Improved monitoring of emerging environmental biocontaminants through (nano)biosensors and molecular analyses

Maria Virginia Riquelme

Dissertation submitted to the faculty of the Virginia Polytechnic Institute and State University in partial fulfillment of the requirements for the degree of

Doctor of Philosophy
In
Civil Engineering

Peter J. Vikesland, Co-Chair
Amy J. Pruden, Co-Chair
Masoud Agah
Michael F. Hochella Jr.

October 27, 2016
Blacksburg, VA

Keywords: Emerging biocontaminants, antibiotic resistance genes, ARGs, wastewater treatment, WWTP, nanosensors, biosensors, impedimetric biosensors, qPCR.

Improved monitoring of emerging environmental biocontaminants through (nano)biosensors and molecular analyses

Maria Virginia Riquelme

ABSTRACT

Outputs of human-derived chemicals and constituents to the environment, and shifts in these outputs, can result in unintended consequences to human and ecological health. One such shift is the advent of the modern antibiotic era, in which mass production and outputs of antibiotics, which are mostly naturally-derived microbial defense compounds and include a few synthetic antimicrobials, has profound implications for contributing to the spread of antibiotic resistance. Antibiotic resistance arises from mutations and/or sharing of antibiotic resistance genes (ARGs) among bacteria via horizontal gene transfer, with carriage of ARGs by pathogenic bacteria of particular concern to human health. While most attention to stopping the spread of antibiotic resistance has been devoted to the clinic, it is critical to consider the environmental origin, ecology and pathways by which antibiotic resistance spreads in order to develop comprehensive strategies to combat antibiotic resistance. In particular, wastewater treatment plants (WWTPs) represent a potentially key critical control point given that they receive antibiotic resistant bacteria (ARB) and ARGs from the population, which are then routed to activated sludge biological treatment, consisting of high density, highly active microbial populations. The research projects described in this dissertation aimed to explore the occurrence of ARGs in WWTPs, particularly WWTPs in developing countries representing the extremes of what is expected to be encountered in terms of potential to spread antibiotic resistance, and to improve and apply novel technologies for monitoring key markers of antibiotic resistance in WWTPs and affected environments. The pathogen *Staphylococcus aureus* and a corresponding ARG (methicillin resistance *mec*A gene) were chosen as model biocontaminants of concern due to their environmental and public health relevance. The results reported in Chapters 3-5 advance the knowledge of bio(nano)sensing techniques and highlight areas of promise and challenge. The results reported in Chapter 2 provided insight into the baseline levels of ARGs expected in a highly impacted WWTP in India, thereby highlighting the magnitude and global scale of the problem of antibiotic resistance as well as the need for innovative solutions.

Improved monitoring of emerging environmental biocontaminants through (nano)biosensors and molecular analyses

Maria Virginia Riquelme

GENERAL AUDIENCE ABSTRACT

Release of human-derived pollutants into the environment can result in unintended consequences to human and environmental health. The rise of antibiotic resistance in disease-causing bacteria serves as a notorious example. Antibiotic resistance arises from mutations and/or sharing of antibiotic resistance genes (ARGs), which are the genetic elements that enable the resistance to occur. While most attention to stopping the spread of antibiotic resistance has been devoted to the clinic, it is critical to consider the environmental factors by which antibiotic resistance spreads in order to develop well-informed strategies to combat it. In particular, wastewater treatment plants (WWTPs) represent a potentially key critical control point given that they receive antibiotic resistant bacteria (ARB) and ARGs from the population, which are then routed to a highly active biological treatment process. The research projects described in this dissertation aimed to explore the occurrence of ARGs in WWTPs, particularly WWTPs in developing countries representing the extremes of what is expected to be encountered in terms of potential to spread antibiotic resistance, and to improve and apply novel technologies for monitoring key markers of antibiotic resistance in WWTPs and affected environments. The disease-causing bacterium *Staphylococcus aureus* and a corresponding ARG (methicillin antibiotic resistance *mec*A gene) were chosen as model biological contaminants of concern due to their environmental and public health relevance. The results reported in Chapters 3-5 advance the knowledge of integrated microbiology and nanotechnology techniques, and also highlight some associated limitations. The results reported in Chapter 2 provide insight into the baseline levels of ARGs expected in a highly impacted WWTP in India, thereby highlighting the magnitude and global scale of the problem of antibiotic resistance as well as the need for innovative solutions.

ACKNOWLEDGEMENTS

I feel grateful about all of the people and circumstances in my life that have led to today. A few people have been particularly impactful in my journey through higher education, and it would be inaccurate to say that I have only grown intellectually. First the obvious person, Dr. Amy Pruden, my ‘extremophile’ coadvisor and mentor, whom I look up to as a role mode and who has made an enormous impact in my life since I was an undergraduate student pretending to know what I was doing. Thank you for sharing and extending part of your life with me, and for welcoming me with unconditional patience, guidance and, dare I say, love. Ironic but funny, if you were a bacterium, you would probably be a ‘superbug.’

Dr. Peter Vikesland (Dr. Pete), I feel a very special appreciation for having you as my coadvisor and mentor. By example, you have taught me to reach for the stars because they are closer than we tend to think. It was through you that I first traveled beyond the Americas! What amazing opportunities you have extended. Besides valuable lessons about science and research, from you I have learned perseverance, trust, and to drop my illusory limitations. Thank you for extending your kindness and dedication.

Committee members, Dr. Masoud Agah and Dr. Mike Hochella, thank you for your kind and open expert and practical advice. I see you as outstanding, sensible, ethical, and passionate professors and mentors, and I hope to emulate those qualities and values when my turn comes, hopefully not too long from now.

I feel particularly fortunate about the wonderful lab and office friends and colleagues that I have had throughout my time Virginia Tech, both in the Pruden and Vikesland groups, and beyond. I have learned so very much from all of you, and I have so enjoyed sharing professional help, casual talks, food, jokes, and even tears with all of you. I cannot tell you how fortunate I feel to have had you as my companions and how much I do love you.

Thank Grace for putting an unconventional angel on the desk next to mine: MamaJi.

Finally, I would like to acknowledge and thank my family for their support, presence and huge(mongous) patience throughout this journey (Like, a lot of patience). I love you.

TABLE OF CONTENTS

LIST OF FIGURES

LIST OF TABLES

CHAPTER 1. Introduction

ENVIRONMENTAL BIOCONTAMINANTS AND THE NEED FOR SUSTAINABLE WATER SOLUTIONS THAT ALSO PROTECT PUBLIC HEALTH

The concept of the "wicked problem" has been introduced, in recognition that not all problems have straightforward solutions.[1] These are unique, complex and convoluted problems that may be directly or indirectly connected to other problems, could be considered as symptoms of other problems, and have no clear solutions.[1, 2] Wicked problems do not have a well-defined cause, but rather, may be the effect of a collection of contributing factors, which may also be interconnected.[1, 2] Furthermore, they are elusive, and, although their effects may be readily-evident, they are difficult to measure and even more so to predict.[1, 2] This concept describes the majority of environmental and human health problems faced by humanity today. Because human activities themselves form the roots of wicked problems, it is evident that mitigation strategies must necessarily be considerate of human behavior, societal practices, and policy. Solutions will clearly require an interdisciplinary perspective and should aim to be in harmony with other critical goals, such as sustainable development and a high standard of public health, in order to most effectively guide us towards homeostasis with our environment and natural resources.[3]

The relationship between microbes and human health can be considered, thus, a wicked one. Thousands of years of coevolution have resulted in intricate interdependent associations between humans and microbial ecosystems;[4] thus, the human body cannot be said to be separate nor independent from its microbe-laden environment. Major scientific advances have recently been made in beginning to understand human-microbiome interactions, revealing significant interdependencies.[4, 5] However, we now have more questions than answers when it comes to characterizing, understanding and predicting these relationships and their benefits/consequences. In particular, as anthropogenic activities take their toll on environmental ecosystems, unanticipated and undesirable effects are being reflected on human health itself. This is so, in part, because microbes evolve and microbial communities adapt in unpredictable ways in responding to human-induced shifts in their environments. Thus, understanding microbe-human

health relationships as well as the effect of anthropogenic activities on microbial communities underlying critical ecosystems, are important first steps in advancing human health and sustainable development.

One of the most globally-relevant and urgent 'wicked problems,' with dire implications to human health, is the emergence antibiotic resistance.[6] The general pattern that has been observed is that, within a few years of releasing a new antibiotic onto the market, bacteria resistant to that antibiotic are discovered in the clinic. Antibiotic resistance can then lead to higher medical costs, prolonged illnesses and increased mortality,[7] with an estimated yearly health care cost of $21 to $34 billion in the US alone.[8] Antibiotic resistance has been associated with more than 2 million illnesses and 23,000 deaths per year in the US alone;[9] however, socioeconomic factors are also at play in antibiotic resistance-related outcomes.[10] In order to combat the spread of antibiotic resistance, it is critical to gain an understanding of the root causes in terms of its origin, evolution and pathways by which it spreads.[11] After seven decades of observations and research, the occurrence and dissemination of antibiotic resistance remains an elusive threat. This is partly due to the complexity of microbial community dynamics taking place within human and environmental systems and partly due to the intricacies surrounding the mechanisms of emergence, carriage, and dissemination of antibiotic resistance.[12, 13] Interestingly, clinically-relevant antibiotic resistance genes (ARGs) are thought to have largely originated from nonpathogenic environmental bacteria,[6, 14] thus highlighting the magnitude of environmental reservoirs as a source of potentially new ARGs.[5] This underscores the importance of advancing understanding of the role of human-induced selective pressures and inputs of exogenous antibiotic resistant bacteria (ARBs) and pathogens to receiving environments, particularly those that interconnect human and natural ecosystems. ARGs are often carried in clusters via self-transmissible or mobilizable elements, such as plasmids and transposons, and can be transferred vertically or horizontally to progeny and other bacteria. Moreover, selective pressures may result in genetically-linked ARGs of different classes to be simultaneously co-selected and amplified in response to exposure to only one antibiotic or selective agent.[15] In this way, different ARGs can become co-enriched within microbial communities, thereby magnifying the concern of dissemination.

Integrons are key genetic elements that can provide an adaptive advantage to bacteria by acquiring, accumulating, and rearranging gene cassettes.[16] Integrons are known to be controlled by the SOS genetic response, which is triggered by DNA damage under stress conditions and induces genetic repair and mutagenesis.[17] One relevant example that highlights their significance with respect to antibiotic resistance was reported in a recent study by Marathe and colleagues.[18] The study characterized the antibiotic resistance profiles of bacteria isolated from a WWTP in India receiving influent from a drug production industry where high levels of antibiotics were found. The authors reported integrase class 1 *intI*1 gene concentrations that were consistently higher than levels of 16S ribosomal RNA genes, a housekeeping gene essential to cell survival and present in all bacteria with a range of copies per genome.[18, 19] In addition, 86% of isolated bacteria were resistant to 20 or more antibiotics, while two isolates were resistant to 35 and 36 of the 39 antibiotics tested.[18] Because integrons can acquire and integrate multiple gene cassettes into their mobile platforms, ARGs are often associated with other bacterial protection genes such as those imparting resistance to metals and other biocides, and thus, may be coselected.[20, 21]

Considering that ARGs can spread among microorganisms, and even be assimilated from dead bacteria via transformation, they have been described to be environmental contaminants.[22, 23] It is evident that ARGs and ARG-associated genetic elements behave unlike typical contaminants in the environment.[23, 24] Mitigation of the complex problem of antibiotic resistance must be truly multidimentional and interdisciplinary (i.e., cover clinical, environmental, cultural and other aspects), as a clear-cut solution is unlikely to be reached.[24, 25] However, there are major gaps associated with global antibiotic resistance characterization and mitigation such as lack of coordinated surveillance, lack of globalized methodology and standards, and lack of concerted global action, especially in developing countries where administration of antibiotics is less regulated.[8, 10] Although antibiotic overuse contributes to the increased occurrence of ARBs, it is not logical to totally abandon antibiotic use, as antibiotics are critical life-saving drugs that have vastly improved human health and well-being. For this reason, an extensive analysis and characterization of the problem, followed by concerted action, are needed with the primary objective of effectively minimizing the impacts of human activities to the

environment and our own well-being.[26] Overall, a balance between innovative and sustainable mitigation techniques, their feasibility, and impacts, both intentional and not, must continually be assessed and recalibrated.[11, 25]

Control of bacterial pathogens has long been the focus of hygiene and environmental policy, with water treatments aimed at their removal and disinfection before discharging to water bodies or distributing to consumers. Bacterial pathogens are of particular concern when they carry ARGs, which can increase their fitness when exposed to selective environments, such as those containing high levels of antibiotics.[6] Since the advent of the antibiotic era and onset of widespread antibiotic use, infections caused by multidrug-resistant bacteria have gradually increased in incidence, causing increased morbidity, mortality, length of illness and treatment, and treatment costs.[7, 27] An important example is multidrug resistant tuberculosis (MDR-TB), which infects over 480,000 people each year and has been identified in 92 countries.[7] Other multidrug resistant life-threatening infections caused by pathogens, such as *Klebsiella pneumoneae* and *Escherichia coli* have been found to essentially be untreatable, and failure of the last resort antibiotic for treatment of gonorrhea has been reported in 10 countries.[7] Resistance to Colistin, a last resort antibiotic for treatment of carbapenem-resistant Enterobacteriaceae, has also recently been reported.[7, 28]

Methicillin-resistant *Staphylococcus aureus* (MRSA), a species of Gram-positive spherical bacteria that has become increasingly resistant to a variety of antibiotics, [29, 30] is a key exemplar of a critical antibiotic-resistant pathogen. *S. aureus* can form part of the normal human flora and can be hosted and transferred by asymptomatic carriers. However, it is also a leading cause of bacterial infection in humans and can infect virtually any tissue of the human body given the right set of conditions.[31] Although *S. aureus* is the most common cause of skin and soft tissue infections, it can also cause more invasive infections that can quickly progress and become systemic and/or life threatening. MRSA infections are more likely to be fatal.[7] Staphylococcal food poisoning is also common, as *S. aureus* is known to produce seven different enteric toxins.[32] Reports of MRSA incidence range between 30 and 90%.[7, 33] One study specific to India characterized *S. aureus* isolates from different sources around the country.[34] The authors reported about 45% MRSA incidence and, more alarmingly, more than 10% vancomycin (an antibiotic of

last resort) resistance *S. aureus* (VRSA) incidence.[34] Due to its high virulence and opportunistic nature, to its resistance and resilience to environmental stresses and antibiotics, and to its adaptability to a range of different environments, *S. aureus* can be considered a relevant opportunistic pathogen of concern.[30] Although MRSA infections were initially primarily limited to the healthcare setting, community acquired infections have become more prevalent worldwide and have been observed to displace other emergent and endemic strains.[35, 36] In addition, *S. aureus* and MRSA strains have been detected in WWTP influents and effluents,[29, 37-39] highlighting the need for monitoring of this emerging aquatic contaminant.

Water is a vital resource to human existence, but can also be a source of waterborne disease and other contamination. Water can facilitate the physical mobility of many colloidal and molecular contaminants, and thus the water cycle is an important conduit to consider for transmitting bacteria, pathogens, and ARGs. In particular, wastewater treatment plants (WWTPs) have been developed and emplaced, mainly within the last century, as barriers to decrease the loads and direct effects of anthropogenic contaminants on the environment and human health. However, WWTPs have not been designed bearing in mind the effects of increasing loads of ARBs and ARGs. Contaminated waters from a variety of human-impacted sources; including hospital, industrial, and domestic sources, converge at WWTPs, thereby creating an efficient and well-mixed medley that may increase interactions between selective agents and microbes. The potential for WWTPs to serve as a hub for horizontal gene transfer and dissemination must be carefully considered and is subject to debate.[40] Untreated and emerging contaminants (e.g., ARB, ARGs and selective agents such as antibiotics, antimicrobials, metabolites, metals, etc.) can potentially enter the environment and/or reenter the human use/consumption grid via direct or indirect water (and biosolids) reuse.[11, 41] Thus, WWTPs not only act as foci for biocontaminant emergence, transfer and proliferation, but also as intermediaries for dissemination via contaminated effluents. Accordingly, WWTPs represent an important point of control for monitoring, characterization and mitigation of emerging biocontaminants of concern.[42, 43]

Considering the rapidly evolving nature of emerging contaminants, a paradigm shift where traditional wastewater treatment methods are adapted to minimize the emergence and

dissemination of amplifiable biocontaminants may be necessary. A critical need for guiding the future development of our water infrastructure is baseline data on occurrence of ARBs, pathogens, and ARGs. In particular, widespread application of low-cost detection and monitoring technologies can help in addressing critical knowledge gaps in understanding the magnitude of the problem as well as in characterizing and prioritizing potential solutions.[44] Thus, the **overarching goal** of this dissertation was to develop, refine, and apply novel detection and monitoring technologies for environmental biocontaminants of concern, especially key markers of antibiotic resistance. The pathogen *S. aureus* and corresponding ARGs (methicillin resistance *mec*A gene in Chapter 5, specifically) were chosen as model biocontaminants of concern due to their environmental and public health relevance and recent reporting of their occurrence in wastewater and reclaimed water.

This dissertation discusses an exploration of electrochemical (Chapter 4) and nanotechnology-enabled (Chapters 3 and 5) detection mechanisms, as well as the application of traditional molecular analyses (Chapter 2) for detection and quantification of biocontaminants. A description of each chapter and its status, as well as a list of authors for each manuscript are described as follows.

ANNOTATED DISSERTATION OUTLINE

Chapter 1 – Introduction. This chapter provides background regarding the motivation of the dissertation, an overview of its contents, and a list of attributions for chapter coauthors.

Chapter 2 – Antibiotic Resistance Gene Distribution in Two WWTPs in Chennai, India. This chapter describes the characterization of antibiotic resistance gene distributions across two WWTPs and their effluent-receiving environments in a densely-populated Indian coastal city. The results thus far suggest relatively high levels of ARGs in WWTP influents and effluents, as well as high background ARG concentrations in receiving environments likely due to direct discharge of unregulated untreated waste and wastewater.

These preliminary results are part of the initial sampling event of the VT PIRE HEARD project. Halting Environmental Antimicrobial Resistance Dissemination (HEARD) is a Virginia Tech project funded by the NSF Partnerships for International Research and

Education (PIRE) program. The project is aimed at improving understanding about different aspects of global wastewater-mediated dissemination of antibiotic resistance.

Chapter authors: Maria V. Riquelme, Jacob Metch, Gargi Singh, Ramya, Indumathi Nambi, Amy Pruden, Peter Vikesland.

Chapter 3 – Aptamer-functionalized Gold Nanoparticles for the Rapid Detection of *Staphylococcus aureus*. This chapter describes the development of aptamer-functionalized gold nanosensors for surface enhanced Raman spectroscopy (SERS)-based detection of a model opportunistic human pathogen of concern: *S. aureus*. The nanosensors have shown promise in terms of specificity and stability, as well as challenges associated with assay reproducibility. We plan to submit a manuscript describing the demonstration of the approach and discussing the limitations and challenges that we have encountered.

Chapter authors: Maria V. Riquelme, Weinan Leng, Matthew S. Hull, Chad W. McKinney, Amy Pruden, and Peter J. Vikesland.

Chapter 4 – Optimizing Blocking of Nonspecific Bacterial Attachment to Impedimetric Biosensors. This manuscript describes the evaluation of a variety of low- and high-molecular weight blocking agents in terms of their ability to minimize nonspecific bacterial binding onto impedimetric gold electrodes. The results demonstrate that some blocking agents can promote differential binding of closely-related bacterial species and highlights the importance of strategically optimizing the blocking of nonspecific bacterial binding in a chemical and biological agent-specific manner. This work led to a publication in *Sensing and Bio-Sensing Research 8 (2016) 47-54*. Available via: http://dx.doi.org/10.1016/j.sbsr.2016.04.003.

Chapter authors: Maria V. Riquelme, Huaning Zhao, Vaishnavi Srinivasaraghavan, Amy Pruden, Peter Vikesland, Masoud Agah.

Chapter 5 – Gold Nanosensor Enabled Detection of Antibiotic Resistance Genes for Environmental Monitoring. The manuscript presented in this chapter describes the development and application of gold nanosensors for the detection of ARGs in complex environmental matrices. Specifically, the stability, selectivity and applicability of *mec*A gene-specific nanosensors were demonstrated in effluents from four WWTPs, including one from a large, densely-populated city in India. The manuscript is in preparation.

Chapter authors: Maria V. Riquelme, Weinan Leng, Marcos Carzolio, Amy Pruden, Peter Vikesland.

Chapter 6 – Conclusions. The major outcomes of the research described in this dissertation are discussed and directions for future work are highlighted in this chapter.

ATTRIBUTIONS

The work reported in this dissertation is the product of collaborations between experts from multiple fields. Each coauthor is credited for his/her contributions to the work described herein.

Dr. Peter Vikesland and Dr. Amy Pruden (Civil and Environmental Engineering). Ph.D. coadvisors, committee co-chairs and project co-PIs. Co-authors of Chapters 2, 3, 4 & 5. Provided guidance regarding experimental design, interpretation of data and communication of results. Assisted with writing manuscripts and reviewed this dissertation.

Jacob Metch (Civil and Environmental Engineering). Coauthor of Chapter 2. Involved in experimental design, sample collection and processing, and sample analyses.

Dr. Gargi Singh, Dr. Indumathi Nambi and Ramya Srinivasan. Coauthors of Chapter 2. Involved in sample collection and processing.

Dr. Weinan Leng (Civil and Environmental Engineering). Coauthor of Chapters 3 and 5. Involved in experimental design, implementation, and analyses relating to Chapters 3 and 5. Provided training on nanoparticle synthesis and functionalization and in instrument use, including surface enhanced Raman spectroscopy (SERS). Performed TEM imaging reported in Chapters 3 and 5.

Chad McKinney. Coauthor of Chapter 3. Assisted with bacterial cultures relating to some of the experiments reported in Chapter 3.

Dr. Matthew Hull. Coauthor of Chapter 3. Assisted with experimental design relating to Chapter 3.

Dr. Masoud Agah (Electrical and Computer Engineering). Committee member. Coauthor of Chapter 4. Provided guidance regarding experimental design, data interpretation and communication of results pertaining to Chapter 4. Also collaborated in other works that are not part of this dissertation.

Huaning Zhao (Biomedical Engineering). First coauthor of Chapter 4. Co-designed experiments, prepared impedance devices and SEM-imaging chips, performed impedance measurements, and assisted in SEM image collection.

Dr. Vaishnavi Srinivasaraghavan (Electrical Engineering). Coauthor of Chapter 4. Assisted with experimental design, implementation and analyses relating to experiments reported in Chapter 4.

Dr. Marcos Carzolio (Statistics). Coauthor of Chapter 5. Performed data modeling and fitting and statistical analyses related to Chapter 5.

REFERENCES

1. Rittel, H. W. J.; Webber, M. M., Dilemmas in a general theory of planning. *Policy Sciences* **1973,** *4*, 155-169.
2. Kreuter, M. W.; De Rosa, C.; Howze, E. H.; Baldwin, G. T., Understanding wicked problems: A key to advancing environmental health promotion. *Health Educ. Behav.* **2004,** *31*, 441-454.
3. van Bueren, E. M.; van Bueren, E. T. L.; van der Zijpp, A. J., Understanding wicked problems and organized irresponsibility: Challenges for governing the sustainable intensification of chicken meat production. *Current Opinion in Environmental Sustainability* **2014,** *8*, 1-14.
4. Clemente, J. C.; Ursell, L. K.; Parfrey, L. W.; Knight, R., The Impact of the gut microbiota on human health: An integrative view. *Cell* **2012,** *148*, 1258-1270.
5. Allen, H. K.; Donato, J.; Wang, H. H.; Cloud-Hansen, K. A.; Davies, J.; Handelsman, J., Call of the wild: Antibiotic resistance genes in natural environments. *Nature Reviews Microbiology* **2010,** *8*, 251-259.
6. Finley, R. L.; Collignon, P.; Larsson, D. G. J.; McEwen, S. A.; Li, X. Z.; Gaze, W. H.; Reid-Smith, R.; Timinouni, M.; Graham, D. W.; Topp, E., The scourge of antibiotic resistance: The important role of the environment. *Clin. Infect. Dis.* **2013,** *57*, 704-710.
7. WHO, Antimicrobial resistance fact sheet. Accessed in 2016. http://www.who.int/mediacentre/factsheets/fs194/en/
8. WHO, *Antimicrobial resistance: Global report on surveillance*; 2014.
9. CDC, Antibiotic resistance threats in the United States. In Services, U. D. o. H. a. H., Ed. 2013.
10. Okeke, I. N.; Lamikanra, A.; Edelman, R., Socioeconomic and behavioral factors leading to acquired bacterial resistance to antibiotics in developing countries. *Emerging Infect. Dis.* **1999,** *5*, 18-27.
11. Berendonk, T. U.; Manaia, C. M.; Merlin, C.; Fatta-Kassinos, D.; Cytryn, E.; Walsh, F.; Burgmann, H.; Sorum, H.; Norstrom, M.; Pons, M. N.; Kreuzinger, N.; Huovinen, P.; Stefani, S.; Schwartz, T.; Kisand, V.; Baquero, F.; Martinez, J. L., Tackling antibiotic resistance: The environmental framework. *Nature Reviews Microbiology* **2015,** *13*, 310-317.

12. Baym, M.; Lieberman, T. D.; Kelsic, E. D.; Chait, R.; Gross, R.; Yelin, I.; Kishony, R., Spatiotemporal microbial evolution on antibiotic landscapes. *Science* **2016,** *353*, 1147-1151.
13. Martinez, J. L.; Baquero, F., Emergence and spread of antibiotic resistance: setting a parameter space. *Ups. J. Med. Sci.* **2014,** *119*, 68-77.
14. D'Costa, V. M.; King, C. E.; Kalan, L.; Morar, M.; Sung, W. W. L.; Schwarz, C.; Froese, D.; Zazula, G.; Calmels, F.; Debruyne, R.; Golding, G. B.; Poinar, H. N.; Wright, G. D., Antibiotic resistance is ancient. *Nature* **2011,** *477*, 457-461.
15. Aminov, R. I.; Mackie, R. I., Evolution and ecology of antibiotic resistance genes. *FEMS Microbiol. Lett.* **2007,** *271*, 147-161.
16. Cambray, G.; Guerout, A. M.; Mazel, D., Integrons. In *Annual Review of Genetics, Vol 44*, Campbell, A.; Lichten, M.; Schupbach, G., Eds. 2010; Vol. 44, pp 141-166.
17. Guerin, E.; Cambray, G.; Sanchez-Alberola, N.; Campoy, S.; Erill, I.; Da Re, S.; Gonzalez-Zorn, B.; Barbe, J.; Ploy, M. C.; Mazel, D., The SOS response controls integron recombination. *Science* **2009,** *324*, 1034-1034.
18. Marathe, N. P.; Regina, V. R.; Walujkar, S. A.; Charan, S. S.; Moore, E. R. B.; Larsson, D. G. J.; Shouche, Y. S., A treatment plant receiving waste water from multiple bulk drug manufacturers is a reservoir for highly multi-drug resistant integron-bearing bacteria. *PLoS One* **2013,** *8*.
19. Vetrovsky, T.; Baldrian, P., The variability of the 16S rRNA gene in bacterial genomes and its consequences for bacterial community analyses. *PLoS One* **2013,** *8*.
20. Pal, C.; Bengtsson-Palme, J.; Kristiansson, E.; Larsson, D. G. J., Co-occurrence of resistance genes to antibiotics, biocides and metals reveals novel insights into their co-selection potential. *BMC Genomics* **2015,** *16*.
21. Di Cesare, A.; Eckert, E. M.; D'Urso, S.; Bertoni, R.; Gillan, D. C.; Wattiez, R.; Corno, G., Co-occurrence of integrase 1, antibiotic and heavy metal resistance genes in municipal wastewater treatment plants. *Water Res.* **2016,** *94*, 208-214.
22. Pruden, A.; Pei, R. T.; Storteboom, H.; Carlson, K. H., Antibiotic resistance genes as emerging contaminants: Studies in northern Colorado. *Environ. Sci. Technol.* **2006,** *40*, 7445-7450.
23. Sanderson, H.; Fricker, C.; Brown, R. S.; Majury, A.; Liss, S. N., Antibiotic resistance genes as an emerging environmental contaminant. *Environ. Rev.* **2016,** *24*, 205-218.
24. Martinez, J. L.; Baquero, F.; Andersson, D. I., Predicting antibiotic resistance. *Nature Reviews Microbiology* **2007,** *5*, 958-965.
25. Baquero, F.; Lanza, V. F.; Canton, R.; Coque, T. M., Public health evolutionary biology of antimicrobial resistance: Priorities for intervention. *Evolutionary Applications* **2015,** *8*, 223-239.
26. Cars, O.; Hedin, A.; Heddini, A., The global need for effective antibiotics-Moving towards concerted action. *Drug Resistance Updates* **2011,** *14*, 68-69.
27. Ogeer-Gyles, J. S.; Mathews, K. A.; Boerlin, P., Nosocomial infections and antimicrobial resistance in critical care medicine. *Journal of Veterinary Emergency and Critical Care* **2006,** *16*, 1-18.
28. Du, H.; Chen, L.; Tang, Y. W.; Kreiswirth, B. N., Emergence of the mcr-1 colistin resistance gene in carbapenem-resistant Enterobacteriaceae. *Lancet Infect. Dis.* **2016,** *16*, 287-288.

29. Goldstein, R. E. R.; Micallef, S. A.; Gibbs, S. G.; Davis, J. A.; He, X.; George, A.; Kleinfelter, L. M.; Schreiber, N. A.; Mukherjee, S.; Sapkota, A.; Joseph, S. W.; Sapkota, A. R., Methicillin-resistant *Staphylococcus aureus* (MRSA) detected at four US wastewater treatment plants. *Environ. Health Perspect.* **2012,** *120*, 1551-1558.
30. Shinefield, H. R.; Ruff, N. L., Staphylococcal Infections: A Historical Perspective. *Infect. Dis. Clin. North Am.* **2009,** *23*, 1-+.
31. Kluytmans, J.; vanBelkum, A.; Verbrugh, H., Nasal carriage of *Staphylococcus aureus*: Epidemiology, underlying mechanisms, and associated risks. *Clin. Microbiol. Rev.* **1997,** *10*, 505-&.
32. Dinges, M. M.; Orwin, P. M.; Schlievert, P. M., Exotoxins of *Staphylococcus aureus*. *Clin. Microbiol. Rev.* **2000,** *13*, 16-+.
33. Pathare, N. A.; Asogan, H.; Tejani, S.; Al Mahruqi, G.; Al Fakhri, S.; Zafarulla, R.; Pathare, A. V., Prevalence of methicillin resistant *Staphylococcus aureus* MRSA colonization or carriage among health-care workers. *Journal of Infection and Public Health* **2016,** *9*, 571-576.
34. Mendem, S. K.; Gangadhara, T. A.; Shivannavar, C. T.; Gaddad, S. M., Antibiotic resistance patterns of *Staphylococcus aureus*: A multi center study from India. *Microb. Pathog.* **2016,** *98*, 167-170.
35. Stryjewski, M. E.; Corey, G. R., Methicillin-resistant *Staphylococcus aureus*: An evolving pathogen. *Clin. Infect. Dis.* **2014,** *58*, S10-S19.
36. Klein, E. Y.; Sun, L. V.; Smith, D. L.; Laxminarayan, R., The changing epidemiology of Methicillin-resistant *Staphylococcus aureus* in the United States: A national observational study. *Am. J. Epidemiol.* **2013,** *177*, 666-674.
37. Gomez, P.; Lozano, C.; Benito, D.; Estepa, V.; Tenorio, C.; Zarazaga, M.; Torres, C., Characterization of staphylococci in urban wastewater treatment plants in Spain, with detection of methicillin resistant *Staphylococcus aureus* ST398. *Environ. Pollut.* **2016,** *212*, 71-76.
38. Thompson, J. M.; Gundogdu, A.; Stratton, H. M.; Katouli, M., Antibiotic resistant *Staphylococcus aureus* in hospital wastewaters and sewage treatment plants with special reference to methicillin-resistant *Staphylococcus aureus* (MRSA). *J. Appl. Microbiol.* **2013,** *114*, 44-54.
39. Borjesson, S.; Matussek, A.; Melin, S.; Lofgren, S.; Lindgren, P. E., Methicillin-resistant *Staphylococcus aureus* (MRSA) in municipal wastewater: An uncharted threat? *J. Appl. Microbiol.* **2010,** *108*, 1244-1251.
40. Baquero, F.; Martinez, J. L.; Canton, R., Antibiotics and antibiotic resistance in water environments. *Curr. Opin. Biotechnol.* **2008,** *19*, 260-265.
41. Garner, E.; Zhu, N.; Strom, L.; Edwards, M.; Pruden, A., A human exposome framework for guiding risk management and holistic assessment of recycled water quality. *Environmental Science-Water Research & Technology* **2016,** *2*, 580-598.
42. Pruden, A.; Larsson, D. G. J.; Amezquita, A.; Collignon, P.; Brandt, K. K.; Graham, D. W.; Lazorchak, J. M.; Suzuki, S.; Silley, P.; Snape, J. R.; Topp, E.; Zhang, T.; Zhu, Y. G., Management options for reducing the release of antibiotics and antibiotic resistance genes to the environment. *Environ. Health Perspect.* **2013,** *121*, 878-885.
43. Pruden, A., Balancing water sustainability and public health goals in the face of growing concerns about antibiotic resistance. *Environ. Sci. Technol.* **2014,** *48*, 5-14.

44. Pehrsson, E. C.; Tsukayama, P.; Patel, S.; Mejia-Bautista, M.; Sosa-Soto, G.; Navarrete, K. M.; Alderon, M. C.; Abrera, L. C.; Hoyos-Arango, W.; Bertoli, M. T.; Berg, D. E.; Gilman, R. H.; Dantas, G., Interconnected microbiomes and resistomes in low-income human habitats. *Nature* **2016,** *533*, 212-+.

CHAPTER 2. Antibiotic resistance gene distributions across two WWTPs and their effluent-receiving environments in a densely-populated Indian city.

Maria V. Riquelme, Jacob Metch, Gargi Singh, Ramya Srinivasan, Indumathi Nambi, Peter Vikesland, Amy Pruden.

Project in progress

ABSTRACT

The pandemic propagation of antibiotic resistance calls for concerted global action. From an environmental perspective, wastewater treatment plants (WWTPs) are potentially critical control points for antibiotic resistance emergence, proliferation and dissemination. As part of a larger effort aimed at understanding and mitigating wastewater treatment-associated antibiotic resistance, the primary focus of this project was to characterize antibiotic resistance gene distributions across two WWTPs and their effluent-receiving bodies in a densely-populated Indian coastal city. Real-time quantitative polymerase reaction (qPCR) was applied to quantify bacterial 16S rRNA genes and three antibiotic resistance genes (ARGs), *tet*(W), *tet*(O), and *sul*1, and an associated class I integron, *intI*1. In general, gene abundances followed the pattern 16SrRNA>*intI*1≥*sul*1> *tet*(O)>*tet*(W). Influent ARG concentrations were relatively high (in the order of 10^8 gene copies/mL) and similar in both WWTPs. Absolute and relative (i.e., normalized to 16S rRNA genes) gene abundances were similar throughout both treatment trains, while the WWTP effluent impact on the receiving water bodies could not be resolved due to high background ARG levels, likely due to direct discharge of unregulated untreated waste and wastewater. Metagenomic analyses will be applied in a future study to provide a broader and comprehensive profile of the ARGs to validate trends observed here in the WWTPs and further explore the potential effects of their effluents on receiving environments.

INTRODUCTION

Antibiotic resistance is a multicausal and dynamic problem of pandemic proportions affecting human health worldwide.[1] Mitigation strategies require global and interdisciplinary concerted action with an aim to minimize ARG emergence, proliferation

and dissemination via priority 'hotspots.'[1-3] In particular, the role of the environment is gaining attention, including means by which human activities may amplify natural background antibiotic resistance genes (ARGs) and their tendency to be transferred or the potential for clinical sources of resistance to spread via environmental routes. As central points of convergence of human waste and a plethora of selective agents (e.g., metals, antibiotics), wastewater treatment plants (WWTPs) are of key interest as potential hot-spots for ARG amplification, horizontal gene transfer, and spread to the environment.[4, 5] These attributes also place WWTPs in a potentially key position for limiting the spread of antibiotic resistance, underscoring the importance of establishing an understanding of the effects of different treatment processes and technologies on ARG behavior. For example, some wastewater treatment processes have been reported to increase ARG concentrations relative to the influent,[6, 7] while others have been observed to decrease levels.[8, 9] Increase in ARG concentration during wastewater treatment has been associated with selective conditions coupled with recycling of biosolids,[6, 10] supporting the idea that the degree of WWTP-associated ARG emergence may be impacted synergistically by various factors. Thus, characterizing and categorizing the efficacy of existing treatment strategies and their influence on receiving environments are necessary steps in designing more effective and sustainable treatment waste management systems, while ensuring utmost protection of public health.

Antibiotic resistance is a complex global challenge driven by varying antibiotic use and disposal policies in different countries, as well as distinct socioeconomic conditions and standards of sanitation and waste management. Thus, it is critical to begin to gain perspective about the baseline occurrence and function of ARGs in WWTPs across the globe. Indian WWTPs are of strong interest as potential worst-case-scenarios, both in terms of the levels and kinds of resistant bacteria and selective agents in the influent. Also noteworthy are the lack of regulation of antibiotic use, unfettered disposal of industrial sources of antibiotics,[11] and the prominent emergence and incidence of multi-drug resistant "super-bugs".[10, 12] In 2010, India was the world's largest human health-related consumer of antibiotics, followed by China and the United States.[13] Factors such as low regulation of antibiotic distribution, poor public health infrastructure, rising incomes,

high population densities and high incidence of disease, are likely synergistic forces in driving emergence of antibiotic resistance.[14]

Here we examined occurrence of key ARG markers and a gene transfer element in two WWTPs located in a densely-populated Indian city with the objectives of: (1) characterizing ARG distributions throughout the treatment system, (2) characterizing ARG distributions in receiving bodies and exploring relationships with the WWTP effluent, and (3) validating sample preservation and DNA extraction methodology to support international comparisons of ARG distributions. We quantified the bacterial 16S rRNA gene, a conserved gene among bacteria and a marker for total bacterial concentrations; the *intI*1 class 1 integrase gene, which encodes an integrase enzyme implicated in the acquisition of ARGs for their subsequent expression within the bacterial cell;[15] and the *tet*(W) and *tet*(O) genes that encode tetracycline resistance; and the *sul*1 gene, which encodes sulfonamide resistance. This approach provided a cross-section of genes of clinical, environmental, and ecological relevance. In combination with novel metagenomic-based ARG fingerprinting, the ARG quantification results reported herein are expected to provide insights about local patterns and relative sources contributing to the global emergence and dissemination of antibiotic resistance.

MATERIALS AND METHODS

WWTP description and sample collection. A schematic of the two WWTP relative locations within the city and their configurations are shown in Figure 2.1. WWTP 1 was the newest (about 1-year-old) of a three-train WWTP complex that treated influent from separate districts of the surrounding city. The 54 MLD (14 MGD) WWTP consisted of conventional activated sludge treatment with diffused oxygen followed by a chlorination step (without dechlorination) prior to effluent release into a channel that led to a nearby river (≈ 0.25 mi away). The combined biosolids were anaerobically digested prior to dewatering via centrifugation; however, the dewatering centrifuge was out of operation at the time of sampling. Samples were collected from the influent, primary clarifier effluent, activated sludge basin effluent, secondary clarifier effluent, final effluent, combined solids, and final (digested) solids. Samples were also collected from the receiving river upstream and downstream of the WWTP effluent discharge; however, it is important to note that

both the river and the canal connecting the WWTP to the river also received discharge from unregulated sources. For this reason, it may be difficult to determine the actual impact that the WWTP effluent had on the receiving river water quality.

WWTP 2 was a 54 MLD (14 MGD) conventional activated sludge treatment (mechanically aerated) without a disinfection step. The secondary effluent flowed into a shallow retention pond (sunlight exposure was expected to partially disinfect) before discharging into a marshland. The marshland was also home to a solid waste dump site, known to be impacted by leaching of high levels of heavy metals (e.g., lead) and other contaminants (personal communication). The influent to the plant was partially composed of septic tank sewage transported on trucks and disposed onto partially open channels that led to combination with the bulk influent. The WWTP had an infinite secondary SRT, thus the final solids composition was made up of anaerobically-digested settled solids from primary clarification only. The solids dewatering centrifuge was also out of service at this plant. Areas of turbulent hydraulic flow throughout the plant generated high quantities of foam that was lifted and dispersed by the wind. Samples were collected from the influent, primary clarifier effluent, activated sludge aeration basin near the discharge point (effluent collection was inaccessible due to foaming), secondary clarifier effluent, final effluent, and primary solids before and after anaerobic digestion (i.e., anaerobic digester influent and effluent). Because the WWTP effluent receiving water body was a marshland, there were no clear upstream and downstream points available for sampling. In addition, the location near the WWTP effluent discharge into the marshland was not accessible, thus sampling of the marshland took place near the solid waste dumpsite and at the marshland outfall, where the marshland discharged into a canal that ran parallel to the coastline.

Where necessary samples were collected by dipping a bucket attached to a string into the water, then transferring the sample into a previously washed sampling container for transport to the lab. The plastic collection containers were prepared by scrubbing with bleach and rinsing thoroughly with tap water before rinsing three final times with DI water. For influent, primary effluent, and activated sludge sampling, a bucket provided by the WWTP was rinsed five times with sample water before using for sample collection. For secondary effluent, final effluent, and receiving water body sampling, a bucket brought from the lab was rinsed with DI water, wiped with ethanol, and pre-rinsed five times with

sample water prior to using for sample collection. Temperature, dissolved oxygen (DO), and pH were measured on-site on a fraction of each sample collected. Solids samples were collected directly into sterile 50 mL centrifuge tubes. The samples were immediately transported to the lab and either processed immediately (within 2-4 h of collection) or stored in a 4 °C fridge until processing on the same day.

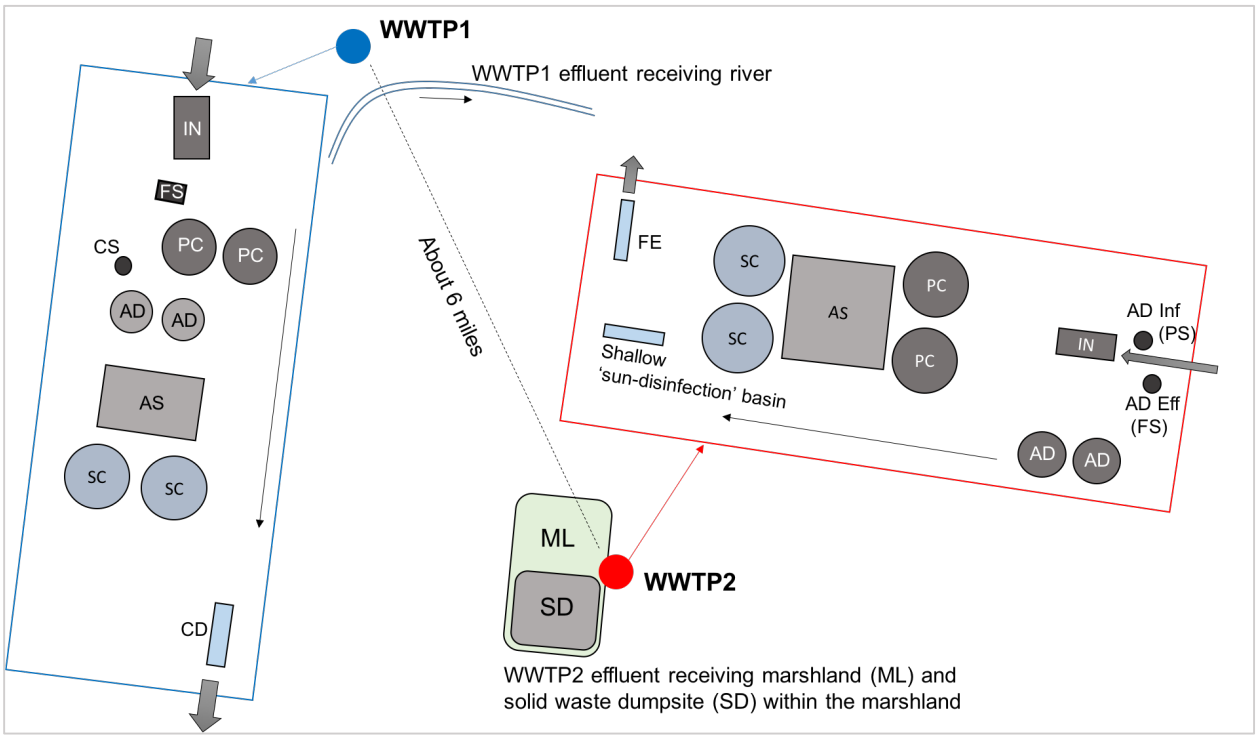

Figure 2.1. Map of WWTP relative locations and WWTP process schematics (magnified in blue and red for WWTPs 1 and 2, respectively). WWTPs were located within a densely populated coastal Indian city. WWTP1 effluent-receiving river was about 0.25 mi away from the WWTP. Abbreviations: IN (influent), PC (primary clarifiers), AS (activated sludge basin), SC (secondary clarifiers), CD (Chlorine disinfection), FE (Final effluent), AD (anaerobic digesters), CS (Combined solids), FS (final solids), ML (marshland), SD (solid waste dump site). WWTP2 secondary solids had infinite retention time, and final effluent did not undergo disinfection.

Sample processing. Liquid samples (influent, primary effluent, secondary effluent, final effluent, and upstream and downstream of receiving body) were shaken and concentrated onto 0.22 μm-pore size mixed cellulose esters filters (Millipore, Catalog # GSWP047S0)

via vacuum filtration until clogging. Triplicate samples were filter-concentrated and their volume recorded before the filter was folded using flame-sterilized tweezers, placed in a 2-mL O-ring screw-cap sterile tube, and submerged in 1.5 mL of 50% ethanol in sterile MilliQ water. Activated sludge and solids samples were homogenized by shaking and 500 uL or 500 mg were mixed 500 μL of 100% ethanol inside of a 2-mL O-ring screw-cap sterile tube. All ethanol-fixed samples were stored at -20 °C before shipping (expedited) on ice to our home lab at Virginia Tech, where they were immediately stored at -20 °C until DNA extraction.

DNA extraction. DNA was extracted from the samples using the Fast DNA SPIN Kit for Soil (MP Bio, Catalog # 116560200). For DNA extraction from the filtered liquid samples, the filters were first removed from the 2-mL storage tube and torn into small (≈5 mm × 5 mm pieces) using flame-sterilized tweezers before placing inside of a lysing matrix tube E. This step was done directly above a sterile Petri dish with care not to drop any filter pieces outside of the plate area. The 2-mL storage tubes containing the remaining ethanol solution were then centrifuged at 5,000 ×g for 10 min, the ethanol decanted, and the pellet resuspended in Sodium Phosphate Buffer (978 μL) and MT Buffer (122 μL) (i.e., the first two solutions applied during DNA extraction). This mix was then transferred to the lysing matrix tubes (along with the torn filters), before carrying on with DNA extraction according to kit manufacturer's instructions. For DNA extraction from activated sludge and solids samples, the 2-mL tubes were centrifuged at 5,000 ×g for 10 min, the ethanol decanted, and the pellet resuspended in Sodium Phosphate Buffer and MT Buffer (978 μL and 122 μL, respectively), before transferring to the lysing matrix tubes and carrying out DNA extraction as directed in the kit manual. DNA extracts were stored in O-ring tubes at -20 °C prior to molecular analyses.

Real-time, quantitative polymerase chain reaction (qPCR). First, four representative samples were chosen from each of the two WWTPs in order to determine the optimum sample dilution required for maximizing enzyme-based amplification while minimizing contaminant-induced inhibition. Three dilutions (1:20, 1:50, and 1:100) were prepared for DNA extracted from influent, final effluent, activated sludge and final solids samples obtained from both WWTPs. An initial qPCR-based 16S rRNA gene quantification was

done for these dilutions, and an optimum dilution of 1:50 was chosen. Triplicate qPCR quantifications of the 16S rRNA, i*ntI*1, *tet*(W), *tet*(O) and *sul*1 genes were then carried out for all the samples. Each 10 μL reaction consisted of 400 nM of each primer, 1X EVA Green Supermix (BioRad), and 1 μL of 1:50 diluted sample. Each reaction underwent an initial denaturation step of 2 min at 98 °C followed by 40 cycles of denaturing at 98 °C and annealing-extension at the temperature specified in Table 2.1. A melt-curve was collected after each run. A list of genes and primer information is reported in Table 2.1.

Table 2.1. List of qPCR-quantified genes and their respective primer information.

Gene	Annealing temp. (°C)	Amplicon size (bp)	Reference
16S rRNA	60	124	Suzuki et al., 2000
*intI*1	60	473	Hardwick et al., 2008
tet(W)	60	167	Aminov et al., 2001
tet(O)	50.3	171	Aminov et al., 2001
*sul*1	69.9	163	Pei et al., 2006

RESULTS & DISCUSSION

Sample collection and characterization. Samples were collected from the WWTPs and their effluent receiving bodies as illustrated in Figure 2.2. Each sample was characterized in terms of temperature, DO and pH (Table 2.2). On average, sample temperature was about 30.6 ±0.59 °C, excluding the marshland outfall (34 °C). The pH ranged from 7.46 (WWTP1 PE) to 8.43 (Marshland outfall).

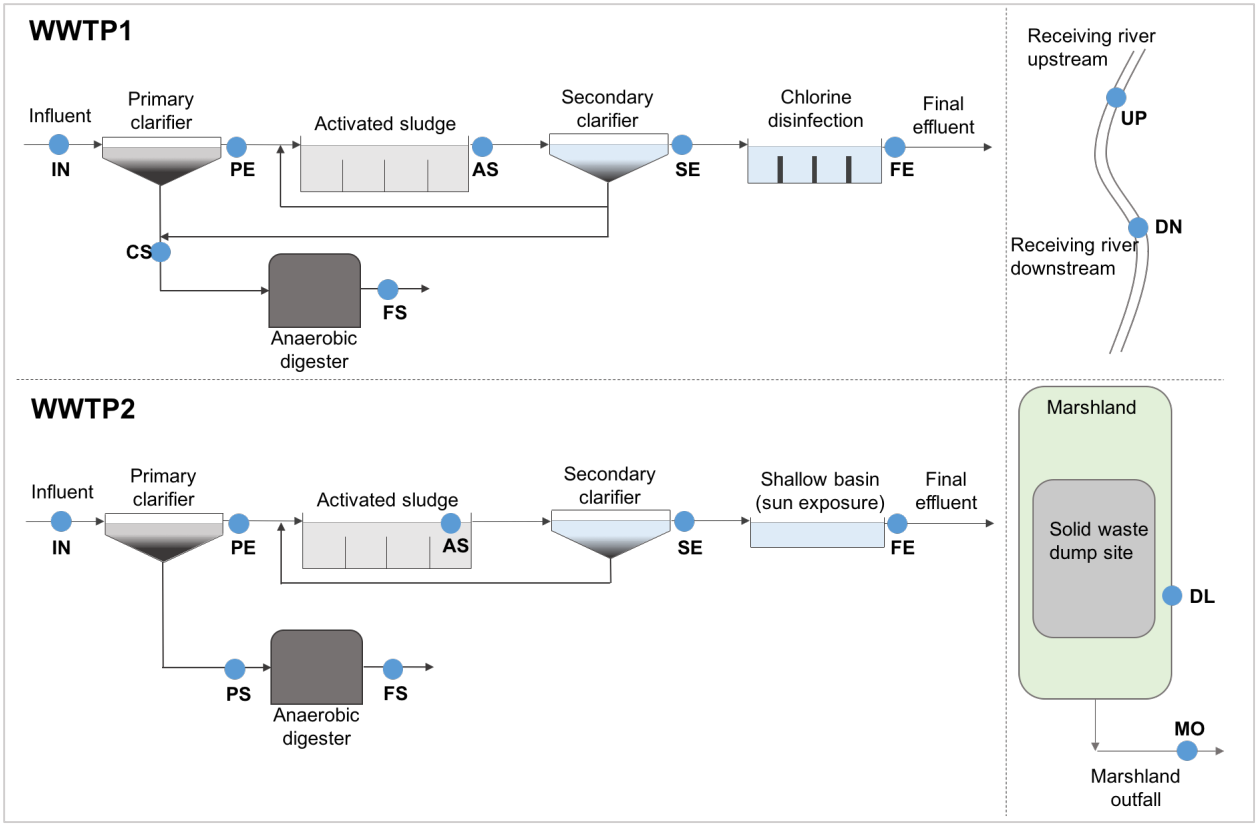

Figure 2.2. WWTP configuration and sampling locations. Blue dots accompanied by a two-letter sample abbreviation (in bold) represent sampling locations within each WWTP and their receiving bodies (right). Abbreviations: IN (influent), PE (primary effluent), AS (activated sludge basin), SE (secondary effluent), FE (Final effluent), PS (primary solids), CS (combined solids), FS (final solids), UP (receiving river upstream from WWTP), DN (receiving river downstream from WWTP), DL (Solid waste dumpsite leachate), MO (marshland outfall).

Table 2.2. Temperature, dissolved oxygen (DO) and pH characteristics of samples.

WWTP (Capacity)	Sampling location	Temp. (°C)	DO (mg/L)	pH
WWTP1 (54 MLD)	Influent (IN)	29.8	0.94	7.96
	Primary effluent (PE)	30.0	0.60	7.46
	Activated sludge (AS)	30.6	2.83	7.61
	Secondary effluent (SE)	30.8	4.71	7.79
	Final effluent (FE)	30.5	5.29	7.86
WWTP2 (54 MLD)	Influent (IN)	30.9	0.22	7.64
	Primary effluent (PE)	31.5	1.56	7.55
	Activated sludge (AS)			7.91
	Secondary effluent (SE)	30.8	2.76	7.96
	Final effluent (FE)	31.4	4.01	8.18
Marshland receiving WWTP2 effluent	Marsh- Near Solid Dump (DL)	29.9	7.20	8.00
	Marsh- Outfall (MO)	34.0	15.11	8.43

Gene occurrence trends. All collected samples were screened for *intI*1, *tet*(W), *tet*(O) and *sul*1 genes. Relative gene abundances were estimated via normalization to corresponding 16S rRNA gene copies. Preliminary gene quantification results are shown in Figures 2.3, 2.4 and 2.5. All genes were detected in all samples at relatively high concentrations in comparison to levels reported in other countries,[9, 16-18] except in the dumpland leachate-impacted marshland sample (DL) associated with WWTP2. Class 1 integron *intI*1 abundances were generally comparable to *sul*1 gene but higher than other ARG abundances for all samples, following a general pattern where *tet*(O) was slightly, and consistently, higher than *tet*(W). In general, gene abundances followed the pattern 16SrRNA>*intI*1≥*sul*1>*tet*(O)>*tet*(W). WWTP ARG-associated gene concentrations ranged from 5.4×10^{8} (*intI*1) to 1×10^{8} (*tet*(W)) gene copies/mL in the influent, 6.7×10^{9} (*intI*1) to 1.4×10^{8} (*tet*(W)) gene copies/mL in the activated sludge, and from 9.8×10^{6} (*intI*1) to 8.0×10^{5} (*tet*(W)) gene copies/mL in the final effluent. Relative gene abundances ranged from 2.3×10^{-1} (*intI*1) to 4.2×10^{-2} (*tet*(W)) in the influent, 3.6×10^{-1} (*intI*1) to 7.2×10^{-3} (*tet*(W)) in the activated sludge, and from 1.6×10^{-1} (*intI*1) to 1.3×10^{-2} (*tet*(W)) in the final effluent. Absolute gene concentrations and ARG relative abundances were similar upstream and downstream of WWTP1 in the receiving river. ARG-associated gene concentrations

ranged from 1.7×10^{7} (*intI*1) to 9.4×10^{5} (*tet*(W)) gene copies/mL upstream, and from 3.0×10^{7} (*intI*1) to 1.0×10^{6} (*tet*(W)) gene copies/mL downstream of the WWTP; with relative abundances ranging from 1.8×10^{-1} (*intI*1) to 9.8×10^{-3} (*tet*(W)) upstream, and from 1.4×10^{-1} (*intI*1) to 4.8×10^{-3} (*tet*(W)) downstream of the WWTP. Based on these results, there was no evidence of a direct impact of WWTP effluents on increased ARG occurrence downstream of the river. However, inputs from WWTP1 were likely overshadowed by the dominating influence of unregulated discharge into the river itself and into the canal leading the WWTP effluent into the river. Metagenomic analyses are expected to provide broader and deeper ARG fingerprints to help elucidate the relative impacts of different sources on the ARG composition of the receiving environment.

Similar gene distribution patterns were observed for WWTP2. ARG-associated gene concentrations ranged from 4.5×10^{8} (*intI*1) to 8.6×10^{7} (*tet*(W)) gene copies/mL in the influent, 4.6×10^{9} (*intI*1) to 3.3×10^{8} (*tet*(W)) gene copies/mL in the activated sludge, and from 1.4×10^{7} (*intI*1) to 1.9×10^{6} (*tet*(W)) gene copies/mL in the final effluent. Relative gene abundances ranged from 2.3×10^{-1} (*intI*1) to 4.3×10^{-2} (*tet*(W)) in the influent, 1.7×10^{-1} (*intI*1) to 1.1×10^{-2} (*tet*(W)) in the activated sludge, and from 9.0×10^{-2} (*intI*1) to 1.2×10^{-2} (*tet*(W)) in the final effluent. Relative gene abundances in the solids samples from both WWTPs followed a similar pattern.

ARG concentrations followed the same occurrence pattern as described above, where *intI*1≥*sul*1>*tet*(O)>*tet*(W), throughout the WWTP and also in the marshland outfall (except in the solid waste dumpsite leachate-impacted marshland sample). Marshland outfall gene concentrations were similar to those in the WWTP effluent. However, it is unknown to what extent these concentrations are impacted by WWTP effluent versus unregulated wastewaters channeled into the marshland. Gene concentrations in the solid waste dumpsite-impacted marshland samples were lowest in comparison to all other samples. Gene concentrations were 2.3×10^{6} (*intI*1), 3.0×10^{3} (*tet*(W)), 2.6×10^{4} (*tet*(O)), and 3.2×10^{6} (*sul*1), with relative abundances of 1.5×10^{-2}, 1.7×10^{-4}, 1.7×10^{-3}, and 2.1×10^{-2}, respectively. Because this solid waste leachate-impacted marshland may contain higher levels of PCR inhibitors, additional optimizations will be carried out to test for inhibition and corroborate the values reported here.

Absolute and relative ARG concentrations were very similar in the influent to both WWTPs, suggesting the possibility of a relatively homogeneous antibiotic use and antibiotic resistance distribution among the areas where the wastewater is generated. Microbial community composition dependence on seasonal antibiotic wastewater concentrations has been reported.[19] The same study reported a positive correlation between temperature and sulfonamide resistant heterotrophs and enterobacteria.[19] ARG and *intI*1 concentrations reported elsewhere are variable and also tend to reflect local and seasonal patterns of antibiotic use.[7, 12, 20] The concentrations reported herein appear to be relatively higher when compared to other reports;[9, 16-18] however, this is not surprising considering that antibiotic use in India is among the highest in the world.[14] One study quantified *intI*1 concentrations in an extreme WWTP receiving influent from a drug production plant.[10] The authors highlighted the occurrence of high drug levels in the WWTP environment, and reported unusually high levels of ARGs, including *intI*1 concentrations that were higher than 16S rRNA gene concentrations and that increased throughout the wastewater treatment train.[10] Because bacteria usually harbor multiple 16S rRNA gene copies within their genomes, this finding suggested the potential for occurrence of multiple *intI*1 genes in a single cell and highlighted the effect of selective pressures on the enrichment of ARG-associated genetic elements.[10]

Compared to other sampling locations, ARG abundances were enriched in the activated sludge. This is consistent with the hypothesis of the biosolids recycling practices and the active growth conditions within these reactors contributing to selection and transfer of ARGs,[7] although a recent metagenomics-based study of Danish WWTPs suggested that horizontal gene transfer may be limited in activated sludge.[21] The presence of selective agents such as pharmaceuticals, heavy metals, disinfectants, antibiotics (even at subtherapeutic doses), or a combination thereof, theoretically can enhance ARG emergence and coselection,[22-25] potentially making the activated sludge process a fertile ground for selection of antibiotic-resistant bacteria. Further metagenomic analysis is expected to provide broader and deeper resolution profiling of ARGs and gene transfer elements to help elucidate relationships between wastewater treatment and ARG emergence and dissemination.[12, 22, 26]

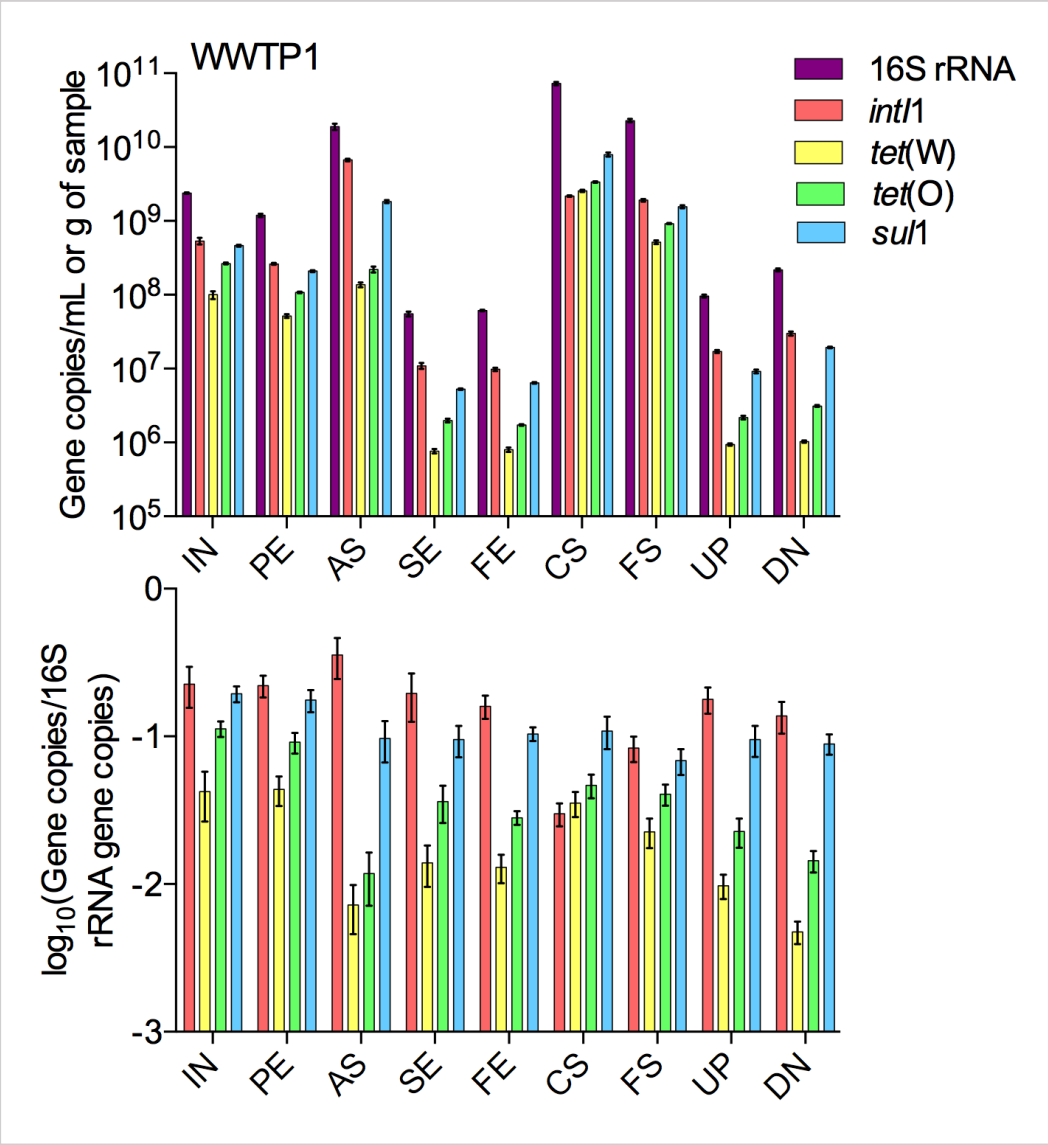

Figure 2.3. qPCR-quantified gene concentrations in samples obtained from WWTP1. Absolute gene concentrations per copy numbers (top), and 16S rRNA gene normalized gene proportions (bottom). Error bars include analytical and experimental replicates, accounting for error propagation of standard deviations. Samples: IN (Influent), PE (Primary effluent), AS (Activated sludge), SE (Secondary effluent), FE (Final effluent), CS (Combined solids), FS (Final solids), UP (River upstream), DN (River downstream).

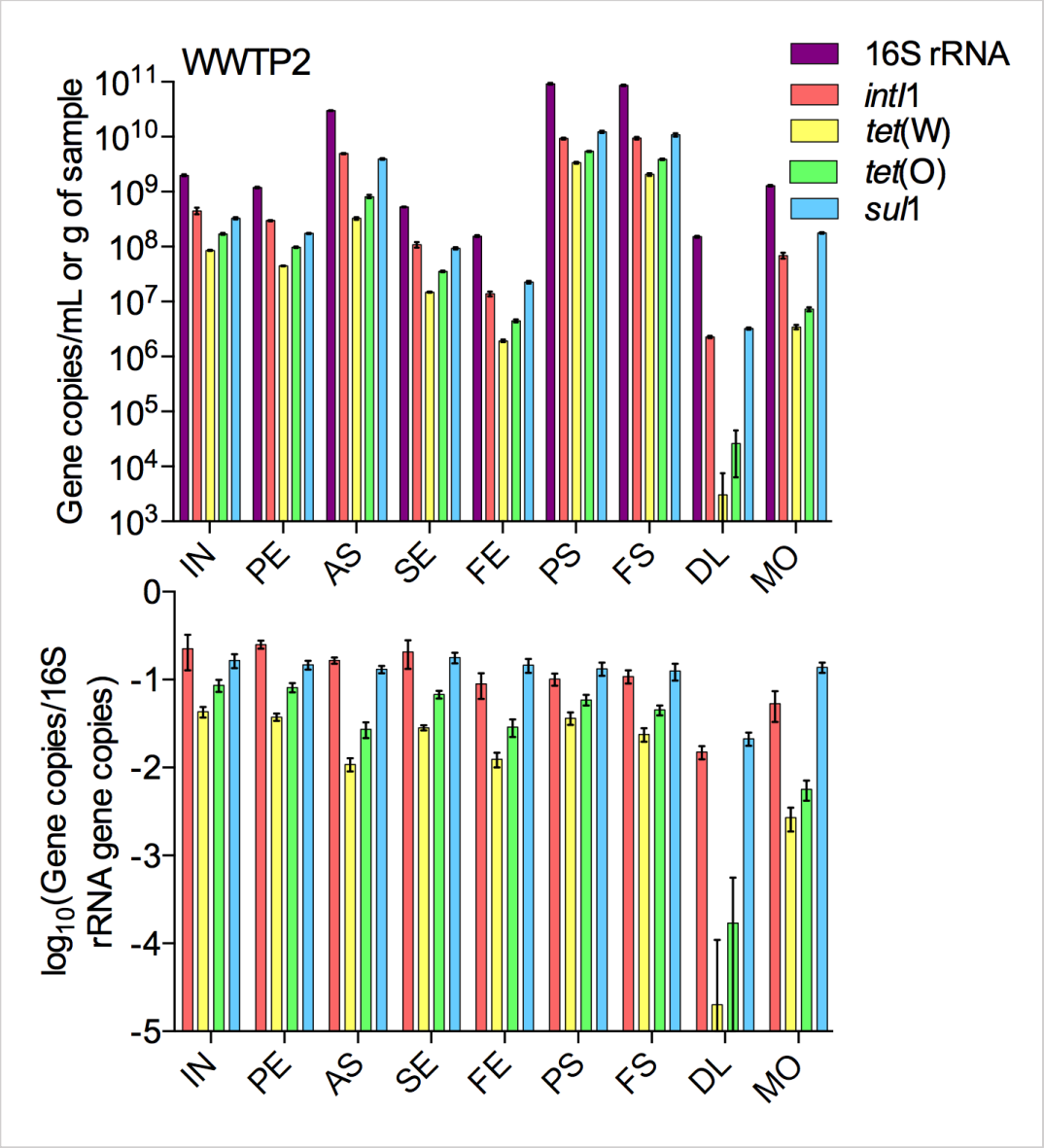

Figure 2.4. qPCR-quantified gene concentrations in samples obtained from WWTP2. Absolute gene concentrations per copy numbers (top), and 16S rRNA gene normalized gene proportions (bottom). Error bars include analytical and experimental replicates, accounting for error propagation of standard deviations. IN (Influent), PE (Primary effluent), AS (Activated sludge), SE (Secondary effluent), FE (Final effluent), PS (Primary solids), FS (Final solids), DL (Dump land leachate), MO (Marshland outfall).

In addition to characterizing ARG concentrations within the WWTP and effluent-receiving environments, we also compared the effect of DNA extraction directly from freshly processed samples (in India), versus extracting DNA from ethanol-fixed samples shipped

to the United States. The DNA extraction was carried out by the same person in both places in order to minimize person-to-person bias; however, many other factors independent from the DNA extraction process (e.g., sample fixation, shipping and extended storage) could also influence the results. Triplicate samples from three locations of WWTP1 were selected for this comparison: Influent (IN), activated sludge (AS) and secondary effluent (SE). The results, shown in Figure 2.5, indicate that there were minor differences in DNA extract yields, and suggest that sample stability is minimally compromised by fixation, shipping and storage.

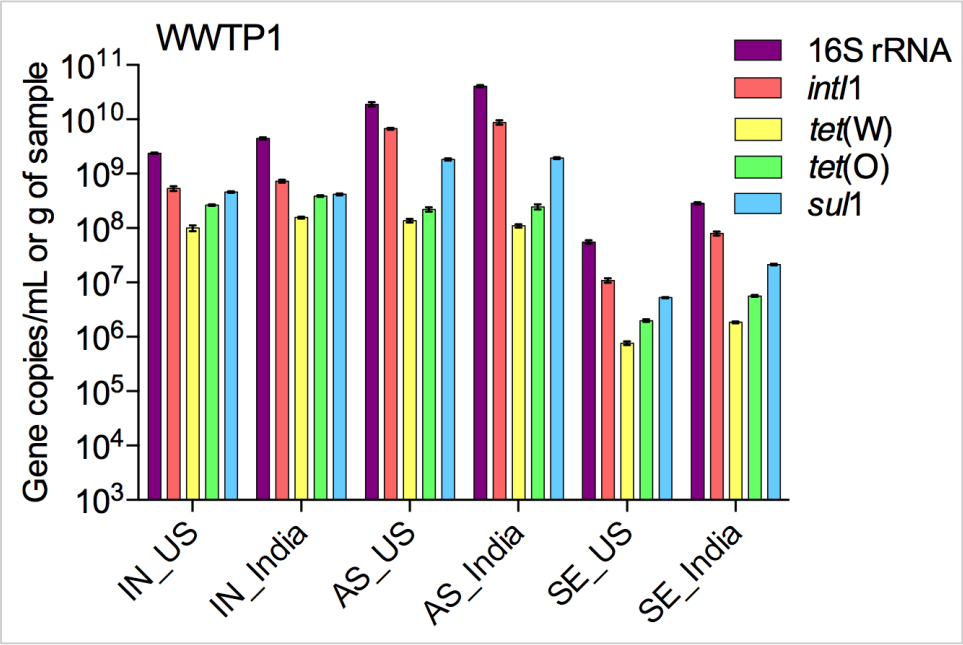

Figure 2.5. Comparison of DNA extraction from fresh samples in India Vs. fixed samples in the US. DNA extraction was performed by the same person in both places. Error bars include analytical and experimental replicates, accounting for error propagation of standard deviations. Samples: IN (Influent), AS (Activated sludge), SE (Secondary effluent), US (DNA extracted in the US from ethanol-fixed samples), India (DNA extracted from freshly collected samples in India).

CONCLUSIONS AND FUTURE WORK

The preliminary results reported here begin to reflect the distinctive antibiotic resistance distributions within a developing economy exhibiting poor sanitation infrastructure and unregulated antibiotic consumption. Little differences in absolute and relative ARG

concentrations were observed within the two WWTPs; however, it is expected that subtler differences will become resolved with the application of metagenomics analyses. Metagenomic data can provide broad and deep-resolution ARG fingerprints expected to shed light on the relative contributions of different influents (e.g., WWTP effluent versus unregulated non-point sources) on the receiving body ARG composition. In addition, scaffolding of metagenomics sequences can provide further insight about associations between ARGs and other genetic elements. Further wastewater characterization as well as seasonal sampling events are also important for discerning relationships between antibiotic resistance enrichment and selective agents such as unmetabolized antibiotics at subtherapeutic doses.

REFERENCES

1. Baquero, F.; Lanza, V. F.; Canton, R.; Coque, T. M., Public health evolutionary biology of antimicrobial resistance: Priorities for intervention. *Evolutionary Applications* **2015,** *8*, 223-239.
2. Cars, O.; Hedin, A.; Heddini, A., The global need for effective antibiotics-Moving towards concerted action. *Drug Resistance Updates* **2011,** *14*, 68-69.
3. Baquero, F.; Martinez, J. L.; Canton, R., Antibiotics and antibiotic resistance in water environments. *Curr. Opin. Biotechnol.* **2008,** *19*, 260-265.
4. Pruden, A.; Larsson, D. G. J.; Amezquita, A.; Collignon, P.; Brandt, K. K.; Graham, D. W.; Lazorchak, J. M.; Suzuki, S.; Silley, P.; Snape, J. R.; Topp, E.; Zhang, T.; Zhu, Y. G., Management options for reducing the release of antibiotics and antibiotic resistance genes to the environment. *Environ. Health Perspect.* **2013,** *121*, 878-885.
5. Pruden, A., Balancing water sustainability and public health goals in the face of growing concerns about antibiotic resistance. *Environ. Sci. Technol.* **2014,** *48*, 5-14.
6. Luo, Y.; Yang, F. X.; Mathieu, J.; Mao, D. Q.; Wang, Q.; Alvarez, P. J. J., Proliferation of multidrug-resistant New Delhi Metallo-β-lactamase genes in municipal wastewater treatment plants in northern China. *Environ. Sci. Technol. Lett.* **2014,** *1*, 26-30.
7. Mao, D. Q.; Yu, S.; Rysz, M.; Luo, Y.; Yang, F. X.; Li, F. X.; Hou, J.; Mu, Q. H.; Alvarez, P. J. J., Prevalence and proliferation of antibiotic resistance genes in two municipal wastewater treatment plants. *Water Res.* **2015,** *85*, 458-466.
8. Breazeal, M. V. R.; Novak, J. T.; Vikesland, P. J.; Pruden, A., Effect of wastewater colloids on membrane removal of antibiotic resistance genes. *Water Res.* **2013,** *47*, 130-140.
9. Munir, M.; Wong, K.; Xagoraraki, I., Release of antibiotic resistant bacteria and genes in the effluent and biosolids of five wastewater utilities in Michigan. *Water Res.* **2011,** *45*, 681-693.

10. Marathe, N. P.; Regina, V. R.; Walujkar, S. A.; Charan, S. S.; Moore, E. R. B.; Larsson, D. G. J.; Shouche, Y. S., A treatment plant receiving waste water from multiple bulk drug manufacturers is a reservoir for highly multi-drug resistant integron-bearing bacteria. *PLoS One* **2013,** *8*.
11. Larsson, D. G. J.; de Pedro, C.; Paxeus, N., Effluent from drug manufactures contains extremely high levels of pharmaceuticals. *J. Hazard. Mater.* **2007,** *148*, 751-755.
12. Kristiansson, E.; Fick, J.; Janzon, A.; Grabic, R.; Rutgersson, C.; Weijdegard, B.; Soderstrom, H.; Larsson, D. G. J., Pyrosequencing of Antibiotic-Contaminated River Sediments Reveals High Levels of Resistance and Gene Transfer Elements. *PLoS One* **2011,** *6*.
13. Van Boeckel, T. P.; Gandra, S.; Ashok, A.; Caudron, Q.; Grenfell, B. T.; Levin, S. A.; Laxminarayan, R., Global antibiotic consumption 2000 to 2010: an analysis of Cross Mark 742 national pharmaceutical sales data. *Lancet Infect. Dis.* **2014,** *14*, 742-750.
14. Laxminarayan, R.; Chaudhury, R. R., Antibiotic Resistance in India: Drivers and Opportunities for Action. *PLoS Med.* **2016,** *13*.
15. Cambray, G.; Guerout, A. M.; Mazel, D., Integrons. In *Annual Review of Genetics, Vol 44*, Campbell, A.; Lichten, M.; Schupbach, G., Eds. 2010; Vol. 44, pp 141-166.
16. Gao, P.; Munir, M.; Xagoraraki, I., Correlation of tetracycline and sulfonamide antibiotics with corresponding resistance genes and resistant bacteria in a conventional municipal wastewater treatment plant. *Sci. Total Environ.* **2012,** *421*, 173-183.
17. Czekalski, N.; Berthold, T.; Caucci, S.; Egli, A.; Burgmann, H., Increased levels of multiresistant bacteria and resistance genes after wastewater treatment and their dissemination into Lake Geneva, Switzerland. *Front. Microbiol.* **2012,** *3*.
18. Makowska, N.; Koczura, R.; Mokracka, J., Class 1 integrase, sulfonamide and tetracycline resistance genes in wastewater treatment plant and surface water. *Chemosphere* **2016,** *144*, 1665-1673.
19. Novo, A.; Andre, S.; Viana, P.; Nunes, O. C.; Manaia, C. M., Antibiotic resistance, antimicrobial residues and bacterial community composition in urban wastewater. *Water Res.* **2013,** *47*, 1875-1887.
20. Caucci, S.; Karkman, A.; Cacace, D.; Rybicki, M.; Timpel, P.; Voolaid, V.; Gurke, R.; Virta, M.; Berendonk, T. U., Seasonality of antibiotic prescriptions for outpatients and resistance genes in sewers and wastewater treatment plant outflow. *FEMS Microbiol. Ecol.* **2016,** *92*.
21. Munck, C.; Albertsen, M.; Telke, A.; Ellabaan, M.; Nielsen, P. H.; Sommer, M. O. A., Limited dissemination of the wastewater treatment plant core resistome. *Nature Communications* **2015,** *6*.
22. Zhang, T.; Zhang, X. X.; Ye, L., Plasmid metagenome reveals high levels of antibiotic resistance genes and mobile genetic elements in activated sludge. *PLoS One* **2011,** *6*.
23. Peltier, E.; Vincent, J.; Finn, C.; Graham, D. W., Zinc-induced antibiotic resistance in activated sludge bioreactors. *Water Res.* **2010,** *44*, 3829-3836.
24. Di Cesare, A.; Eckert, E. M.; D'Urso, S.; Bertoni, R.; Gillan, D. C.; Wattiez, R.; Corno, G., Co-occurrence of integrase 1, antibiotic and heavy metal resistance genes in municipal wastewater treatment plants. *Water Res.* **2016,** *94*, 208-214.

25. Li, A. D.; Li, L. G.; Zhang, T., Exploring antibiotic resistance genes and metal resistance genes in plasmid metagenomes from wastewater treatment plants. *Front. Microbiol.* **2015,** *6*.
26. Yang, Y.; Li, B.; Ju, F.; Zhang, T., Exploring Variation of Antibiotic Resistance Genes in Activated Sludge over a Four-Year Period through a Metagenomic Approach. *Environ. Sci. Technol.* **2013,** *47*, 10197-10205.

CHAPTER 3. Aptamer-functionalized gold nanoparticles for the rapid detection of *Staphylococcus aureus*

Maria V. Riquelme, Weinan Leng, Matthew S. Hull, Chad W. McKinney, Amy Pruden, and Peter J. Vikesland

ABSTRACT

Staphylococcus aureus is one of the leading causes of a wide range of opportunistic infections in humans. Because of its increased resistance to multiple antibiotics and frequent detection in environmental matrices such as wastewater, *S. aureus* is considered an emerging environmental pathogen of concern. Herein we describe a method for the rapid detection of *S. aureus* that couples highly specific aptamer-functionalized gold nanoparticles (Apt-AuNPs) with sensitive surface enhanced resonance Raman spectroscopy (SERRS). Stable Apt-AuNPs include a Raman reporter that enables rapid and sensitive SERRS detection, a *S. aureus*-specific aptamer, and a PEG linker and monolayer that acts as an Au-aptamer spacer as well as a colloid stabilizer. Our Apt-AuNP prototype facilitates detection of *S. aureus* while remaining stable for an extended period of time. Although optimization is necessary for reproducible results, the technology reported here represents a novel and more sustainable alternative to existing pathogen detection methods that require additional time and preparation.

INTRODUCTION

Staphylococcus aureus is the causative agent of a growing number of disease outbreaks within the United States and worldwide.[1-3] Although transmission of this organism has historically been associated with hospitals, recent environmental outbreaks of methicillin resistant *S. aureus* (MRSA) as well as its detection in wastewater effluent have inaugurated MRSA as an emerging environmental pathogen of concern.[1, 2, 4] Unfortunately, the established methods for *S. aureus* monitoring are generally slow and rely on laborious and lengthy cell culture techniques that are not conducive to rapid detection. Furthermore, PCR-based methods can be lengthy and inaccurate because they rely on the extraction and purification of intracellular DNA, are enzyme-dependent,

and do not yield whole cell numbers. Clearly, there is a need for improved techniques to rapidly detect the presence of whole and potentially infectious *S. aureus* cells.

Gold nanoparticle-based assays for the optical detection and quantification of intact pathogenic organisms in biological and environmental matrices have recently elicited interest due to their capacity to detect single cells.[5-7] In these assays, biosensor specificity is realized through the use of recognition elements such as antibodies or aptamers that detect antigens or other epitopes on the pathogen surface. Biosensor sensitivity is then achieved via surface plasmon-enhanced optical signals that develop in response to the interaction between the pathogen and the recognition element. Aptamers, engineered single-stranded nucleic acid sequences (2-25 kDa, 30-80 nt) with high affinity and specificity towards target species, are one antibody alternative that has elicited great interest due to their increased stability under a range of non-physiological conditions, ease of isolation, ease and reproducibility of synthesis and functionalization, and low toxicity and immunogenicity, among others.[8-12] Given the rapidly expanding list of pathogen-specific aptamers,[9, 13-21] it is now feasible to produce biosensor assays that utilize aptamers for pathogen detection.

The Apt-AuNP probe produced in this study consists of a gold nanoparticle core that is covalently functionalized with a SERRS active reporter molecule and aptamers specific to *S. aureus* (Figure 3.1). The highly specific interaction between SERRS active Apt-AuNPs and *S. aureus* enhances the SERRS signal intensity such that single *S. aureus* cells are quickly and easily detected, while unbound Apt-AuNPs are not detected due to their lower signal intensity. XY Raman imaging enables rapid quantification of the *S. aureus* concentration. Our results suggest that this type of detection strategy can be multiplexed to enable simultaneous quantitative detection of numerous pathogens in environmentally-relevant matrices.

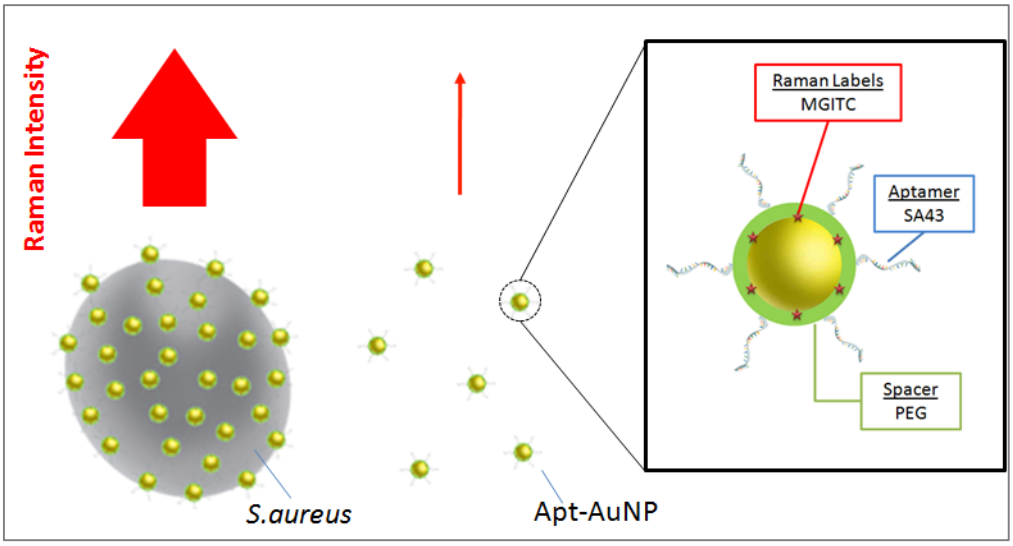

Figure 3.1. Representation of Apt-AuNPs and mechanism of detection. Left: Laser excitation produces different Raman signal intensities for Apt-AuNPs agglomerated on a S. aureus cell versus discrete individual Apt-AuNPs. Right: Structure of Apt-AuNP probe.

MATERIALS AND METHODS

Materials. Chloroauric acid ($HAuCl_4 \cdot 3H_2O$), sodium citrate dehydrate (99+%), N-hydroxysulfosuccinimide (Sulfo-NHS), and ethyl dimethylaminopropyl carbodiimide (EDC) were purchased from Sigma-Aldrich (St. Louis, MO) and were used without further purification. Malachite green isothiocyanate (MGITC) and the amine-functionalized aptamer SA43 (5'- GCAATGGTACGGTACTTCC-TCGGCACGTTCTCAGTAGCGCTCGCTGGTCATCCCACAGCTACGT-CAAAAGTGCACGCTACTTTGCTAA-$(CH_2)_6$-NH_2-3') were acquired from Invitrogen Corp. (Grand Island, NY). Ethanol (99+%) and phosphate-buffered saline (PBS, pH 7.4) were obtained from Fisher Scientific (Pittsburgh, PA). PBS (137 mM NaCl, 2.7 mM KCl, 10 mM Na_2HPO_4, 1.76 mM KH_2PO_4, pH 7.4) was prepared and autoclaved for use in culture washing and aptamer assays. Nanopure water (>18 MΩ·cm) was used to produce all aqueous solutions.

Apt-AuNP synthesis. Spherical gold nanoparticles (AuNPs) at a concentration of ~5 × 10^{10} NPs/mL were prepared by seed-mediated growth.[22, 23] These citrate-capped particles were characterized using a JEOL 100 CX-II transmission electron microscope (TEM) and an Agilent Cary 5000 UV-Vis-NIR spectrometer. Average particle diameters were determined based upon the location of the localized surface plasmon band in the

UV-Vis spectrum[24] and via ImageJ (http://rsbweb.nih.gov/ij/) analysis of the collected TEM images (Figure 3.2A). These two measures of nanoparticle diameter qualitatively agree with one another. Previously described ssDNA aptamer SA43 specific to *S. aureus* was used to functionalize the gold nanoparticle surface. The synthesis of Apt-AuNPs was performed as described by Qian et al.[25] It consisted of three general steps:

(A) *Attachment of Raman active dyes*: A freshly prepared MGITC ($\varepsilon=1\times10^5 M^{-1}cm^{-1}$) solution was added dropwise to the gold nanoparticle suspension under rapid mixing. A 1:6 MGITC:AuNP volume ratio was used to facilitate even distributions of the reporter molecules, while a 300:1 molar ratio was applied in order to maximize SERS intensities and minimize colloid aggregation [25]. Nanoparticle stability was checked via UV-Vis spectroscopy and dynamic light scattering (DLS).

(B) *PEGylated Apt-AuNP preparation*: PEGylated Apt-AuNPs (Apt-PEG-AuNPs) were prepared following a process described by Qian et al.[25] 10 μM HS-PEG (NANOCS), and 1 μM HS-PEG-COOH (NANOCS) were first prepared. The heterofunctional thiolated and carboxylated PEG linker (HS-PEG-COOH) was added at a ratio of 3,000 molecules per AuNP to the previously Raman dye-labeled 46 nm AuNPs under rapid mixing. Additional mixing for 15 minutes was done to ensure even distribution of the molecule over the nanoparticle surface. The gold nanoparticles were subsequently exposed to excess thiolated PEG in order to saturate the nanoparticle surface, and mixed for 15 min. Assuming that each thiolated-PEG molecule occupies ≈0.35 nm^2 of nanoparticle surface, [26] there should be ≈16,000 HS-PEG molecules conjugated to each AuNP. The solution was then adjusted to contain a final 1X PBS concentration and was shaken overnight to allow complete coverage and stabilization of the molecules on the nanoparticle surface.

(C) *Aptamer functionalization*: After five rounds of cleaning by centrifugation at 10,000 × g for 10 min and resuspension in 1X PBS and 0.01% Tween 20, the nanoparticle numbers were checked by UV-Vis spectroscopy ($\varepsilon=1.2\times10^{10}\ M^{-1}cm^{-1}$). The carboxyl terminus of the PEG linker on ~10^{10} AuNPs was activated for covalent reaction with aminated aptamer by adding 50 μl of 4mg/ml ethyl dimethylaminopropyl carbodiimide (EDC, Fluka) and 55 μl of 10 mg/ml sulfo-NHS (Sigma-Aldrich) and mixing vigorously. The activated PEGylated AuNPs was then functionalized by allowing amide bond formation with excess (~12 nmol) aminated aptamer SA43, shaken for 2 h at room temperature and incubated

in the dark at 4°C overnight to ensure complete coverage. Excess reagents were removed through 5 rounds of centrifugation at 10,000 × g for 10 min and resuspension in 1X PBS, containing 0.01% Tween 20 (Sigma-Aldrich). Prepared and stabilized Apt-PEG-AuNPs were stored at 4°C.

Cell culturing and quantification. *S. aureus* (ATCC 12600), *Staphylococcus epidermidis* (ATCC 14990), and *Enterococcus faecium* (ATCC 19434) were cultured in brain heart infusion agar or broth. *Pseudomonas aeruginosa* PAO1 (ATCC 47085) and *Escherichia coli* K5808 (ATCC 53832) were cultured in trypticase soy agar or broth. All controls were cultured in 100 mL of their respective broth medium at 37 °C and 165 rpm to the exponential growth phase (OD600 ~0.5), and then washed via three rounds of centrifugation and resuspension in 1× PBS. Cell quantification was done microscopically using a hemocytometer, and was verified by colony forming unit (CFU) counting. For qualitative analysis, MRSA (ATCC BAA-1556) was cultured at 37 °C in brain heart infusion (BHI) broth. BL21(DE3) *E. coli* (Bio-Rad Laboratories, Inc.) was grown in TB/Amp medium at 37 °C. Individual suspensions with ~2 × 10^7 *S. aureus*/mL and ~1 × 10^8 *E. coli*/mL were stored at -40 °C prior to use.

Aptamer affinity measurement. The affinity of the Sa43 aptamer toward *S. aureus* was validated via an affinity measurement where a series of aptamer concentrations ranging from 0.5 to 1000 nM were incubated with a fixed number of *S. aureus* cells (1x10^8). Prior to incubation with the bacteria, the aptamers were refolded by denaturing at 95 ^oC for 5 min and immediately transferring to ice. The aptamer-bacteria mixture was incubated for 1 hr at room temperature in order to allow sufficient interaction time. After this, the unbound or loosely bound aptamer was washed away via three rounds of centrifugation (5,000 ×g for 10 min) and resuspension in PBS. Following this process, the bound aptamer was eluted by heating the cell-aptamer complexes to 95 ^oC for 10 min, and immediately centrifuging at 13,100 ×g for 5 min. The aptamer-containing supernatant was diluted to 1:10, and quantified via qPCR using the primers described by Cao et al.[17] qPCR was carried out in triplicate 10-µL reactions containing 400 nM of each primer, 1× SsoFast™ Eva Green® Supermix (Bio-Rad), and 1 µL of 1:10 diluted aptamer. The temperature cycling program consisted of an initial 2-min enzyme activation step at 98 ^oC, and 50 cycles of denaturing at 98 ^oC for 5 s and annealing/extension at 65 ^oC for 5 s.

The best-fit values for Kd and Bmax were calculated via GraphPad Prism (Version 6.0a for Mac) software, by fitting the formula $Y = B_{max}*X / (K_d + X)$ to the measured qPCR data.

Sample Preparation. Excess Apt-AuNPs (~2.5×10^9 Apt-AuNPs) were added to 100 µL each of 10^7, 10^6, and 10^5 *S. aureus* and *S. epidermidis* cells/ml; 100 µL of 10^6 *E. coli, P. aeruginosa,* and *E. faecium* cells; or 100 µL of 1× PBS in the absence of bacteria (background control). All tubes were mixed horizontally at 300 rpm and 37 °C for 45 minutes and concentrated by centrifugation at 5,000 ×g for 10 min before discarding all but 40 µL of the supernatant. The pellet was then resuspended in the remaining supernatant plus 60 µL glycerol in order to increase the viscosity of the sample. After thoroughly mixing, 3 µL of the contents from each tube were transferred to one of the wells of a microscope slide containing 2 etched 13 mm circles (Electron Microscopy Sciences). A 22 mm No. 1 cover glass (Fisher Scientific) was placed on each sample, and the edges of the slide were sealed using clear nail polish.

Additional qualitative comparisons between optical and Raman images were made with the purpose of verifying the specificity of the Apt-AuNPs. For this, 10-µL drops containing ~20,000 *S. aureus* (ATCC BAA-1556) or *E. coli* BL21(DE3) cells were dropped onto SuperStick microscope slide wells (Waterborne Inc.). The solution on each well was allowed to dry before washing excess unbound Apt-AuNPs with PBS, covering with a cover slip, and sealing with clear nail polish. Optical and Raman images were obtained within the same location of each sample in order to compare the position of the cells relative to the Raman signal.

Raman Measurements. Confocal Raman microscopy was performed using a WITec Alpha 500R (Ulm, Germany) at room temperature. Samples were mounted on a piezoelectric scanning stage. An edge filter placed in the path of the signal effectively cuts off the excitation radiation. The signal was dispersed using a 300-groove/mm grating and collected by a Peltier cooled charge coupled device (CCD). A 785-nm TOPTICA diode laser associated with a Nikon Fluor (100×, NA=1.25) oil immersion objective was used to collect Raman spectra from the samples fixed between a coverslip and a SuperStick microscope slide. A 2-D array of Raman spectra was recorded using 0.5-µm steps and 100-ms integration time. A 10× Olympus objective (NA=0.3) with laser excitation at 633 nm was used to rapidly monitor Raman signals from sandwiched

samples between a coverslip and a Teflon-printed 2-well glass slide. Large area image scans from 1-25 mm^2 were collected using 0.667-μm steps and 10-ms acquisition times. Raman images were generated by integrating the characteristic MGITC Raman peak at 1172 cm^{-1} from the region of 1075 cm^{-1} to 1250 cm^{-1} and rendering the integrated intensity as brightness at each pixel location.

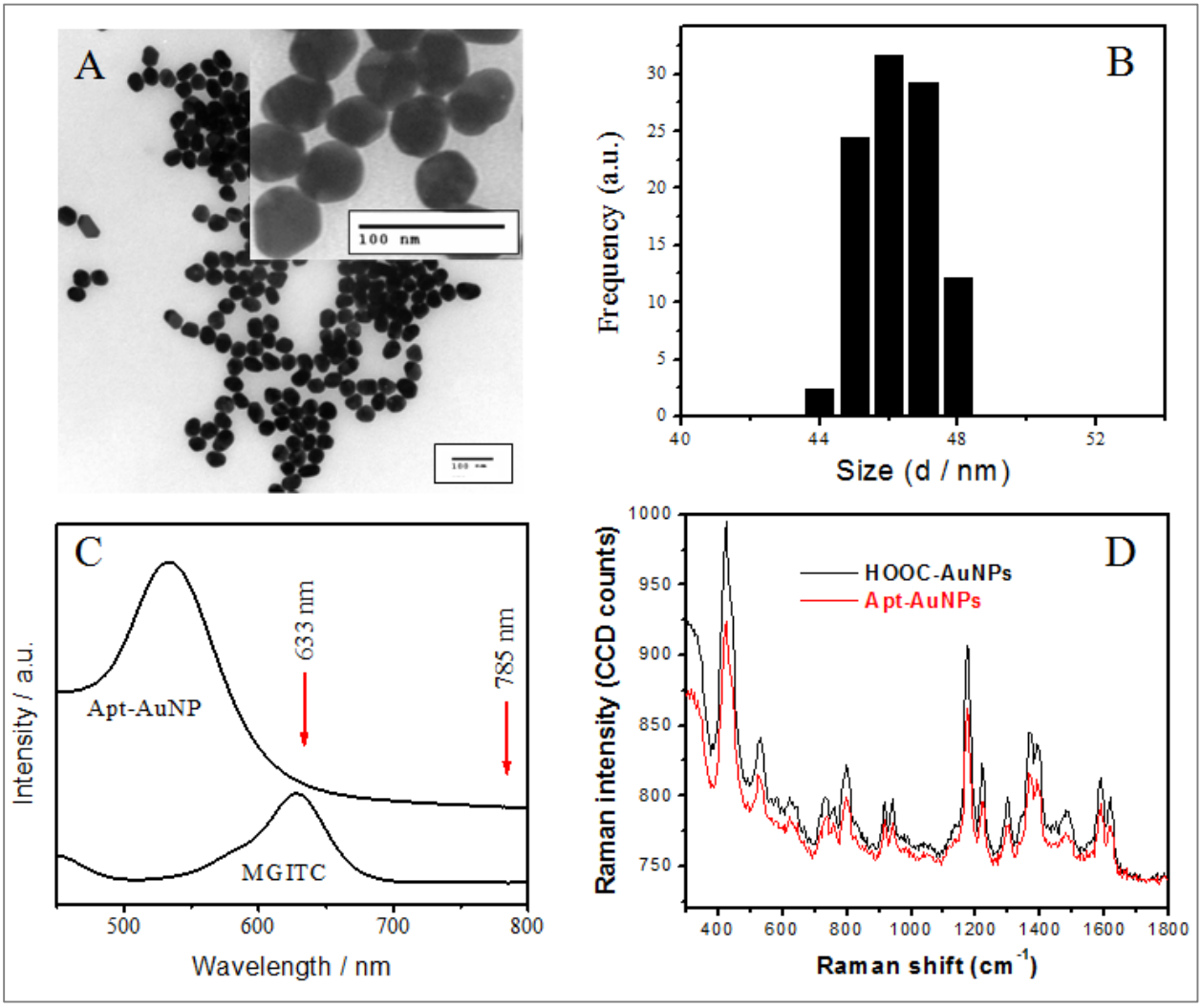

Figure 3.2. AuNP and Apt-AuNP characterization. A) TEM image and B) size distribution of synthesized AuNP with an average diameter of 46.0 nm. Insert: size distribution derived from TEM measurement. C) Absorption spectra of MGITC and Apt-AuNP solutions. The excitation wavelengths used in this paper are indicated. D) Single Raman spectra of particles of HOOC-AuNP and Apt-AuNP under 785 nm excitation and 20 s accumulation time.

RESULTS AND DISCUSSION

Apt-AuNP Design and Stability. Using a subtractive complex target SELEX process, Cao and colleagues isolated and reported sequences and secondary structures for five different ssDNA aptamers specific to *S. aureus.*[17] Each of the isolated aptamers exhibited similar selectivity and through the use of a competition assay it was determined that each aptamer binds to a particular epitope expressed on the *S. aureus* cell surface. Importantly, the aptamers either when used alone or when used collectively were highly specific and did not adhere to *S. epidermidis*, *Streptococcus,* or *E. coli.*[17] For this effort, we chose to use the aptamer SA43 isolated and described by Cao *et al.,*[17] because this aptamer qualitatively appeared to be slightly more sensitive (with the highest EC50 value) than the other aptamers. The high affinity of this aptamer toward *S. aureus* (Kd ~156 nM) was verified via a binding assay (Figure 3.3).

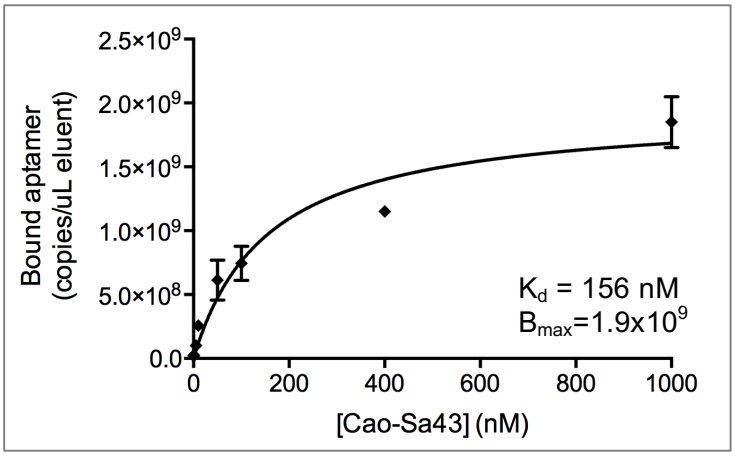

Figure 3.3. Sa43 aptamer affinity for *S. aureus* cells. A range of aptamer concentrations (0.5 to 1000 nM) was incubated with $1x10^8$ *S. aureus* cells. The bound aptamers were eluted and quantified via qPCR. The best-fit values for Kd and Bmax were calculated via GraphPad Prism (Version 6.0a for Mac) software, by fitting the formula $Y = B_{max}*X / (K_d + X)$ to the measured qPCR data. Error bars represent standard deviation of analytical replicates.

The size of a gold nanoparticle affects the spectral location of its localized surface plasmon band resonance (LSPR) with larger nanoparticles exhibiting a red-shifted LSPR relative to smaller nanoparticles.[27, 28] To optimize SERRS it is important that the LSPR

band falls within the optical range such that the band has some overlap with the excitation laser wavelength. Previous studies by our laboratory and others[29-31] have shown that gold nanoparticles with average diameters <50 nm are more spherical in shape and elicit more highly reproducible SERRS enhancements than larger particles. For this reason, our Apt-AuNP probe for *S. aureus* was produced by functionalizing 46-nm citrate-stabilized AuNPs with a MGITC Raman-active reporter. Both the absorption band of MGITC and the LSPR band of Apt-AuNP show sufficient overlap with 633-nm laser excitation to facilitate SERRS detection (Figure 3.2B). When using 785-nm laser excitation there is less resonance enhancement, but the potential for laser induced sample damage is decreased. As documented herein, it is possible to use either 633- or 785-nm excitation for *S. aureus* detection. Figure 3.2C shows that the SERS spectra for Apt-AuNP and HOOC-AuNP using 785-nm excitation are identical, thus indicating that the presence of the aptamer does not alter the SERRS signal.

In order to increase their stability, the Apt-AuNPs were coated with a polyethylene glycol (PEG) layer that was then further functionalized with the SA43 aptamer. As documented in Figure 3.4, Apt-AuNPs produced for this effort are stable for extended periods of time and in a variety of different solution media. Each of these characteristics facilitates the long-term storage and use of these functionalized nanomaterials.

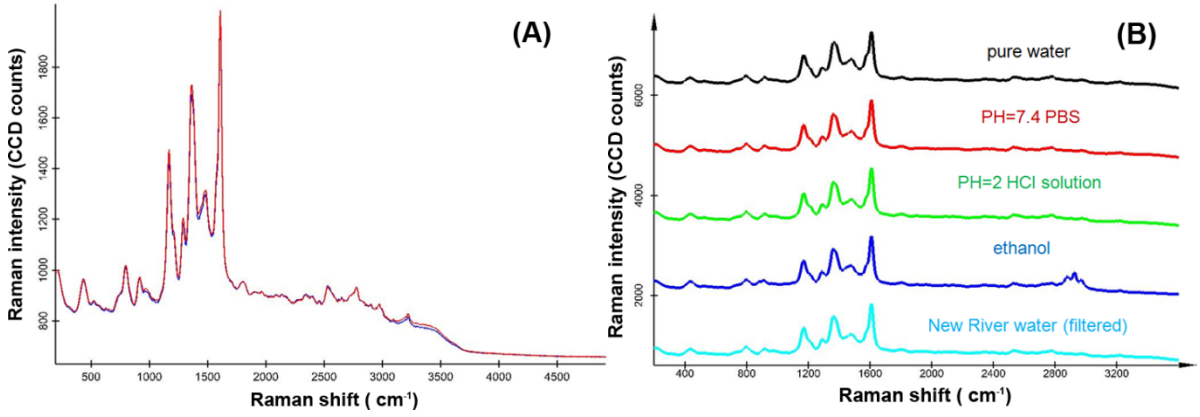

Figure 3.4. SERS reproducibility and stability of synthesized Apt-AuNPs. Raman spectra were collected in a 2 mm flow cell for (A) fresh prepared solution (blue line) and stock solution after 1 month (red line), (B) Apt-AuNPs suspended in different solvents exhibit consistent spectra. Experimental parameters: 633 nm laser, 10× objective, 10 s acquisition times and laser power at samples was normalized by Si Raman intensity at 520 cm^{-1}.

Apt-AuNP Specificity and *S. aureus* detection. Following purification and characterization, an excess of prepared Apt-AuNP was incubated with *S. aureus* and negative controls in PBS solution at 37 °C to enable aptamer-cell interaction. Excess unbound Apt-AuNPs were not removed. As shown in Figure 3.5A, a SERRS XY-image based upon the integrated intensity of the MGITC Raman band at 1172 cm^{-1} correlates exceptionally well with a light microscopy image obtained simultaneously. This result shows that the aptamer-functionalized particles adhere to *S. aureus* and provide a readily detectable and quantifiable signal over a 25 $\mu m \times 25$ μm area with minimal sample preparation and analysis. Control experiments using probes produced without the aptamer biorecognition agent (HOOC-AuNPs) did not adhere to *S. aureus* and in these control samples no MGITC signal was detected under the same experimental conditions (Figure 3.5B). Importantly, in experiments using *E. coli* as a negative control, no SERRS signal from Apt-AuNP was detected in the vicinity of the *E. coli* cells (Figure 3.5C). The latter result indicates the specificity of the particles is sufficient to readily differentiate these two bacterial species. As shown in Figure 3.5C; however, there is a background signal that resulted due to the agglomeration of Apt-AuNP. This background signal reflects Apt-AuNP that clustered during production and is negligible relative to the signal observed when bound to *S. aureus*.

The average Raman enhancement factors are around $10^2 - 10^3$ for individual gold nanoparticles[27] and thus the SERRS signals of MGITC are not detectable for non-aggregated Apt-AuNPs (i.e., the areas without a signal in Figures 3.5A and 1C) or isolated HOOC-AuNPs (Figure 3.5B) incubated with either *S. aureus* or *E. coli*. Only when sufficient numbers of Apt-AuNP agglomerate on an individual *S. aureus* cell is a substantial signal observable (Figure 3.5A). It is well established that SERRS “hotspots” with large signal enhancements occur when individual gold nanoparticles come into close contact with one another.[32] As shown in Figure 3.5, the high surface density of Apt-AuNP on each *S. aureus* cell results in such signal amplification.

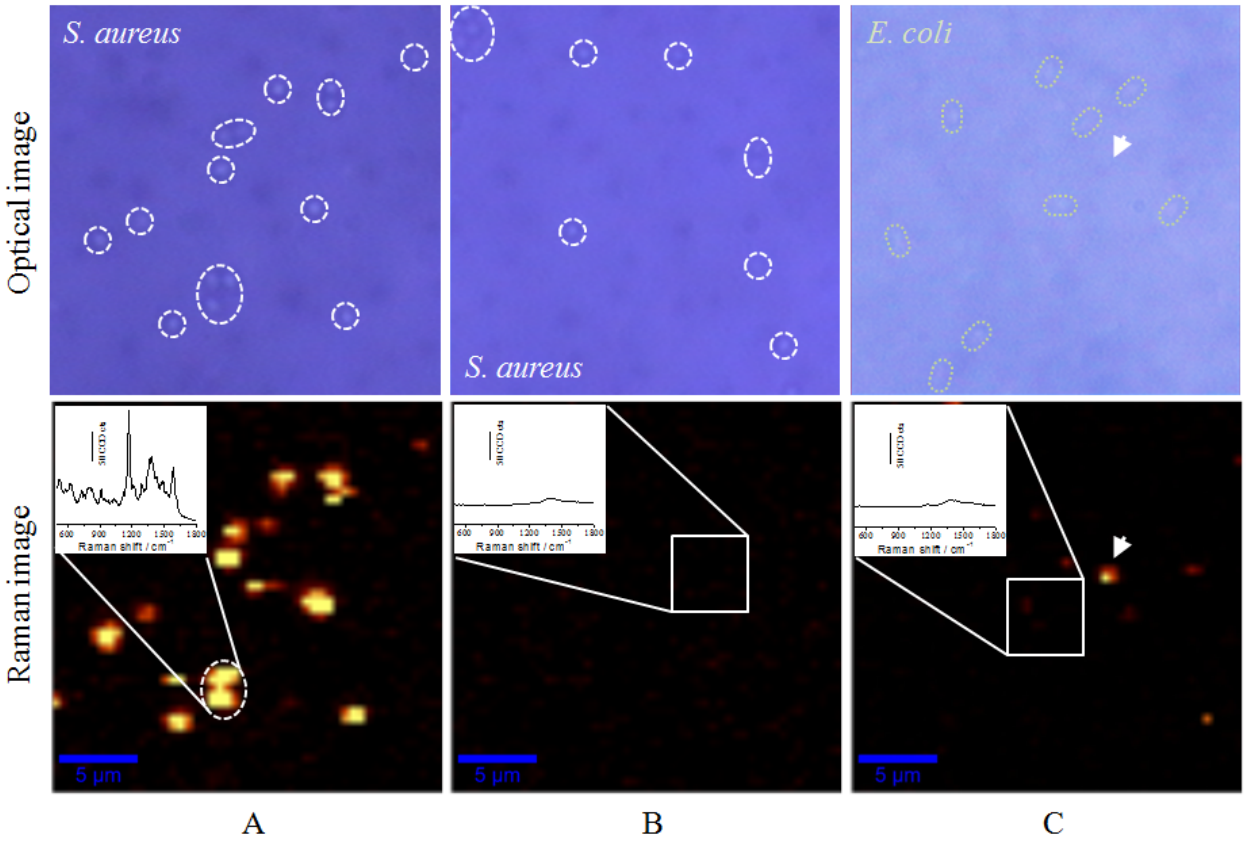

Figure 3.5. Optical and Raman images of bacterial detection. Light microscope images (top) and Raman images with inset indicating the average Raman spectra within the selected area (bottom) of *S. aureus treated with either (A) Apt-AuNPs or (B) HOOC-AuNPs. (C) E. coli treated with Apt-AuNPs. All samples* were prepared using a SuperStick microscope slide. The optical images indicate the location of organisms focused within the depth of field of the microscope. Additional 'shadow' organisms were either above or below the depth of field and were not detected via SERRS. The Raman images are based on the integrated intensity of the MGITC spectrum from 1075 to 1250 cm^{-1} using a consistent intensity scale from 0-850 CCD counts. Total scan range: 25 μm × 25 μm, 50 × 50 pixels, 2500 spectra with 0.1 s per spectrum; 785 nm diode laser with 100× oil immersion objective. The negative bright spot in the Raman image of C is the result of clustering of Apt-AuNPs. Its location is also marked in the optical image and clearly shows there are no *E. coli* cells present in that region.

***S. aureus* quantification.** Additional results suggest that Apt-AuNP enable the simple and standard-free SERRS-based estimation of *S. aureus* cell numbers (Figures 3.6 and 2.7). Samples for this purpose were prepared by suspending nanoparticle-treated bacteria in 60% glycerol/40% PBS solution. This solution was then sandwiched in a

PTFE-printed 2-well microscope slide and covered with a coverslip. When the 3-μL sample chamber was completely filled, the thickness of the liquid layer was 22 μm, which is less than the focal depth of 50 μm for the 633-nm laser and the 10× objective (NA=0.25) employed. Figure 3.6 summarizes the Raman based quantification of 3,000 cell- and 300 cell-containing samples as well as controls. The 46-nm AuNP used in this assay exhibit a LSPR band ($\lambda_{max} \approx 533$ nm) that is extremely sensitive to 633-nm excitation. Because of the enhanced resonance effect from MGITC, a scan of a 5 mm × 5 mm area can be performed within 2 hours. Using a step size of 0.67 μm, all SERRS signals can be detected in the scan area. Hotspots indicative of cells were counted using NIH ImageJ software and the total number of cells was calculated based upon extrapolation from the scan area to the entire surface area of the well. Compared to the expected cell numbers, scanning of a larger area results in decreased error relative to smaller scan areas. Error in the measurements may be the result of cell clumping and overlap and/or of variability in nanoparticle-cell interactions.

Herein we presented replicated experiments illustrating the viability of aptamer based nanoparticle probes for *S. aureus* detection. We note, however, that there are often challenges associated with aptamer functionalization of the nanoparticle surface. Numerous times throughout the course of this study we produced probes that lacked specificity or extensively aggregated in the absence of the target. These challenges may reflect improper aptamer production by the manufacturer, issues with oligonucleotide stability during storage, improper surface functionalization, water chemistry effects, or any combination of these and other challenges. Our assay requires AuNP agglomeration on the *S. aureus* surface for the development of SERS hotspots and the production of a quantifiable signal,[33, 34] thus stable monomeric nanosensors that bind on the cell surface at high densities are required. We are currently evaluating possible ways to overcome these limitations. The results, nonetheless, illustrate the great potential of aptamers for biological detection.

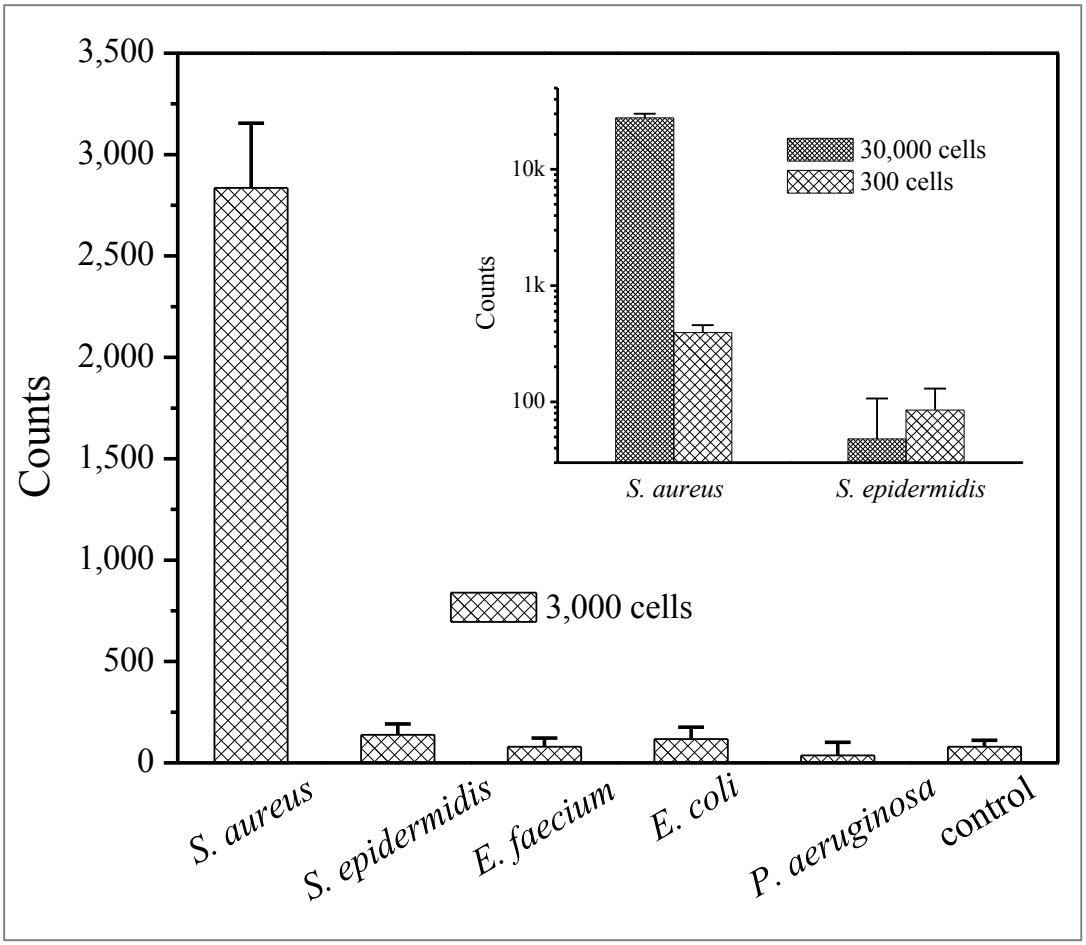

Figure 3.6. SERRS determined counts of *S. aureus*, and comparison with negative controls, in samples containing 3,000 cells (inset: 30,000 and 300 cells/sample). A solution of Apt-NPs in 60/40% glycerol/PBS in the absence of cells, but treated in the same way was used as a control. Raman images were recorded in large area scans up to 25 mm^2 under 633 nm excitation using a 10× objective. 0.01 s of integration time was used for each single Raman spectrum. The data are reported as mean ± standard deviation for three randomly chosen locations in the scan area with 1 mm^2.

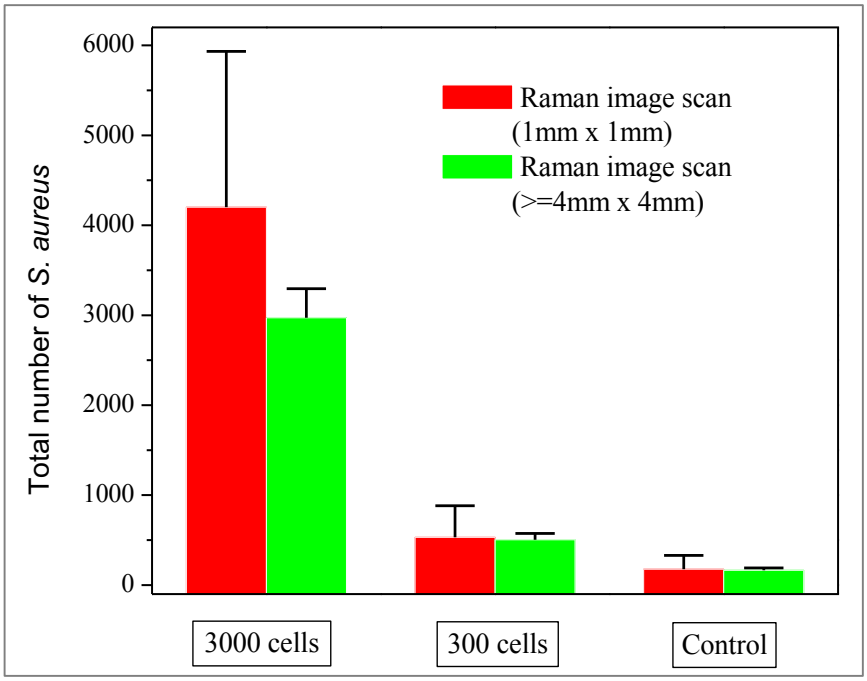

Figure 3.7. SERRS determined numbers of *S. aureus* in samples containing either 3,000 cells or 300 cells (based upon qPCR and serial dilution of stock suspensions). A solution of Apt-NPs in 60/40% glycerol/PBS was used as a control. Raman images were recorded in three different locations under 633 nm excitation using a 10× objective. 0.01 s of integration time was used for each single Raman spectrum. The data are reported as mean ± standard deviation.

CONCLUSIONS

The technology presented here represents a novel alternative to existing pathogen detection methods that require additional time and preparation. For example, PCR-based technologies have been preferred due to their high specificity, high sensitivity, and rapid application. However, a variety of steps including DNA extraction, standard preparation, and reaction setup, render PCR a more labor intensive method, especially when applied to multiple targets simultaneously. Here we present a technology that promises minimal preparation and sample disturbance, while providing comparable specificity and sensitivity under optimal conditions, as well as the potential for portability. Furthermore, the potential for multiplex detection of a variety of pathogens of concern is possible with minimal sample preparation. Although we have initially focused on the detection of *S. aureus*, the rapidly growing number of aptamers being reported in the literature for the

detection of whole cells, as well as the evolving ease of aptamer isolation, highlight the potential for the detection of a number of pathogens of great environmental, food safety, and medical concern. Thus, we envision this technology evolving in simplicity of use as well as expanding in fields of application. Additional experiments to validate these probes under a variety of experimental conditions are required to fully determine their ultimate range of application; however, as demonstrated herein, aptamer-based probes for pathogenic organisms are viable alternatives to antibody-based sensors.

ACKNOWLEDGMENTS

This work was supported by grants from the Virginia Tech Institute of Critical Technology and Applied Science and NSF Awards CBET-0547342 & CBET-1133746. We thank Dr. Hezhong Wang for providing the *E. coli* BL21(DE3) cells.

REFERENCES

1. Klevens, R. M.; Morrison, M. A.; Nadle, J.; Petit, S.; Gershman, K.; Ray, S.; Harrison, L. H.; Lynfield, R.; Dumyati, G.; Townes, J. M.; Craig, A. S.; Zell, E. R.; Fosheim, G. E.; McDougal, L. K.; Carey, R. B.; Fridkin, S. K.; Investigators, A. B. M., Invasive methicillin-resistant *Staphylococcus aureus* infections in the United States. *Jama-Journal of the American Medical Association* **2007,** *298*, 1763-1771.
2. Grundmann, H.; Aires-De-Sousa, M.; Boyce, J.; Tiemersma, E., Emergence and resurgence of meticillin-resistant *Staphylococcus aureus* as a public-health threat. *Lancet* **2006,** *368*, 874-885.
3. DeLeo, F. R.; Chambers, H. F., Reemergence of antibiotic-resistant *Staphylococcus aureus* in the genomics era. *J. Clin. Invest.* **2009,** *119*, 2464-2474.
4. Borjesson, S.; Matussek, A.; Melin, S.; Lofgren, S.; Lindgren, P. E., Methicillin-resistant *Staphylococcus aureus* (MRSA) in municipal wastewater: An uncharted threat? *J. Appl. Microbiol.* **2010,** *108*, 1244-1251.
5. Ravindranath, S. P.; Wang, Y. L.; Irudayaraj, J., SERS driven cross-platform based multiplex pathogen detection. *Sensor Actuat. B-Chem.* **2011,** *152*, 183-190.
6. Vikesland, P. J.; Wigginton, K. R., Nanomaterial enabled biosensors for pathogen monitoring - A review. *Environ. Sci. Technol.* **2010,** *44*, 3656-3669.
7. Wigginton, K. R.; Vikesland, P. J., Gold-coated polycarbonate membrane filter for pathogen concentration and SERS-based detection. *Analyst* **2010,** *135*, 1320-1326.
8. James, W., Aptamers in the virologists' toolkit. *J. Gen. Virol.* **2007,** *88*, 351-364.
9. So, H. M.; Park, D. W.; Jeon, E. K.; Kim, Y. H.; Kim, B. S.; Lee, C. K.; Choi, S. Y.; Kim, S. C.; Chang, H.; Lee, J. O., Detection and titer estimation of *Escherichia coli* using aptamer-functionalized single-walled carbon-nanotube field-effect transistors. *Small* **2008,** *4*, 197-201.

10. Tombelli, S.; Minunni, M.; Mascini, M., Aptamers-based assays for diagnostics, environmental and food analysis. *Biomol. Eng.* **2007,** *24*, 191-200.
11. Cerchia, L.; Hamm, J.; Libri, D.; Tavitian, B.; de Franciscis, V., Nucleic acid aptamers in cancer medicine. *FEBS Lett.* **2002,** *528*, 12-16.
12. Medley, C. D.; Bamrungsap, S.; Tan, W. H.; Smith, J. E., Aptamer-conjugated nanoparticles for cancer cell detection. *Anal. Chem.* **2011,** *83*, 727-734.
13. Bruno, J. G.; Kiel, J. L., In vitro selection of DNA aptamers to anthrax spores with electrochemiluminescence detection. *Biosens. Bioelectron.* **1999,** *14*, 457-464.
14. Ikanovic, M.; Rudzinski, W. E.; Bruno, J. G.; Allman, A.; Carrillo, M. P.; Dwarakanath, S.; Bhahdigadi, S.; Rao, P.; Kiel, J. L.; Andrews, C. J., Fluorescence assay based on aptamer-quantum dot binding to *Bacillus thuringiensis* spores. *Journal of Fluorescence* **2007,** *17*, 193-199.
15. Chen, F.; Zhou, J.; Luo, F. L.; Mohammed, A. B.; Zhang, X. L., Aptamer from whole-bacterium SELEX as new therapeutic reagent against virulent Mycobacterium tuberculosis. *Biochem. Biophys. Res. Commun.* **2007,** *357*, 743-748.
16. Homann, M.; Goringer, H. U., Combinatorial selection of high affinity RNA ligands to live African trypanosomes. *Nucleic Acids Res.* **1999,** *27*, 2006-2014.
17. Cao, X. X.; Li, S. H.; Chen, L. C.; Ding, H. M.; Xu, H.; Huang, Y. P.; Li, J.; Liu, N. L.; Cao, W. H.; Zhu, Y. J.; Shen, B. F.; Shao, N. S., Combining use of a panel of ssDNA aptamers in the detection of *Staphylococcus aureus*. *Nucleic Acids Res.* **2009,** *37*, 4621-4628.
18. Hamula, C. L. A.; Le, X. C.; Li, X. F., DNA aptamers binding to multiple prevalent M-types of *Streptococcus pyogenes*. *Anal. Chem.* **2011,** *83*, 3640-3647.
19. Li, H.; Ding, X. H.; Peng, Z. H.; Deng, L.; Wang, D.; Chen, H.; He, Q. Z., Aptamer selection for the detection of *Escherichia coli* K88. *Can. J. Microbiol.* **2011,** *57*, 453-459.
20. Dwivedi, H. P.; Smiley, R. D.; Jaykus, L. A., Selection and characterization of DNA aptamers with binding selectivity to Campylobacter jejuni using whole-cell SELEX. *Appl. Microbiol. Biotechnol.* **2010,** *87*, 2323-2334.
21. Pan, Q.; Zhang, X. L.; Wu, H. Y.; He, P. W.; Wang, F. B.; Zhang, M. S.; Hu, J. M.; Xia, B.; Wu, J. G., Aptamers that preferentially bind type IVB pili and inhibit human monocytic-cell invasion by *Salmonella enterica* serovar Typhi. *Antimicrob. Agents Chemother.* **2005,** *49*, 4052-4060.
22. Frens, G., Controlled nucleation for the regulation of the particle size in monodisperse gold suspensions. *Nature Phys. Sci.* **1973,** *241*, 20-22.
23. Turkevich, J.; Stevenson, P. C.; Hillier, J., A study of the nucleation and growth processes in the synthesis of colloidal gold. *Discuss. Faraday Soc.* **1951,** *No. 11*, 55-75.
24. Haiss, W.; Thanh, N. T. K.; Aveyard, J.; Fernig, D. G., Determination of size and concentration of gold nanoparticles from UV-Vis spectra. *Anal. Chem.* **2007,** *79*, 4215-4221.
25. Qian, X. M.; Peng, X. H.; Ansari, D. O.; Yin-Goen, Q.; Chen, G. Z.; Shin, D. M.; Yang, L.; Young, A. N.; Wang, M. D.; Nie, S. M., In vivo tumor targeting and spectroscopic detection with surface-enhanced Raman nanoparticle tags. *Nat. Biotechnol.* **2008,** *26*, 83-90.
26. Wuelfing, W. P.; Gross, S. M.; Miles, D. T.; Murray, R. W., Nanometer gold clusters protected by surface-bound monolayers of thiolated poly(ethylene glycol) polymer electrolyte. *J. Am. Chem. Soc.* **1998,** *120*, 12696-12697.

27. Joseph, V.; Matschulat, A.; Polte, J.; Rolf, S.; Emmerling, F.; Kneipp, J., SERS enhancement of gold nanospheres of defined size. *J. Raman Spectrosc.* **2011,** *42*, 1736-1742.
28. Njoki, P. N.; Lim, I. I. S.; Mott, D.; Park, H. Y.; Khan, B.; Mishra, S.; Sujakumar, R.; Luo, J.; Zhong, C. J., Size correlation of optical and spectroscopic properties for gold nanoparticles. *Journal of Physical Chemistry C* **2007,** *111*, 14664-14669.
29. Brown, K. R.; Walter, D. G.; Natan, M. J., Seeding of colloidal Au nanoparticle solutions. 2. Improved control of particle size and shape. . *Chem. Mater.* **2000,** *12*, 306-313.
30. Kimling, J.; Maier, M.; Okenve, B.; Kotaidis, V.; Ballot, H.; Plech, A., Turkevich method for gold nanoparticle synthesis revisited. *J. Phys. Chem. B* **2006,** *110*, 15700-15707.
31. Rule, K. L.; Vikesland, P. J., Surface-enhanced resonance Raman spectroscopy for the rapid detection of *Cryptosporidium parvum* and *Giardia lamblia*. *Environ. Sci. Technol.* **2009,** *43*, 1147-1152.
32. Lal, S.; Grady, N. K.; Kundu, J.; Levin, C. S.; Lassiter, J. B.; Halas, N. J., Tailoring plasmonic substrates for surface enhanced spectroscopies. *Chem. Soc. Rev.* **2008,** *37*, 898-911.
33. Chen, G.; Wang, Y.; Yang, M.; Xu, J.; Goh, S. J.; Pan, M.; Chen, H., Measuring ensemble-averaged surface-enhanced Raman scattering in the hotspots of colloidal nanoparticle dimers and trimers. *J. Am. Chem. Soc.* **2010,** *132*, 3644-+.
34. Wustholz, K. L.; Henry, A.-I.; McMahon, J. M.; Freeman, R. G.; Valley, N.; Piotti, M. E.; Natan, M. J.; Schatz, G. C.; Van Duyne, R. P., Structure-activity relationships in gold nanoparticle dimers and trimers for surface-enhanced Raman spectroscopy. *J. Am. Chem. Soc.* **2010,** *132*, 10903-10910.

CHAPTER 4. Optimizing blocking of nonspecific bacterial attachment to impedimetric biosensors

Maria V. Riquelme, Huaning Zhao, Vaishnavi Srinivasaraghavan, Amy Pruden, Peter Vikesland, Masoud Agah.

Published: Sensing and Bio-Sensing Research 8 (2016) 47-54.

Available via: http://dx.doi.org/10.1016/j.sbsr.2016.04.003

ABSTRACT

We evaluated the capacity for a variety of commonly used, low and high-molecular weight blocking agents to prevent nonspecific binding of *Staphylococcus aureus* and *S. intermedius* to impedimetric gold electrodes. The blocking agents tested here were mercaptoundecanol (MCU), polyethylene glycol (PEG, MW≈ 1kDa or 5 kDa), bovine serum albumin (BSA), and chicken serum albumin (CSA). The surfactant Tween 20 was applied additionally in some conditions. BSA and MCU in combination with Tween 20 were found to yield the greatest blocking capacities, whereas 5kPEG was found to actually enhance *S. intermedius* attachment. Although genetically and physiologically similar, *S. intermedius* and *S. aureus* differed significantly in their capacity to attach to the gold substrate. Monitoring of gold functionalization kinetics in real-time via impedance spectroscopy indicated that surface functionalization occurred within a few minutes of gold exposure to a given blocking agent. Higher impedance changes were observed with lower molecular weight blocking agents, likely due to denser molecular packing on the gold substrate. Careful optimization of blocking agent with respect to chemical properties, molecular size and potential interactions is recommended.

INTRODUCTION

In the midst of an era of emerging pathogens and a rise in antibiotic resistance, fast, sensitive and specific detection of target microbes is urgently needed. Traditional approaches for detection of pathogenic bacteria include methods such as culturing, antibody-based methods, and polymerase chain reaction (PCR). These methods can be both time and energy intensive, and also require skilled personnel. Although generally offering high specificity, PCR-based techniques may require long processing and

purification steps and are subject to the action of enzyme inhibitors such as organic matter and chelators, which are common in environmental samples.

The detection of pathogenic microorganisms via electrochemical methods is a promising approach because it offers the potential for fast, sensitive, user-friendly, and specific detection. Electrochemical impedance spectroscopy, specifically, is a versatile approach that has been successfully applied in the detection and quantification of a variety of biomolecules such as enzymes, antibodies, antigens, and DNA;[1-3] as well as for the detection of viruses, pathogenic bacteria, and eukaryotic cells.[4-7] Impedance-based detection methods rely upon the measurement of electrical impedance across an electrode that has been functionalized with a target-specific molecule, which is then exposed to a sample containing the target analyte. Here, the electrode acts as an electrical transducer that translates changes in electrical impedance at the analyte-electrode interface thus reflecting the presence or absence of the target. This signal can also be related to analyte concentration, thereby enabling quantification. Gold is a common electrode material because of its electrochemical properties, biocompatibility, and well-known surface chemistry, which allows controlled binding of biomolecules and other surface coatings.[8-11] The advantages of electrochemical impedance over existing methods include label-free detection, direct non-invasive, fast or real-time response, potential for miniaturization and integration into microfabricated systems, ease of use, and potential for low cost and mass production.[5, 12]

Low detection limits of a few colony-forming units (CFUs) have been reported using recently developed impedimetric immunosensors.[5, 13-15] Although the best known and most widely applied pathogen detection systems are based on antigen-antibody interactions (i.e., immunosensors), other recognition elements such as aptamers are quickly gaining ground due to their high stability, comparable selectivity, and ease of synthesis, among other reasons.[16] These molecules are characterized by their smaller size and molecular weight relative to protein antibodies, and may require optimized experimental conditions for their successful application. In this regard, a suitable blocking agent may be required to prevent nonspecific binding while not interfering with the capacity of the recognition element to interact with its target. In addition to limiting nonspecific binding, these materials may be employed simultaneously for multiple

purposes such as spacers, as linkers with functional moieties, or to minimize nonspecific binding of the target molecule to the gold surface, thereby increasing its ability to interact with the target analyte.[17, 18] The minimization of nonspecific binding to the gold electrode is critical because subsequent measurements depend on changes induced by total interactions between the electrode and the analyte. Furthermore, contaminants and other matrix components can contribute to the changes measured, thereby skewing the results. The blocking agents tested here were mercaptoundecanol (MCU), polyethylene glycol (PEG, 1 kDa or 5 kDa), bovine serum albumin (BSA), and chicken serum albumin (CSA). The surfactant Tween 20 was used in combination with some of the mentioned blocking agents. MCU is a hydroxyl-terminated long-chain alkane thiol that produces highly packed self-assembled monolayers (SAMs).[19] PEG is a non-ionic, water-soluble polymer commonly used to form protein-resistant SAMs.[20, 21] PEG molecules in SAMs are surrounded by an ordered shell of water molecules that render the monolayer hydrophilic and thus resistant to protein attachment.[21] Shorter length PEG chains are known to form more densely packed monolayers than longer length chains, likely due to the bending of the longer chains.[20] Serum albumin (e.g., BSA and CSA), casein, and other milk proteins are often used as blocking agents in enzyme-linked immunosorbent assay (ELISA), Western Blotting, and other enzyme-based assays.[22, 23] These proteins are well known for their capacity to prevent nonspecific binding of cells to surfaces, especially in the presence of Tween 20.[23] *Staphylococcus aureus* and *S. intermedius* were applied as model organisms here, both because they are closely related species of the same genus, and because they are pathogens of significant concern to human health. Specifically, *S. aureus* is the leading cause of skin and soft tissue infections and can also cause more invasive and life threatening diseases.[24, 25] *S. intermedius* is a closely related genus to *S. aureus*.[26] *S. intermedius* is generally associated with wound infections that have been either caused by or exposed to animals.[27, 28]

The objective of this research was to compare the aforementioned low and high-molecular weight blocking agents with respect to their capacity to prevent nonspecific bacterial binding to impedimetric gold electrodes. We hypothesized that smaller and more hydrophilic molecules would have a higher blocking capacity for two reasons: (1) It is well known that the capacity of a surface-coating agent to block nonspecific binding of proteins

or whole cells is related to the agent's hydrophilicity;[29, 30] and (2) smaller molecules form more compact SAMs that more thoroughly cover modified surfaces. Thus, blocking agents represent a limiting aspect of the sensitivity and selectivity of impedance-based biosensors, and critical examination is necessary in a manner to optimize their performance.

MATERIALS AND METHODS

Solutions. All buffers and solutions were produced using autoclaved nanopure (>18 MΩ·cm) water. PBS (137 mM NaCl, 2.7 mM KCl, 10 mM Na_2HPO_4, 1.76 mM KH_2PO_4, pH 7.4) was prepared as a stock 10× solution using molecular biology grade reagents, autoclaving, and diluting as necessary. Molecular biology grade ethanol (200 Proof) was purchased from Fisher Scientific. A list of blocking agents, their molecular weights, and their manufacturers is given in Table 4.1. Thiol-modified PEG (HS-PEG) was used for covalent PEG attachment to the gold substrate. Further descriptions of blocking agent concentrations and preparation procedures are given in Table 4.2.

Table 4.1. List of blocking agents and their molecular weights.

Name	Abbreviation	Molecular weight (Da)	Manufacturer
11-Mercapto 1-undecanol	MCU	204.37	Aldrich
HS-PEG (1 kDa)	1kPEG	1,000	NANOCS
HS-PEG (5 kDa)	5kPEG	5,000	NANOCS
Bovine serum albumin	BSA	66,500	Sigma
Chicken serum albumin	CSA	~66,000	Sigma
Tween® 20	T	1,227.54	Promega

Device and imaging-chip fabrication. The impedance measurement device consisted of a 6 × 6 array of electrode circuits as shown in Figure 4.1. Thus, 36 different sensors could be used within the same device to test different conditions. A PDMS mold separated each circuit and allowed for analysis of different aqueous samples thus minimizing the potential for cross-contamination.

The chip fabrication process is shown in Figure 4.1. An initial Si wafer substrate was thermally oxidized to obtain a ≈0.5 μm layer of SiO_2. The wafer was then coated with photoresist (Shipley 1827) using a binder (HMDS) by spin coating and soft baking. The photoresist was patterned and developed using a mask that contained the electrode design, and a gold layer ≈0.1 μm thick was deposited by electron-beam evaporation. The wafer was then acetone washed for 20 min to remove the photoresist. Prior to PDMS bonding, the device was cleaned by oxygen plasma for 10 minutes (Harrick Plasma Cleaner).[31, 32].

For SEM imaging, gold-coated SiO_2 chips were used. A Si wafer was thermally oxidized to form a SiO_2 layer. A gold layer was then deposited by electron-beam evaporation. Finally, a layer of photoresist was applied as a passivation layer prior to cutting the wafer into small squares of $\approx 4 \times 4$ mm^2. Before use, the photoresist layer was washed off using acetone and the chip was cleaned with oxygen plasma.[32]

Bacteria strains and culture. *S. aureus* (ATCC 12600) and *S. intermedius* (ATCC 29663) were cultured in 100 mL of brain heart infusion media (Bactrius Limited, Houston TX) at 37 °C and 165 rpm to the late exponential growth phase (OD600 ≈ 0.8). Cells were then transferred to two sterile 50 mL centrifuge tubes, and subjected to two washes by centrifugation (5000 ×g for 10 min) and re-suspension in 1× PBS. A calibration curve relating OD600 to microscopic cell counts was created and used to quantify the washed bacteria via spectrophotometry thereafter. Cell quantification was done via microscope using a counting chamber, and was verified by colony forming unit (CFU) counts.

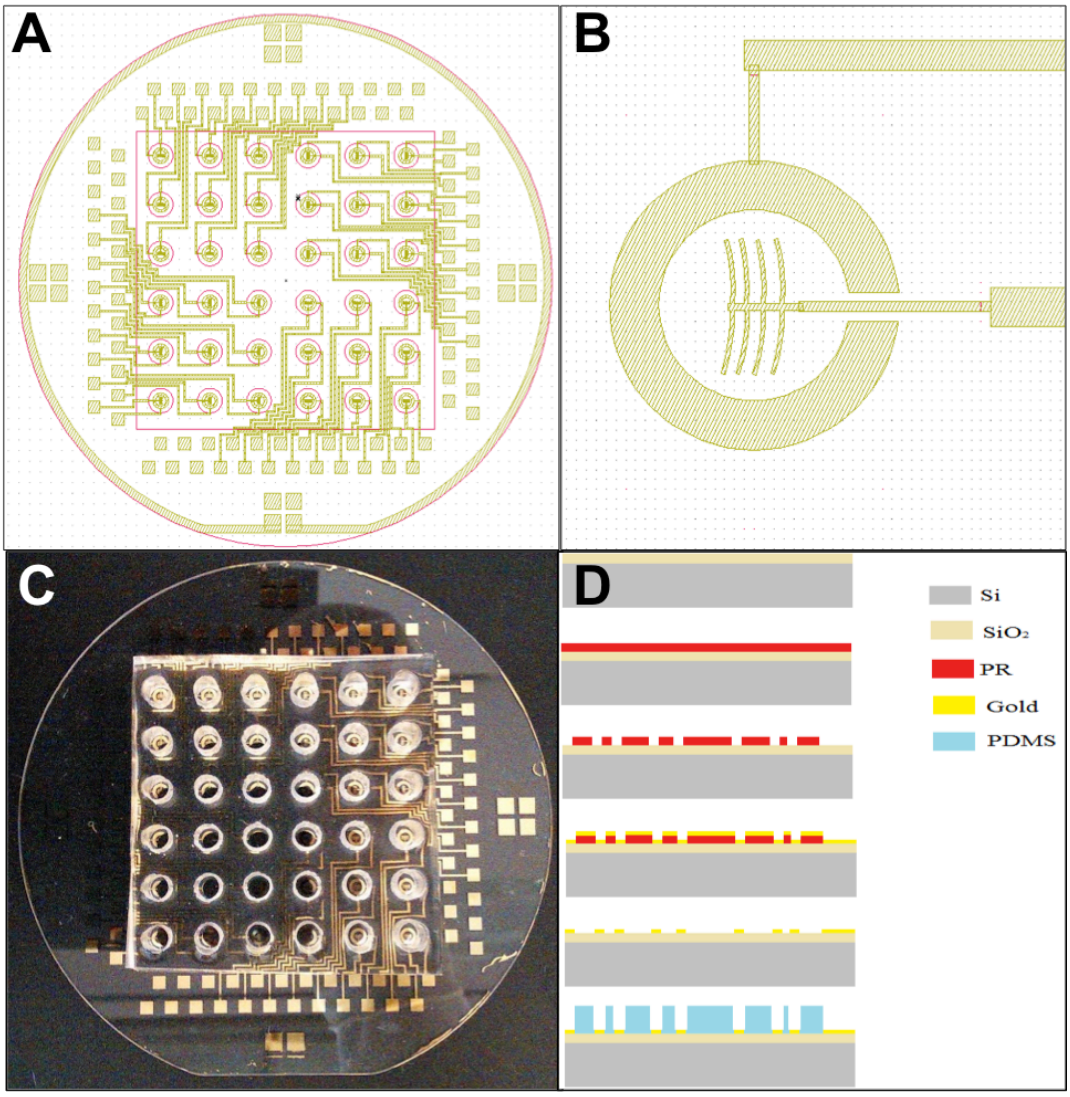

Figure 4.1. Impedance biosensor setup and fabrication. A) 6x6 electrode circuit array. B) Single electrode circuit. C) Picture of fabricated electrode bound to PDMS mold with sample wells. D) Schematic of impedance device fabrication process.

Experimental setup and impedance measurements. An impedance analyzer (Agilent HP4192A) was used to make impedance measurements from each electrode with a log-spaced frequency sweep (30 points in the range 1 kHz–1 MHz). Measurements included both the impedance magnitude (|Z|) and phase (∠Z) values for each electrode.[32] Initial baseline impedance measurements were defined in PBS only. Next, each electrode was exposed to 50 µL of blocking agent solution and measurements were made continuously for 1 h at 37 °C. After washing 3 times with PBS, a second (post-wash) measurement

was collected in PBS for comparison to the initial baseline. After this step, 50 µL of bacteria ($2x10^8$/mL) was introduced into each well, and impedance measurements were made for 2 h at 37 °C. Again, all wells were washed 3× with PBS, and a final measurement was collected in PBS for comparison with the baseline.

For SEM imaging and contact angle measurements, square gold-coated SiO_2 chips were affixed to the bottom of a 24-well plate using silicone grease. The chips were then exposed to 1 mL of blocking agent for 1 h at 37 °C. After 1 h, all pieces were washed 3 times with PBS. Chips used for contact angle measurements were washed with autoclaved nanopure water and allowed to dry before being placed in a vacuum desiccator overnight. Functionalized chips used for SEM imaging were exposed to 1 mL of bacteria ($2x10^8$/mL), and incubated for 2 h at 37 °C. After 2 h, the chips were washed 3 times with PBS, fixed with 500 µL of 3% glutaraldehyde in PBS for 30 min, and dehydrated with sequential exposures to increased ethanol concentrations (25, 50, 75, and 100%) for 5 min each. After exposure, the ethanol was allowed to completely evaporate and the chips were prepared for SEM imaging.

SEM and image analysis. The chips were fixed on SEM stubs using double-sided copper tape, coated with gold/palladium using a Cressington 208HR high-resolution sputter-coater, and then imaged using a Leo 1550 Field Emission Scanning Electron Microscope (SEM; Carl Zeiss Nano Technology systems, International). Each chip was imaged five times: once near each corner, about half way between the edge and the center, and once near the center. The bacterial numbers on each image were determined using ImageJ (NIH) software.

Contact Angle measurements. After functionalization and washing, chips used for contact angle measurements were allowed to dry and stored in a vacuum desiccator overnight. Contact angle measurements were then carried out using a First Ten Angstroms contact angle analyzer, Model FTA 125. A droplet of ~7.5 (± 0.6) µL was deposited on the surface of the functionalized chips, and then imaged and analyzed using FTA 32 Video 2.0 Software.

Statistical analysis. Statistical analyses were performed in R (Version 3.2.1). For comparison of the blocking capacity of different blocking agents, ANOVA and pairwise t-

test were applied. A t-test was applied for analyzing differences between *S. aureus* and *S. intermedius* attachment.

RESULTS AND DISCUSSION

Impedimetric characterization of blocking agent attachment kinetics. The kinetics of blocking agent attachment were characterized via impedance spectroscopy (Figure 4.2A). For all blocking agents, most blocking agent-electrode interactions occurred during the first 5 min of incubation, while the maximum impedance was steadily approached between 30 min and 1 h of incubation. This result is in agreement with a previous study, which reported more than 90% surface coverage of an alkanethiol similar to MCU, specifically hexadecyl mercaptan (5 mM), within the first 1 to 5 min of exposure; followed by slower monolayer formation that resulted in an electronically insulating SAM on gold, within about an hour.[33] It was observed that smaller molecular weight materials induced a higher impedance change than larger molecular weight materials. This is likely a result of more dense packing of smaller molecules than larger ones, thereby forming an ordered packed monolayer that blocks electrochemical interactions at the gold-buffer interface.[34, 35] Although smaller molecules interacted with the gold electrode very quickly after exposure, a steady increase in impedance continued to be observed during the 1 h incubation time. This steady increase was likely due to slower monolayer ordering as packing density increased, and eventually reached a plateau. Campuzano, et al.[36] showed that areas of imperfect alkanethiol adsorption to the electrode surface, called pinholes, are often present; however, some of these pinholes can be filled by extended (up to 20 h) alkanethiol exposure. This is also in agreement with a previous study by Boubour and Lennox[37] who found that extended (40 h) exposure to thiol solution is required to achieve an ideal dielectric SAM. It should be noted that blocking agent exposure time may require optimization in order to prevent displacement of the recognition element. Lee et al.[18] optimized exposure time of an alkylthiol onto an oligonucleotide functionalized surface and found that a 30 min exposure was ideal and that longer times may lead to undesirable oligonucleotide displacement. Thus, a balance is required in order to maximize blocking agent coverage while minimizing displacement of recognition elements.

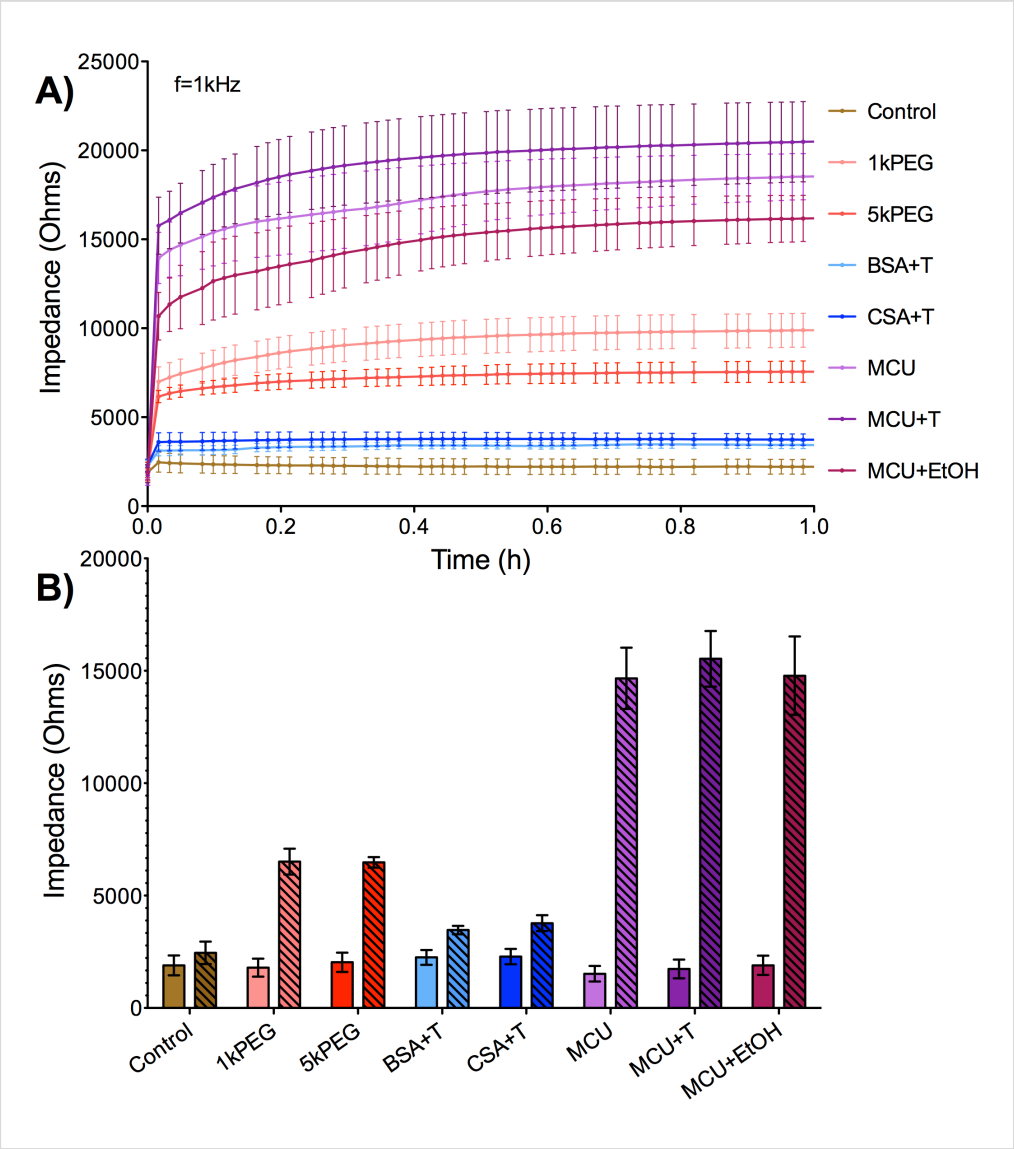

Figure 4.2. Impedance-based measurements of blocking agent attachment. A) Real-time monitored kinetics of BA attachment. B) PBS baseline (plain bars) and post-wash (striped bars) impedance measurements. Gold electrodes were exposed to 50 µL of each blocking agent in four replicates and immediately placed in the impedance instrument. Measurements for two separate devices were collected for 1 h at 37 °C. A baseline measurement and a post-wash measurement (after washing excess blocking agent) were collected before and after treatment with blocking agent, respectively. Control is bare (unfunctionalized) gold exposed to DI water during the incubation time.

Impedimetric and contact angle characterization of functionalized gold electrodes.

A washing step was applied to remove excess and loosely adsorbed blocking agents and

a post-wash impedance measurement was then collected. Upon comparison of baseline and post-wash measurements, the relationship between the measured impedance and the blocking agent size was apparent (Figure 4.2B). Consistent with their higher molecular weight, and thus likely looser surface packing, the impedance change was lowest for BSA and CSA. Next, the 5kPEG- and 1kPEG-induced impedance change was intermediate, in agreement with their relatively intermediate molecular weights. Finally, the lowest molecular weight blocking agent, MCU, induced the highest impedance change. Again, this was likely due to the denser molecular packing on the gold surface, which consequentially resembles an ideal dielectric material.[37]

Water contact angles were determined to quantify and compare the hydrophobicity of each functionalization scheme (Table 4.2). Although most contact angles were in the hydrophilic range (<90°), three blocking agents stood out in terms of their lower contact angles: BSA-T (79°), 1 mM 5kPEG (PEG MW≈5 kDa, 73°) and MCU-T (62°). Compared to the bare gold surface (94°), these three functionalities were more hydrophilic, and therefore should be expected to block bacterial attachment more effectively. Past studies have shown that hydrophilic surface coatings are more effective at blocking protein and bacterial attachment to surfaces.[29, 30]

Table 4.2. Contact angle of blocking agent-functionalized and unfunctionalized gold chips.

Surface Functionalization	Concentration	Contact angle	Stdev
None (Control)		94	4
BSA[a]	5%	82	1
BSA-T[b]	5% BSA, 0.05% T	79	1
CSA[a]	5%	90	1
CSA-T[b]	5% CSA, 0.05% T	86	2
MCU	1 mM	86	2
MCU-T	1 mM MCU, 0.05% T	62	2
MCU-EtOH	1 mM MCU, 75% EtOH	86	10
1kPEG	1 mM	85	2
5kPEG	1 mM	73	1

[a] BSA and CSA solutions were prepared by dissolving in 1× PBS
[b] BSA-T and CSA-T were prepared by dissolving in 1× PBS + Tween®20 solution
All other functionalizations were prepared by dissolving in H_2O (or EtOH where noted).

Contact angles reported in the literature are highly variable and range from about 61° to 78° degrees for bare gold,[38-41] from 31° to 63° for PEG monolayers,[20, 40, 42] from 13° to 37° for MCU monolayers,[42-44] and ~53° (pH dependent) for BSA.[41, 45] Although our measured contact angles are consistently above these ranges, the functionalized substrates invariably displayed increased hydrophilicity relative to the unfunctionalized gold substrate. Taken together with the impedance and bacterial attachment results, the contact angle measurements suggest that blocking agent functionalization occurred successfully.

Comparison of *S. aureus* and *S. intermedius* attachment to gold electrodes. The model organisms employed in this optimization study were two closely related *Staphylococcal* species, both of which are opportunistic human and animal pathogens of concern. Although *S. aureus* and *S. intermedius* are closely related, there are some established differences in their biochemical properties, as well as in the composition of their cell wall polysaccharides and peptidoglycan structures.[26] For example, *S. intermedius* cells have a higher serine content in their peptidoglycan and contain glycerol teichoic acid in their cell walls, rather than ribitol teichoic acid.[46] It is interesting to note that the capacities of *S. aureus* and *S. intermedius* to attach to bare gold surface were significantly different (t-test: $p<0.005$; Figure 4.3). When an unfunctionalized gold chip was exposed to a suspension of either type of bacterial cell (both at the same concentration), ~77,000/mm^2 *S. intermedius* cells attached to the gold surface, whereas only ~6000/mm^2 *S. aureus* cells attached under the same conditions. Nearly 13× more *S. intermedius* cells attached to the gold than did *S. aureus* cells. This is an interesting observation that highlights the difference in behavior in closely related organisms, and therefore the importance of assay optimization for each new target species. Further, this study indicates that the potential for nonspecific attachment likely varies among microbes.

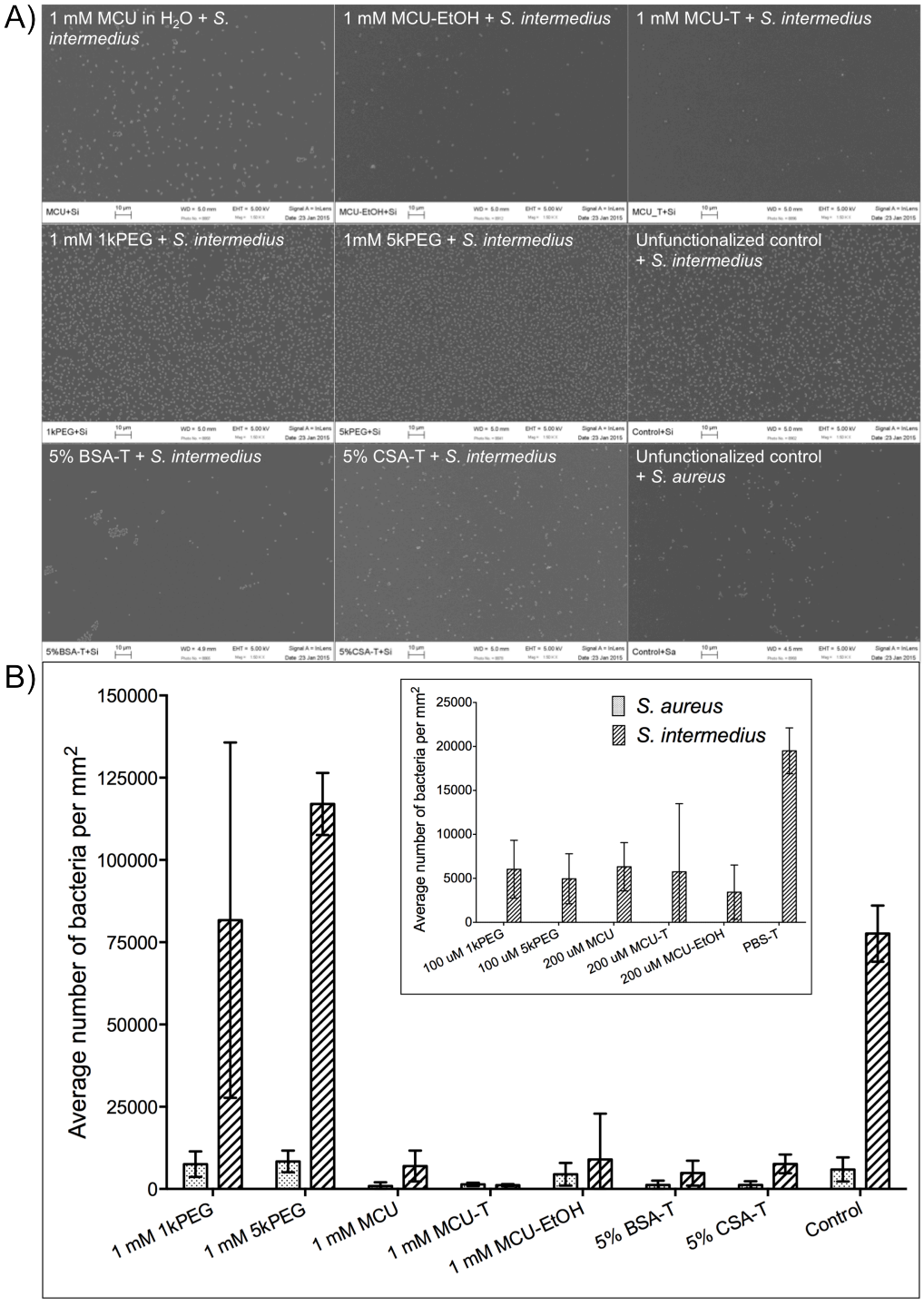

Figure 4.3. Average bacterial counts per mm^2 in blocking agent-functionalized gold chips. Error bars represent standard deviation of 4-6 SEM images. Functionalized gold chips were immersed in 1 mL of $2x10^8$ bacteria/mL for 1 h at 37 °C. Unbound and loosely bound bacteria were removed via three rounds of washing using PBS. Bacteria were fixed in 3% glutaraldehyde, dehydrated via increasing ethanol exposures, and allowed to completely dry before gold-palladium coating and SEM imaging.

Characterization of blocking agent capacity to minimize nonspecific bacterial attachment onto gold electrodes. Based on the water contact angle measurements, the three most hydrophilic functionalities were BSA-T, 5kPEG, and MCU-T (Table 4.2). Interestingly, only two of these widely used materials (BSA-T and MCU-T) were observed to have high blocking capacities, whereas 5kPEG was actually observed to enhance *S. intermedius* attachment (Figure 4.3). In comparison to the unfunctionalized control (via pairwise t-test), significantly fewer bacteria attached to surfaces that were functionalized with BSA-T, CSA-T (5% CSA, 0.05% Tween 20), MCU, and MCU-T ($p<0.001$). However, significantly more bacteria attached to 5kPEG-functionalized gold ($p<0.001$). Here, we excluded MCU-EtOH (1 mM MCU, 75% ethanol) and 1kPEG (PEG, MW≈1 kDa) from the t-test, as their bacterial counts were highly variable and did not meet the normality assumption.

Although the capacity for PEG to inhibit protein attachment has been widely assumed to be associated with resistance to cell attachment, several studies have pointed out that this may not always be the case.[47-49] This result is because adhesion behavior is not only dependent on the substrate chemistry, but also on the cell surface composition and on the interaction medium. Specifically, in a study by Park et al.[48] the grafting of 1kPEG onto polyurethane surfaces did not contribute to the repellence of *Staphylococcus epidermidis*. In fact, 1kPEG-modified surfaces actually showed a slight increase in bacterial adhesion compared to the unmodified hydrophobic polyurethane control. In the same study, bacterial adhesion was shown to be highly dependent on suspension medium.[48] In a different study, Muller et al. [47] observed substantial adhesion of eukaryotic cells to a PEG-modified silicon substrate. In another study by Wei et al.,[49] PEG was shown to prevent protein adsorption onto a stainless steel surface, but made no difference in the adsorption of Gram-negative *Pseudomonas* spp. or Gram-positive *Listeria monocytogenes*.

It is possible that the high affinity of *S. intermedius* towards PEG may be enhanced by a temperature effect, given that our experiments were performed at 37 °C. Prime and Whitesides [50] reported a decrease in protein blocking capacity of a PEG SAM at 37 °C in comparison to 25 or 4 °C. This observation was explained as the result both of the tendency of ethylene oxide chains to have lower solubility limits at higher temperatures

as well as a tendency of the hydrophobic effect to increase at higher temperatures.[50, 51] Ogi, et al. [52] reported nonspecific binding capacities of BSA and PEG for human immunoglobulin G (HIgG) and *Staphylococcus* protein A (SPA). The authors concluded that although both blocking agents show high blocking capacity, the number of binding sites of PEG toward HIgG is significantly larger than that of BSA.[52]

SEM image counts are shown in Figure 4.3B, along with representative SEM images (Figure 4.3A). In contrast to the unexpected affinity of *S. intermedius* for PEG, it can be observed that MCU-T, BSA-T, and CSA-T blocked nonspecific bacterial binding effectively. A previous experiment revealed that BSA or CSA alone are not as effective at blocking nonspecific bacterial binding than BSA or CSA in combination with Tween 20 (Figure S4.1). In addition, Tween 20 alone was found to be ineffective at blocking *S. intermedius* at the concentration tested (Figure 4.4B inset). These results are in agreement with a previous study that quantified the individual and combined blocking effects of BSA and Tween 20 in ELISA microwells.[23] This prior study revealed that although both blocking agents can offer satisfactory results, there was an enhanced effect when they were applied in combination.[23] The same study also advised about the potential interferences that one or the other blocking agents may have, depending on the type of receptor used.[23]

Of the blocking agents tested, MCU-T had the highest capacity for blocking nonspecific bacterial binding (Figure 4.3). For this reason, the blocking capacity of MCU-T at different concentrations was examined further (Figure 4.4). We found that, on average, >85% of *S. intermedius* attachment was blocked at 100 μM MCU-T concentration, >90% attachment was blocked at 1 mM MCU-T concentration, and >99% attachment was blocked at 10 mM MCU-T concentration (Figure 4.4A). The slight but gradual increase in *S. intermedius* attachment at these higher concentrations is likely a combined effect between: (1) the high affinity of *S. intermedius* toward the gold substrate and (2) an increasing frequency of defects (pinholes) in the MCU monolayer with a decrease in MCU concentration. The latter effect is dependent on MCU functionalization time and monolayer defects are expected to decrease with increasing MCU incubation time (e.g., longer than one day).

At concentrations 1 μM and below, the images were not quantifiable, as bacterial attachment occurred irregularly (Figure 4.4A), thus suggesting incomplete surface functionalization. We note that the blocking agent concentrations applied in these experiments were expected to saturate the bare gold chips. Lower blocking agent concentrations may be required if the electrode surface has already been functionalized with a receptor molecule such as an oligomer or an antibody. For example, Lee, Gong, Harbers, Grainger, Castner and Gamble [18] found that an optimum MCU concentration required to block an oligomer-functionalized surface was ≈10 μM.

The impedance values measured from the gold electrodes are expected to rise after bacterial attachment. This is due to the bacterial film forming an effective barrier to the passage of electric current. The functionalized electrodes did not appear to show any significant change in the impedance measurements after exposure to bacteria (Figure S4.2). However, an increase in impedance was observed on electrodes that were not functionalized. It should be noted that these electrodes were originally designed for analyses and detection of mammalian cells,[31, 32, 53] and thus electrode geometries may benefit from specific optimization for bacterial cells, which are 10-100X smaller.

It should be noted that careful choice of blocking agent may be required based on the molecular size of the recognition element being applied and the potential unwanted interactions or inhibitions that the blocking agent may impart. For example, if an oligonucleotide or an aptamer is employed as the recognition element, using BSA or a long chain molecule as blocking agent may also block specific recognition element-target interactions. This case is highlighted in a aptamer-based plant virus detection study by Lautner, et al. [54] who found that although long chain PEGs effectively blocked nonspecific interactions, they also sterically hindered aptamer-target interactions; whereas a short tetraethylene glycol chain allowed excellent specific binding while still minimizing nonspecific interactions. In the case of oligonucleotide targeting molecules, alkylthiols are generally attractive as they not only are successful at preventing nonspecific binding, but also increase the availability of the active oligonucleotide site by preventing nonspecific interactions between the nucleobases and the gold substrate.[18, 55]

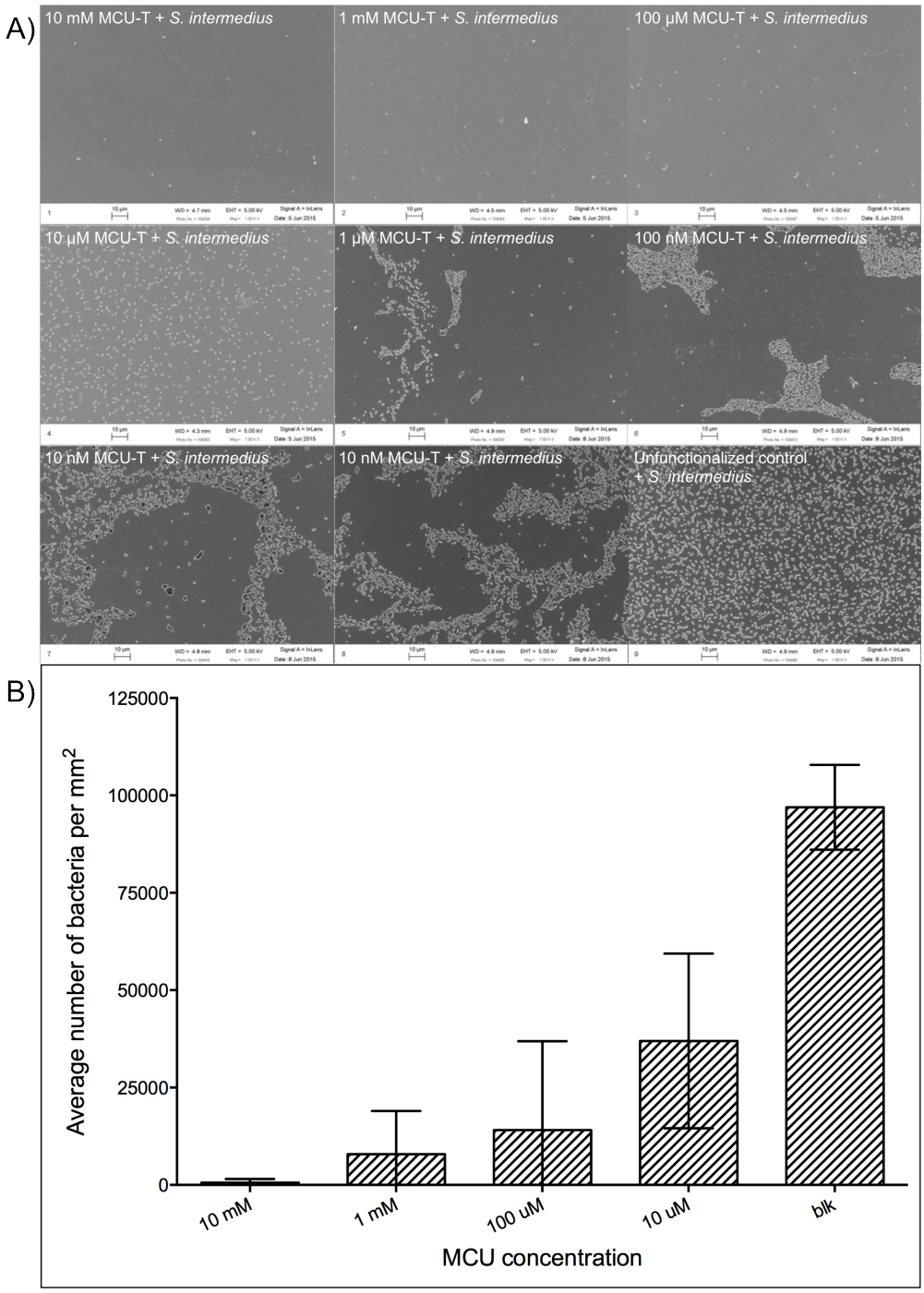

Figure 4.4. Average bacterial counts per mm^2 in MUC-T functionalized gold chips at a range of concentrations. Error bars represent standard deviation of 4-6 SEM images. Functionalized gold chips were immersed in 1 mL of $2x10^8$ bacteria/mL for 1 h at 37 °C. Unbound and loosely bound bacteria were removed via three rounds of washing using PBS. Bacteria were fixed in 3% glutaraldehyde, dehydrated via increasing ethanol exposures, and allowed to completely dry before gold-palladium coating and SEM imaging.

CONCLUSIONS

Several low and high molecular weight blocking agents were compared with respect to their capacity to prevent nonspecific bacterial binding to impedimetric gold electrodes. Hydrophilic BSA-T and MCU-T were found to have the highest blocking capacity. Interestingly, and contrary to our expectations, 5kPEG actually encouraged *S. intermedius* attachment to the functionalized gold substrate. Furthermore, closely related *Staphylococcus* species (*S. intermedius* > *S. aureus*) were found to have significantly different attachment affinities toward the gold substrate, highlighting the need for blocking agent testing and optimization prior to application. Gold functionalization kinetics were also monitored real-time via impedance spectroscopy and found to occur rapidly within a few minutes of gold exposure to blocking agent. Notably, a higher impedance change was observed with lower molecular weight blocking agents, likely due to higher molecular packing on the gold substrate. Careful optimization of blocking agent with respect to molecular size and potential interactions is recommended.

ACKNOWLEDGEMENTS

Funding for this work was provided in part by U.S. National Science Foundation Awards 1310090 (PI Agah) and 1133746 (PI Vikesland) as well as the Virginia Tech Institute for Critical Technology and Applied Science and Interdisciplinary Graduate Education Program.

REFERENCES

1. Cai, D.; Ren, L.; Zhao, H. Z.; Xu, C. J.; Zhang, L.; Yu, Y.; Wang, H. Z.; Lan, Y. C.; Roberts, M. F.; Chuang, J. H.; Naughton, M. J.; Ren, Z. F.; Chiles, T. C., A molecular-imprint nanosensor for ultrasensitive detection of proteins. *Nat. Nanotechnol.* **2010,** *5*, 597-601.
2. Keighley, S. D.; Estrela, P.; Li, P.; Mighorato, P., Optimization of label-free DNA detection with electrochemical impedance spectroscopy using PNA probes. *Biosens. Bioelectron.* **2008,** *24*, 906-911.
3. La Belle, J. T.; Bhavsar, K.; Fairchild, A.; Das, A.; Sweeney, J.; Alford, T. L.; Wang, J.; Bhavanandan, V. P.; Joshi, L., Cytokine immunosensor for multiple sclerosis detection

based upon label-free electrochemical impedance spectroscopy. *Biosens. Bioelectron.* **2007,** *23*, 428-431.
4. Lu, L.; Chee, G.; Yamada, K.; Jun, S., Electrochemical impedance spectroscopic technique with a functionalized microwire sensor for rapid detection of foodborne pathogens. *Biosens. Bioelectron.* **2013,** *42*, 492-495.
5. Barreiros dos Santos, M.; Agusil, J. P.; Prieto-Simon, B.; Sporer, C.; Teixeira, V.; Samitier, J., Highly sensitive detection of pathogen *Escherichia coli* O157:H7 by electrochemical impedance spectroscopy. *Biosens. Bioelectron.* **2013,** *45*, 174-180.
6. Hnaien, M.; Diouani, M. F.; Helali, S.; Hafaid, I.; Hassen, W. M.; Renault, N. J.; Ghram, A.; Abdelghani, A., Immobilization of specific antibody on SAM functionalized gold electrode for rabies virus detection by electrochemical impedance spectroscopy. *Biochem. Eng. J.* **2008,** *39*, 443-449.
7. K'Owino, I. O.; Sadik, O. A., Impedance spectroscopy: A powerful tool for rapid biomolecular screening and cell culture monitoring. *Alectroanal.* **2005,** *17*, 2101-2113.
8. Mohr, F., *Gold chemistry: Applications and future directions in the life sciences*. Wiley: 2009.
9. Austin, L. A.; Mackey, M. A.; Dreaden, E. C.; El-Sayed, M. A., The optical, photothermal, and facile surface chemical properties of gold and silver nanoparticles in biodiagnostics, therapy, and drug delivery. *Arch. Toxicol.* **2014,** *88*, 1391-1417.
10. Daniel, M. C.; Astruc, D., Gold nanoparticles: Assembly, supramolecular chemistry, quantum-size-related properties, and applications toward biology, catalysis, and nanotechnology. *Chem. Rev.* **2004,** *104*, 293-346.
11. Li, G. M., Peng, *Electrochemical analysis of proteins and cells*. Springer: 2013.
12. Daniels, J. S.; Pourmand, N., Label-free impedance biosensors: Opportunities and challenges. *Alectroanal.* **2007,** *19*, 1239-1257.
13. Barreiros dos Santos, M.; Azevedo, S.; Agusil, J. P.; Prieto-Simon, B.; Sporer, C.; Torrents, E.; Juarez, A.; Teixeira, V.; Samitier, J., Label-free ITO-based immunosensor for the detection of very low concentrations of pathogenic bacteria. *Bioelectrochem.* **2015,** *101*, 146-152.
14. La Belle, J. T.; Shah, M.; Reed, J.; Nandakumar, V.; Alford, T. L.; Wilson, J. W.; Nickerson, C. A.; Joshi, L., Label-free and ultra-low level detection of *Salmonella enterica* serovar typhimurium using electrochemical impedance spectroscopy. *Alectroanal.* **2009,** *21*, 2267-2271.
15. Maalouf, R.; Fournier-Wirth, C.; Coste, J.; Chebib, H.; Saikali, Y.; Vittori, O.; Errachid, A.; Cloarec, J.-P.; Martelet, C.; Jaffrezic-Renault, N., Label-free detection of bacteria by electrochemical impedance spectroscopy: Comparison to surface plasmon resonance. *Anal. Chem.* **2007,** *79*, 4879-4886.
16. Ma, X.; Jiang, Y.; Jia, F.; Yu, Y.; Chen, J.; Wang, Z., An aptamer-based electrochemical biosensor for the detection of *Salmonella*. *J. Microbiol. Methods* **2014,** *98*, 94-98.
17. Huang, T. T.; Sturgis, J.; Gomez, R.; Geng, T.; Bashir, R.; Bhunia, A. K.; Robinson, J. P.; Ladisch, M. R., Composite surface for blocking bacterial adsorption on protein biochips. *Biotechnol. Bioeng.* **2003,** *81*, 618-624.
18. Lee, C.-Y.; Gong, P.; Harbers, G. M.; Grainger, D. W.; Castner, D. G.; Gamble, L. J., Surface coverage and structure of mixed DNA/alkylthiol monolayers on gold:

Characterization by XPS, NEXAFS, and fluorescence intensity measurements. *Anal. Chem.* **2006,** *78*, 3316-3325.
19. Chaki, N. K.; Vijayamohanan, K., Self-assembled monolayers as a tunable platform for biosensor applications. *Biosens. Bioelectron.* **2002,** *17*, 1-12.
20. Cerruti, M.; Fissolo, S.; Carraro, C.; Ricciardi, C.; Majumdar, A.; Maboudian, R., Poly(ethylene glycol) monolayer formation and stability on gold and silicon nitride substrates. *Langmuir* **2008,** *24*, 10646-10653.
21. Heuberger, M.; Drobek, T.; Spencer, N. D., Interaction forces and morphology of a protein-resistant poly(ethylene glycol) layer. *Biophys. J.* **2005,** *88*, 495-504.
22. Munoz-Berbel, X.; Godino, N.; Laczka, O.; Baldrich, E.; Xavier Munoz, F.; Javier Del Campo, F., Impedance-based biosensors for pathogen detection. In *Principles of Bacterial Detection: Biosensors, Recognition Receptors and Microsystems*, Zourob, M.; Elwary, S.; Turner, A., Eds. Springer: 2008; pp 341-376.
23. Steinitz, M., Quantitation of the blocking effect of tween 20 and bovine serum albumin in ELISA microwells. *Anal. Biochem.* **2000,** *282*, 232-238.
24. Kluytmans, J.; vanBelkum, A.; Verbrugh, H., Nasal carriage of *Staphylococcus aureus*: Epidemiology, underlying mechanisms, and associated risks. *Clin. Microbiol. Rev.* **1997,** *10*, 505-&.
25. Neyra, R. C.; Frisancho, J. A.; Rinsky, J. L.; Resnick, C.; Carroll, K. C.; Rule, A. M.; Ross, T.; You, Y. Q.; Price, L. B.; Silbergeld, E. K., Multidrug-resistant and methicillin-resistant *Staphylococcus aureus (*MRSA) in hog slaughter and processing plant workers and their community in North Carolina (USA). *Environ. Health Perspect.* **2014,** *122*, 471-477.
26. Hajek, V., *Staphylococcus intermedius*, a new species isolated from animals. *Int. J. Syst. Bacteriol.* **1976,** *26*, 401-408.
27. Pottumarthy, S.; Schapiro, J. M.; Prentice, J. L.; Houze, Y. B.; Swanzy, S. R.; Fang, F. C.; Cookson, B. T., Clinical isolates of *Staphylococcus intermedius* masquerading as methicillin-resistant *Staphylococcus aureus*. *J. Clin. Microbiol.* **2004,** *42*, 5881-5884.
28. Kelesidis, T.; Tsiodras, S., *Staphylococcus intermedius* is not only a zoonotic pathogen, but may also cause skin abscesses in humans after exposure to saliva. *Int. J. Infect. Dis.* **2010,** *14*, E838-E841.
29. Ostuni, E.; Chapman, R. G.; Holmlin, R. E.; Takayama, S.; Whitesides, G. M., A survey of structure-property relationships of surfaces that resist the adsorption of protein. *Langmuir* **2001,** *17*, 5605-5620.
30. Furuya, M.; Haramura, M.; Tanaka, A., Reduction of nonspecific binding proteins to self-assembled monolayer on gold surface. *Biorg. Med. Chem.* **2006,** *14*, 537-543.
31. Srinivasaraghavan, V.; Strobl, J.; Agah, M., Bioimpedance rise in response to histone deacetylase inhibitor is a marker of mammary cancer cells within a mixed culture of normal breast cells. *Lab. Chip.* **2012,** *12*, 5168-5179.
32. Srinivasaraghavan, V.; Strobl, J.; Wang, D.; Heflin, J. R.; Agah, M., A comparative study of nano-scale coatings on gold electrodes for bioimpedance studies of breast cancer cells. *Biomed. Microdevices* **2014,** *16*, 689-696.
33. Forouzan, F.; Bard, A. J.; Mirkin, M. V., Voltammetric and scanning electrochemical microscopic studies of the adsorption kinetics and self-assembly of n-alkanethiol monolayers on gold. *Isr. J. Chem.* **1997,** *37*, 155-163.

34. Hinterwirth, H.; Kappel, S.; Waitz, T.; Prohaska, T.; Lindner, W.; Laemmerhofer, M., Quantifying thiol ligand density of self-assembled monolayers on gold nanoparticles by inductively coupled plasma-mass spectrometry. *ACS Nano* **2013,** *7*, 1129-1136.
35. Xia, X.; Yang, M.; Wang, Y.; Zheng, Y.; Li, Q.; Chen, J.; Xia, Y., Quantifying the coverage density of poly(ethylene glycol) chains on the surface of gold nanostructures. *ACS Nano* **2012,** *6*, 512-522.
36. Campuzano, S.; Pedrero, M.; Montemayor, C.; Fatas, E.; Pingarron, J. M., Characterization of alkanethiol-self-assembled monolayers-modified gold electrodes by electrochemical impedance spectroscopy. *J. Electroanal. Chem.* **2006,** *586*, 112-121.
37. Boubour, E.; Lennox, R. B., Insulating properties of self-assembled monolayers monitored by impedance spectroscopy. *Langmuir* **2000,** *16*, 4222-4228.
38. Rafiee, J.; Mi, X.; Gullapalli, H.; Thomas, A. V.; Yavari, F.; Shi, Y. F.; Ajayan, P. M.; Koratkar, N. A., Wetting transparency of graphene. *Nat. Mater.* **2012,** *11*, 217-222.
39. Ernst, O.; Lieske, A.; Jager, M.; Lankenau, A.; Duschl, C., Control of cell detachment in a microfluidic device using a thermo-responsive copolymer on a gold substrate. *Lab. Chip.* **2007,** *7*, 1322-1329.
40. Joshi, S.; Pellacani, P.; van Beek, T. A.; Zuilhof, H.; Nielen, M. W. F., Surface characterization and antifouling properties of nanostructured gold chips for imaging surface plasmon resonance biosensing. *Sensor Actuat. B-Chem.* **2015,** *209*, 505-514.
41. Shen, W.; Li, S.; Park, M.-K.; Zhang, Z.; Cheng, Z.; Petrenko, V. A.; Chin, B. A., Blocking agent optimization for nonspecific binding on phage based magnetoelastic biosensors. *J. Electrochem. Soc.* **2012,** *159*, B818-B823.
42. Frutos, A. G.; Brockman, J. M.; Corn, R. M., Reversible protection and reactive patterning of amine- and hydroxyl-terminated self-assembled monolayers on gold surfaces for the fabrication of biopolymer arrays. *Langmuir* **2000,** *16*, 2192-2197.
43. Pedri, L. Interaction of bacteria with hydrophobic and hydrophilic interfaces. Lakehead University, Thunder Bay, Canada, 2002.
44. Zaccari, I.; Catchpole, B. G.; Laurenson, S. X.; Davies, A. G.; Walti, C., Improving the dielectric properties of ethylene-glycol alkanethiol self-assembled monolayers. *Langmuir* **2014,** *30*, 1321-1326.
45. Jachimska, B.; Pajor, A., Physico-chemical characterization of bovine serum albumin in solution and as deposited on surfaces. *Bioelectrochem.* **2012,** *87*, 138-146.
46. Schleifer, K. H.; Schumacherperdreau, F.; Gotz, F.; Popp, B.; Hajek, V., Chemical and biochemical studies for differentiation of coagulase-positive *Staphylococci*. *Arch. Microbiol.* **1976,** *110*, 263-270.
47. Muller, R.; Ruhl, S.; Hiller, K. A.; Schmalz, G.; Schweikl, H., Adhesion of eukaryotic cells and *Staphylococcus aureus* to silicon model surfaces. *J. Biomed. Mater. Res. A.* **2008,** *84A*, 817-827.
48. Park, K. D.; Kim, Y. S.; Han, D. K.; Kim, Y. H.; Lee, E. H. B.; Suh, H.; Choi, K. S., Bacterial adhesion on PEG modified polyurethane surfaces. *Biomaterials* **1998,** *19*, 851-859.
49. Wei, J.; Ravn, D. B.; Gram, L.; Kingshott, P., Stainless steel modified with poly(ethylene glycol) can prevent protein adsorption but not bacterial adhesion. *Colloids Surf. B. Biointerfaces* **2003,** *32*, 275-291.

50. Prime, K. L.; Whitesides, G. M., Adsorption of proteins onto surfaces containging end-attached oligo(ethylene oxide) - A model system using self-assembled monolayers. *J. Am. Chem. Soc.* **1993,** *115*, 10714-10721.
51. Privalov, P. L.; Gill, S. J., The hydrophobic effect - A reappraisal. *Pure Appl. Chem.* **1989,** *61*, 1097-1104.
52. Ogi, H.; Fukunishi, Y.; Nagai, H.; Okamoto, K.; Hirao, M.; Nishiyama, M., Nonspecific-adsorption behavior of polyethylenglycol and bovine serum albumin studied by 55-MHz wireless-electrodeless quartz crystal microbalance. *Biosens. Bioelectron.* **2009,** *24*, 3148-3152.
53. Srinivasaraghavan, V.; Strobl, J.; Agah, M., Microelectrode bioimpedance analysis distinguishes basal and claudin-low subtypes of triple negative breast cancer cells. *Biomed. Microdevices* **2015,** *17*.
54. Lautner, G.; Balogh, Z.; Bardoczy, V.; Meszaros, T.; Gyurcsanyi, R. E., Aptamer-based biochips for label-free detection of plant virus coat proteins by SPR imaging. *Analyst* **2010,** *135*, 918-926.
55. Henry, O. Y. F.; Perez, J. G.; Sanchez, J. L. A.; O'Sullivan, C. K., Electrochemcial characterisation and hybridisation efficiency of co-assembled monolayers of PEGylated ssDNA and mercaptohexanol on planar gold electrodes. *Biosens. Bioelectron.* **2010,** *25*, 978-983.

SUPPLEMENTAL FIGURES:

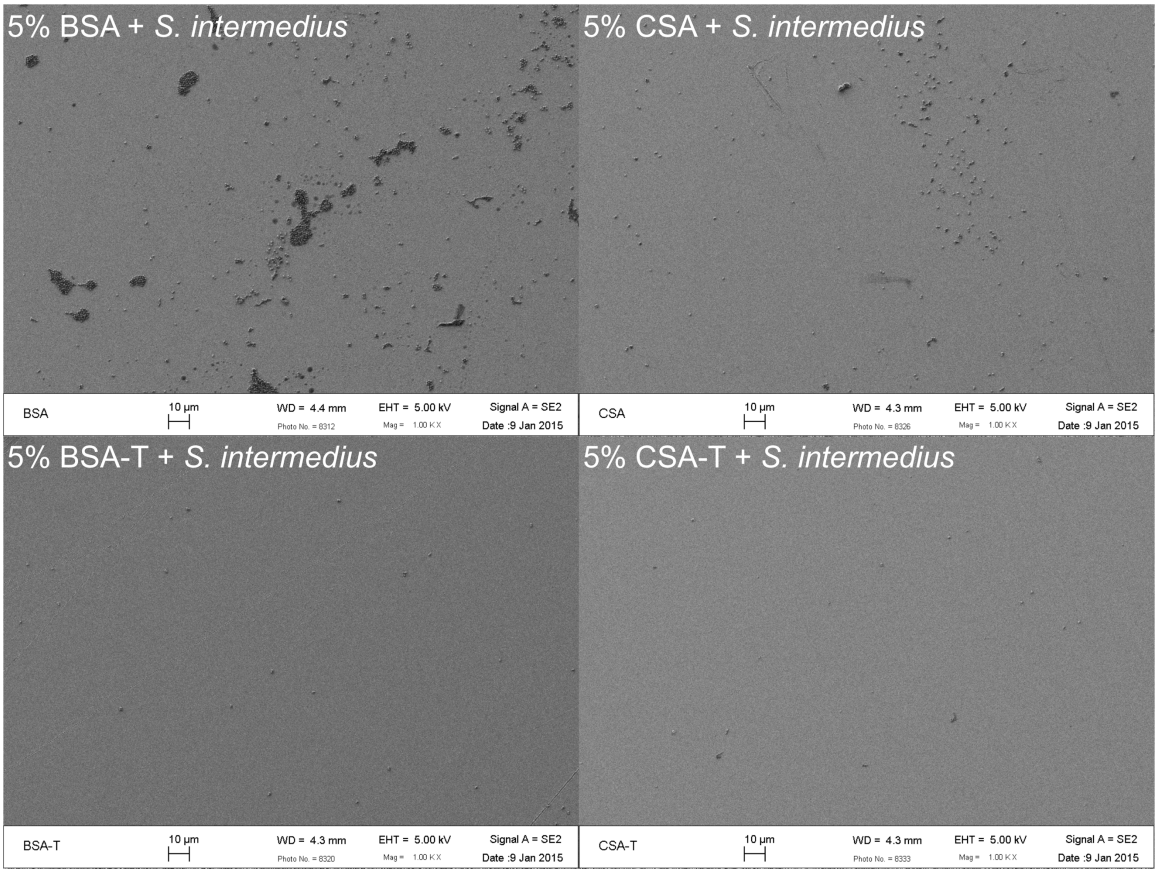

Figure S4.1. Sample SEM images showing difference between BSA Vs. BSA-T AND CSA and CSA-T

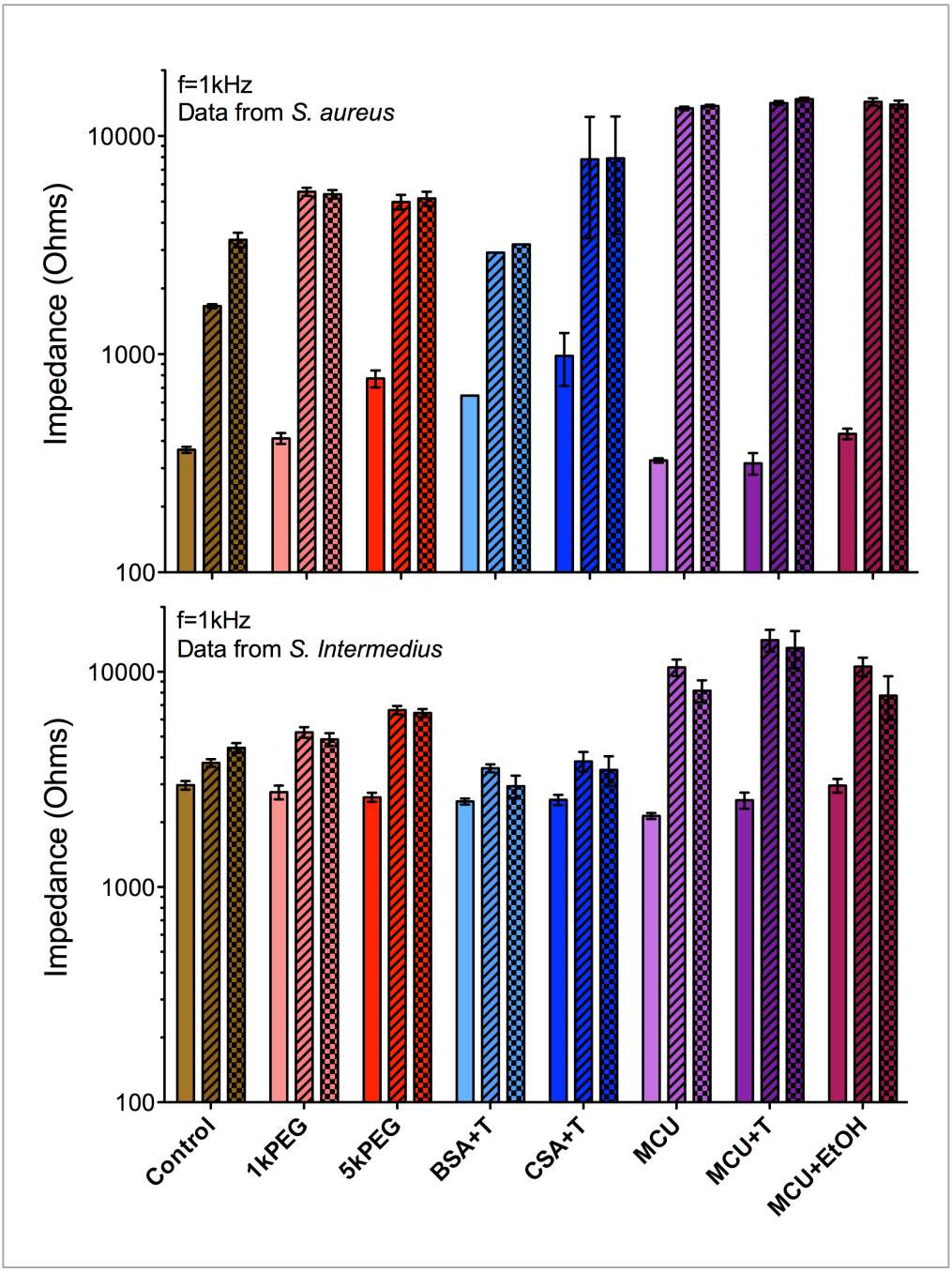

Figure S4.2. Impedance measurements on gold electrodes in PBS before functionalization, after functionalization, and after incubation with bacteria for 2 h. Functionalized gold electrodes were exposed to 50 µL of $2x10^8$ *S. aureus* or *S. intermedius* for 2 h at 37 °C.

CHAPTER 5. Gold nanosensor enabled detection of antibiotic resistance genes for environmental monitoring

Maria V. Riquelme, Weinan Leng, Marcos Carzolio, Amy Pruden, Peter Vikesland.

ABSTRACT

Global strategies for monitoring and mitigating the spread of antibiotic resistance are urgently needed. Here we demonstrate the stability, selectivity and applicability of a gold nanosensor for antibiotic resistance gene (ARG) detection in ARG-spiked effluent from four wastewater treatment plants (WWTPs). The mecA ARG was targeted as a model due to its presence in clinically-relevant pathogens and emergence as an environmental contaminant. The mecA-specific nanosensors showed stability in environmental conditions and in high ionic strength ([MgCl2] < 50 mM), and selectivity against mismatched targets. Target detection was reproducible with an LOD of 70 pM (≈4×107 genes/µL), even in the presence of interferences associated with non-target genomic DNA and complex WWTP effluent. Future work is expected to provide lower LODs via integration with target concentration steps and Surface Enhanced Raman Spectroscopy (SERS)-mediated signal amplification. This provides proof-of-concept for a new line of cost-effective, field-deployable tools needed to support wide-scale ARG monitoring.

INTRODUCTION

Antibiotic resistance is a complex and pervasive public health threat that demands immediate and coordinated global attention.[1, 2] Methicillin resistant *Staphylococcus aureus* (MRSA) is a notorious antibiotic resistant pathogen with the ability to infect multiple tissues and produce toxins. Multidrug resistant MRSA and highly virulent strains, such as USA300, are widespread;[3, 4] while *S. aureus* strains resistant to the antibiotic of last resort, vancomycin, have been reported.[5] *mec*A is the most common ARG detected in MRSA and confers resistance to methicillin and other β-lactam antibiotics.[6, 7] *S. aureus* strains that express this gene are resistant to most, if not all, β-lactam antibiotics. Furthermore, MRSA is commonly known to harbor a broad range of ARGs corresponding to various antibiotic classes.[8, 9]

ARGs can be disseminated from reservoirs of non-pathogenic bacterial hosts and even from naked DNA,[10] which advocates for direct monitoring – particularly in environments that are likely nodes for transfer and amplification (e.g., surface, waste, potable, and reclaimed waters; crop soil; hospitals; and human and animal hosts).[11-13] Wastewater treatment plants (WWTPs) are of special importance as they not only represent a point of ARG convergence, transfer and amplification, but they are also relied upon for inactivation or removal of these contaminants prior to returning treated waters to the environment.[1, 14] Of critical concern is the potential for WWTPs to serve as hot-spots for ARG proliferation.[15, 16] Monitoring WWTPs and their effluents for ARGs can aid in elucidation of their fluxes into the environment and help identify promising treatment technologies. To this end, simple, stable, reliable, fast, efficient and cost-effective ARG monitoring technologies are required.

Gold nanoparticles (AuNPs) are a promising sensing substrate due to their ideal optical properties, stability, and ease of functionalization. Localized surface plasmons (LSPs), or collective oscillations of conduction electrons on the nanoparticle surface, are an important property inherent to metallic nanoparticles. Due to interactions between LSPs and incident light, these particles exhibit extinction cross-sections that are higher than expected based on their size alone. LSP frequency is highly dependent on nanoparticle size and aggregation state and this property can be exploited in aggregation-based detection schemes by monitoring the wavelength of the LSP resonance band (λ_{LSPR}). Furthermore, functionalization of AuNPs with thiol-functionalized oligonucleotides has been previously described and optimized,[17, 18] thereby facilitating their application as gene-specific biosensors.

Here, we applied a sequence-specific target-nanoprobe hybridization assay (Figure 5.1), and demonstrated the applicability of the functionalized nanoprobes for the detection of ARGs in four different treated wastewater effluents. We use *mec*A as a model ARG given its environmental and public health significance. This assay requires minimal sample preparation, does not rely on enzymatic gene amplification, has multiplex application potential, and presents an adaptable platform for environmental monitoring.

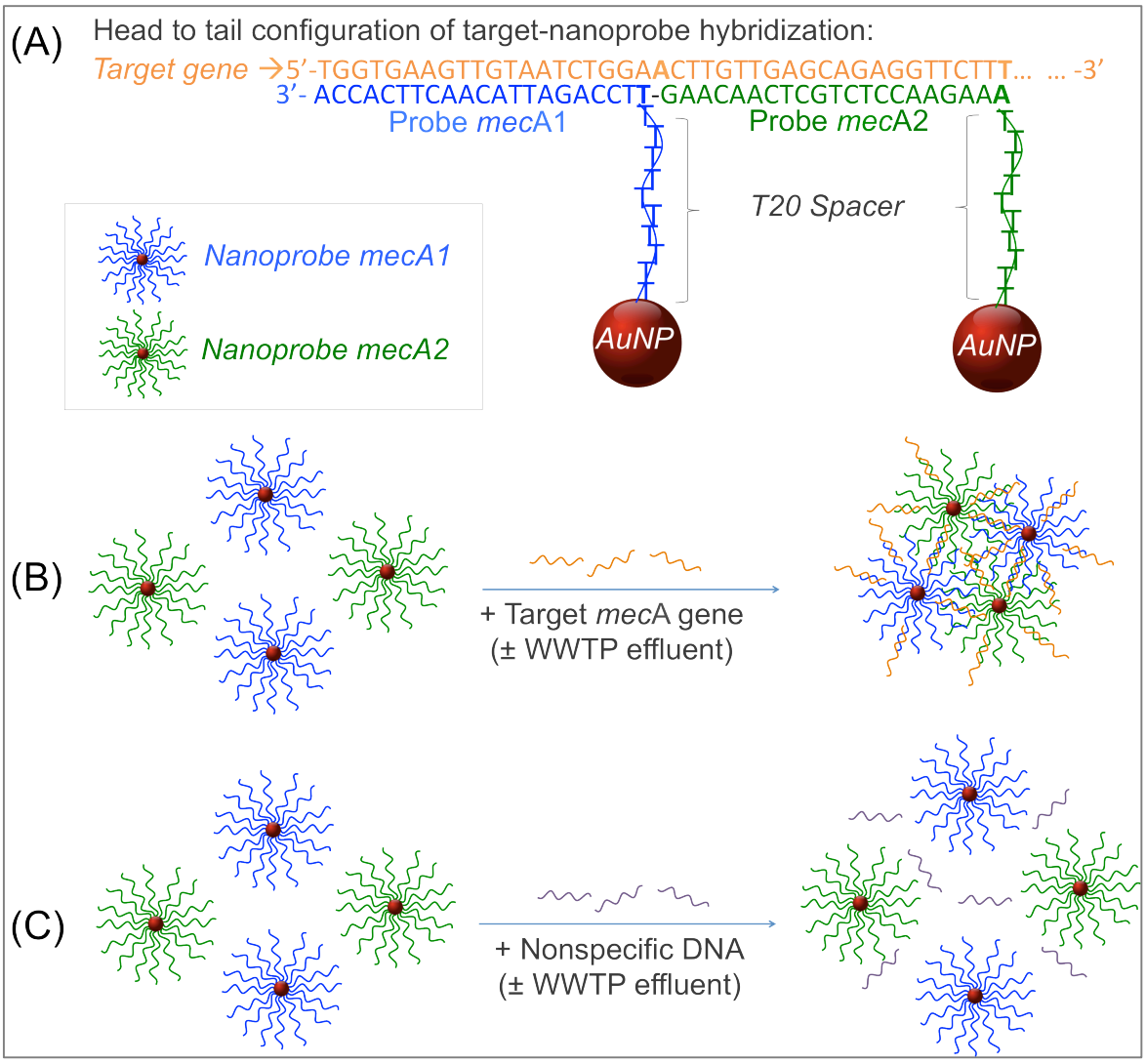

Figure 5.1. Schematic of nanoprobe-DNA interactions. (A) Nanoprobe structure and head-to-tail configuration of nanoprobe-target hybridization. (B) In the presence of target *mec*A gene, nanoprobe-target hybridization induces nanoprobe aggregation, even in the presence of WWTP effluent (C) In the absence of a target gene or in the presence of nonspecific DNA, the nanoprobes remain stably dispersed in solution, even in the presence of WWTP effluent.

MATERIALS AND METHODS

Solutions. All buffers and solutions were prepared using autoclaved nanopure (>18 MΩ·cm) water and molecular biology grade reagents. Phosphate buffered saline (PBS; 137 mM NaCl, 2.7 mM KCl, 10 mM Na_2HPO_4, 1.76 mM KH_2PO_4, pH 7.4) was prepared as a stock solution and autoclaved and diluted as necessary. Chloroauric acid

($HAuCl_4 \cdot 3H_2O$) and sodium citrate dehydrate (99+%) were purchased from Sigma-Aldrich. Citrate buffer (250 mM, pH 3) was prepared by dissolving sodium citrate in water and adjusting the pH using HCl. 5× stock hybridization buffer consisted of 25% formamide, 20% dextran sulfate, and 5 mM $MgCl_2$.[19, 20]

Probe, target and control sequences. *mec*A-specific probe, single-stranded *mec*A target oligonucleotide and nonspecific control oligonucleotide sequences were reported by Storhoff et al.[20] Purified and/or thiolated oligonucleotides were purchased from IDT and are described in Table 5.2. Thiolated probes were activated by incubation in 500 mM DTT in TE buffer.

AuNP synthesis, functionalization and characterization. AuNPs of 42±4 nm diameter (λ_{LSPR} = 532 nm) were prepared via seed-mediated growth.[21, 22] MGITC-AuNPs were prepared by adding diluted MGITC (≈1.5×10^{-7} M) at a ratio of 300 MGITC molecules per AuNP under rapid mixing.[23] MGITC addition enables ARG detection via surface enhanced Raman spectroscopy (SERS); however, SERS-based detection requires optimization and was not evaluated herein. DTT-activated *mec*A-specific probes were subjected to two NAP-10 column purification steps, quantified using the Qbit fluorometer ssDNA quantification kit, and added to MGITC-AuNPs at a ratio of ≈10,000 probes per AuNP in 2 mL Eppendorf tubes (Part # 22363352; Note that other tubes potentially cause AuNP aggregation). The probe-AuNP mixture was vortexed lightly and incubated at room temperature for 30 min. Solution pH was adjusted by addition of citrate buffer (≈25 μL increments every 5 min) up to a 20 mM final concentration.[17] After room temperature incubation for 1 h, the NaCl concentration was adjusted to 300 mM by addition of ≈20 μL aliquots of 5 M NaCl. Note that the citrate buffer and NaCl were added to the inside of the tube lid, then the tubes were closed and vortexed. This process was used to minimize localized high buffer concentrations that may induce AuNP aggregation. After a 30 min room temperature incubation excess 1k-PEG was added as a blocker (at a ratio of ≈50,000 molecules per AuNP) and the PBS-Tween20 concentration adjusted to 1×-0.01%. After 1 h, the particles were washed 3× by centrifugation at 3,000 ×g for 15 min, and resuspended in 1×-0.01% PBS-Tween20. The particles were characterized with an Agilent Cary 5000 UV-Vis-NIR spectrometer and by dynamic light scattering (DLS) with a Malvern Nano-ZS Zetasizer. Characterization by a JEOL 100 CX-II transmission electron

microscope (TEM) was carried out after nanoparticle functionalization. Nanoprobe characteristics are summarized in Figure 5.2.

Sample collection. Local WWTP effluent samples were collected on the day of each experiment in 50 mL tubes, and transported in a cooler (not in ice) to the lab were they were immediately used within 1 hour of collection. In India, the WWTP effluent sample was collected in a 20-gallon container and transported to the lab at around noon. The assay was prepared in the evening at around 9 PM.

Target detection assay. *mec*A gene segments were spiked into four different WWTP effluents to test how potential interferences affect the stability of the assay. A similar approach was reported by Storhoff et al. under controlled conditions;[20] however, we sought to test probe stability and applicability under complex environmental conditions. The characteristics of the WWTP effluents are shown in Table 5.1. Negative controls included unspiked WWTP effluent or effluent containing a nonspecific control oligonucleotide (described in Table 5.2). Nanopure water control samples without wastewater were analyzed for comparison. All reactions contained 10 pM of each nanoprobe, 1× hybridization buffer (5% formamide, 4% dextran sulfate, 1 mM $MgCl_2$), target (T) or nonspecific (NS) oligonucleotides (based on dilutions prepared from concentrated purified oligonucleotide purchased from IDT, Coralville, IA), and 50% WWTP effluent where applicable. After mixing, the samples were denatured for 5 min at ≈98°C and then room temperature-hybridized. An additional test was carried out using genomic MRSA DNA (containing the *mec*A gene) as target, while the probe and buffer concentrations remained constant. A schematic of nanoprobe-target configuration and expected interactions is shown in Figure 5.1.

Table 5.1. WWTP effluent characteristics

WWTP	Capacity (MGD)	TSS (mg/L)	BOD (mg/L)	DO (mg/L)	pH
A[a]	6	3.1	4.0	7.3	7.0
B[a]	9	1.6	2.5[b]	8.3	7.6
C[a]	6	4.0	2.0	8.2	7.3
India[c]	14	-	-	5.3	7.9

[a] Daily averages obtained from WWTP
[b] Values not available for day of sampling and substituted by next day average
[c] Actual sample values measured on day of sampling

Target probe-hybridization kinetics. Hybridization kinetics were monitored using an Agilent Cary 5000 UV-Vis-NIR spectrometer and Scanning Kinetics software. After denaturing, the 200-μL samples were transferred to the ultra-microcuvettes used for analysis. UV-Vis spectra between 350-800 nm were acquired every 15 min for the first two hours and every hour thereafter.

Melting temperature (T_m) analysis. First derivative T_m analyses at λ=535 nm were carried out using the UV-Vis-NIR spectrometer and a temperature controller. UV-Vis spectra were collected between 25-75°C at 1°C intervals with 1 min/degree incubation.

Limit of detection (LOD) determination. Data fitting and LOD determination were carried out in R Version 3.2.1 using the lme4 package version 1.1-12 and a Bootstrap function. A linear mixed effects model was applied to compare λ_{LSPR} values at zero target concentration in the presence and absence of WWTP effluent. This model was applied by considering potential correlations within nanoprobe batches or within experimental runs as random effects and the different media (i.e., WWTP effluent from different plants or control nanopure water) as fixed effects. Because no significant difference was observed among λ_{LSPR} values at zero target concentration, these were grouped and averaged for LOD determination. A cubic polynomial curve was fitted to the log-transformed λ_{LSPR} data corresponding to the non-zero target concentration; then, a bootstrap function was applied in order to determine 95% confidence intervals to the fitted curve (Figure 5.11). Bootstrapping results suggested a lower LOD range between 13 and 23 pM, where the non-zero concentration λ_{LSPR} values were significantly higher than the zero concentration λ_{LSPR} values with 95% confidence. Employing a safety factor of 3× the highest value of this range, a conservative LOD of 70 pM is reported herein. An upper LOD of about 90 nM was also determined.

qPCR quantification of background* mec*A levels in WWTPs. DNA from WWTP effluents was extracted from solids retained in a 0.22 μm polycarbonate filter membrane after filtering a 200 mL volume (Note that the effluent used for these measurements was collected on a different day than the effluent used in the nanoprobe assays). DNA extraction was carried out using the MP-BIO Soil Spin Kit. Quantitative polymerase chain reaction (qPCR) of 1:20 extract dilutions was applied to quantify background 16S, mecA,

and nuc genes in WWTP effluents using a BioRad CFX96 Touch™ Real-Time PCR detection system and primers described by Suzuki et al.[1] (16S rRNA), Volkmann et al.[2] & Oliveira et al.[3] (*mec*A forward and reverse primers, respectively), and Graber et al.[4] (*nuc*). The latter (*nuc*) gene is specific to *S. aureus* thermonuclease. The 10 µL reactions consisted of 40 nM of each primer, 1× SsoFast™ EvaGreen® Supermix (BioRad), 1 uL of template DNA, and molecular biology grade water.

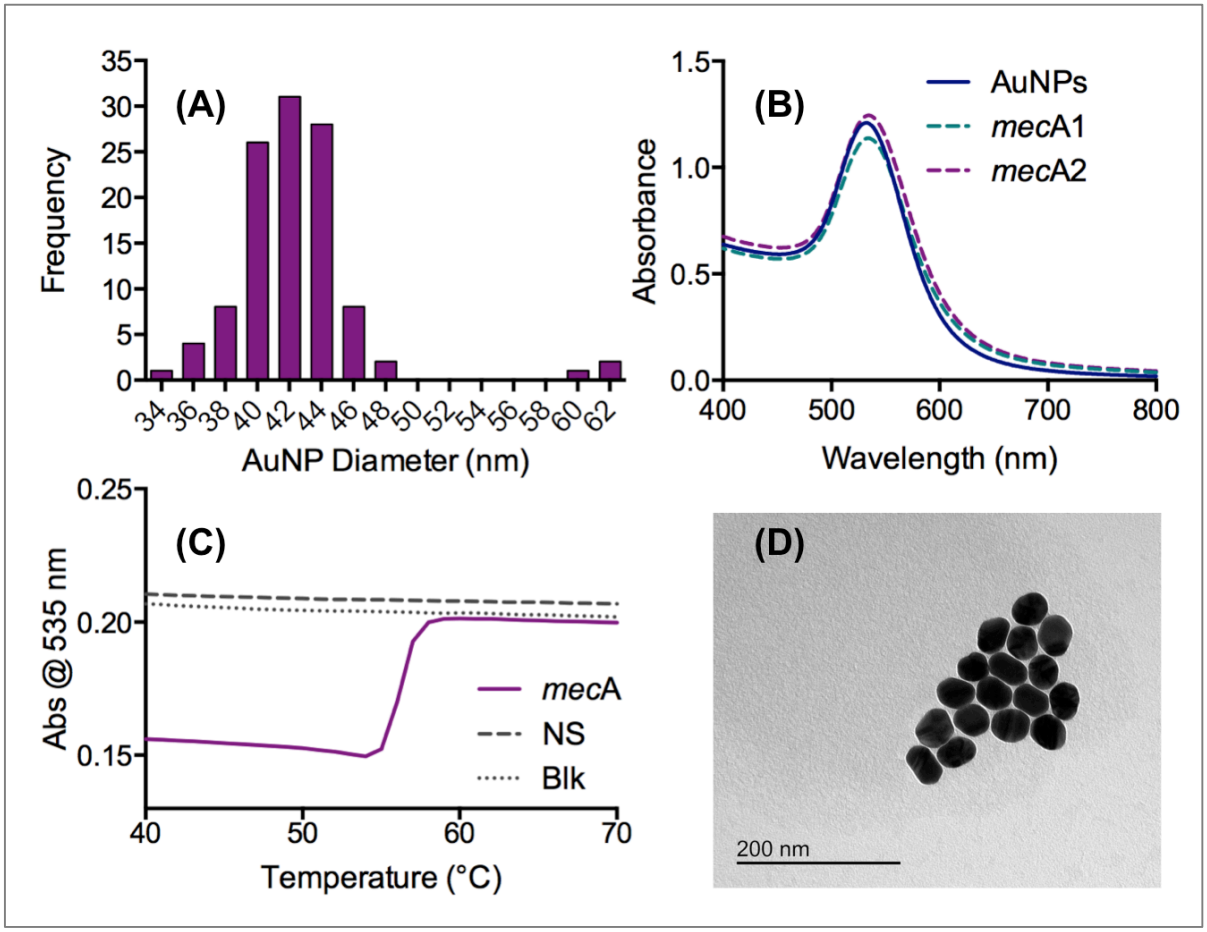

Figure 5.2. Characterization of AuNPs and nanoprobes. (A) Size distribution of AuNPs based on TEM and ImageJ analysis of 111 nanoprobes (Average diameter = 42 nm, StDev = 4). (B) UV-Vis absorption spectra of freshly prepared AuNPs (λ_{LSPR} = 532 nm) and *mec*A1 and *mec*A2 functionalized nanoprobes (λ_{LSPR} = 534-535 nm). (C) Representative melting temperature analysis results of target-nanoprobe hybridized complexes (T_m= 56.8 ± 0.5 °C, n=4). (D) TEM image of nanoprobes.

RESULTS AND DISCUSSION

Target-nanoprobe hybridization-based assay. Our detection scheme relies on sequence-specific nanoprobe-target hybridization. A head-to-tail configuration for target-nanoprobe hybridization was applied as illustrated in Figure 5.1A. This configuration maximizes detection response by minimizing inter-particle distance, as compared to a tail-to-tail configuration, while also minimizing the potential steric hindrance expected for a head-to-head configuration.[24] We functionalized AuNPs with two *mec*A-specific oligonucleotide probes. In the presence of the target oligonucleotide, these functionalized nanoprobes are expected to bind to the gene of interest via sequence-specific hybridization events (Figures 5.1A&B). These binding events induce nanoparticle aggregation, which causes a redshift in the LSPR band that can be detected spectrophotometrically. Our nanoprobes exhibited a λ_{LSPR}=535 nm in the dispersed state. Upon aggregation, a redshift occurs, resulting in change in a change in suspension color indicative of target detection (Figure 5.3). A redshift was observable even in the presence of interferences characteristic of WWTP effluents, including variable ionic strength and natural organic matter content.

Nanoprobe selectivity and stability. Target-specific interaction was confirmed by T_m analyses using both nanopure and WWTP effluent as diluents. Here, the probes were incubated with either a 100% matching DNA sequence, a variety of mismatched targets (containing 1, 3, 5, and 10 base mismatches per binding site; Table 5.2), or in the absence of added DNA for three to four hours. Hybridization and corresponding melting temperatures were observed only in the presence of targets with zero and one mismatch as evidenced by a sharp change in absorbance due to the blueshift caused by the release of hybridization-aggregated particles back into a dispersed state. No hybridization was observed in the presence of targets with three or more mismatched bases (Figure 5.4). In the presence of targets with zero and one mismatch, the *Tm* were found to be 56.8 °C (± 0.5 °C, n=4) and 47.7 °C (± 0.6 °C, n=3) in nanopure water, respectively; and 59 °C and 48.35 °C, respectively, in the presence of WWTPA effluent. In each case, the *Tm* difference was nearly 10 °C, suggesting that the probes are highly specific above ~50 °C. Important to note, due to codon degeneracy, one mismatch may still translate into an identical and functional protein. For a subset of samples prepared with a 100% matching

target and nanopure water as diluent, an initial T_m analysis was done four hours after denaturing. Thereafter, the samples were allowed to rehybridize with the target and the T_m measurement was repeated once again (twice for one sample), yielding a slight (up to one degree) increase in T_m each consecutive cycle. The reproducibility of the T_m results after repeated denaturing and hybridization provides further evidence that the nanoprobes are stable and suggests they may be reusable after a simple denaturing and separation step.

Table 5.2. Probe, target and control oligonucleotide sequences and specifications

	Sequence	nts	Functionalization	Purification
Target *mec*A segment[a]	5'-TGGTGAAGTTGTAATCTGGAACTTGTTGAGCAGAGGTTCTTTTTTATCTTGGGTTAATTTATTATATTCTTCGTTACTCATGCCAT-3'	86	N/A	PAGE
Nonspecific control[a]	5′-ATGGCATGAGTAACGAAGAATATAATAAATTAACCCAAGATAAAAAAGAACCTCTGCTCAACAAGTTCCAGATTACAACTTCACCA-3'	86	N/A	PAGE
1 mismatch per binding site	5′-TGGTGAAGTGGTAATCTGGAACTTGTTGAGCACAGGTTCTTTTTTATCTTGGGTTAATTTATTATATTCTTCGTTACTCATGCCAT-3'	86	N/A	PAGE
3 mismatches per binding site	5'-TGGTTAAGTTCTAATCTGAAACTTGTTTAGCACAGGTTCCTTTTTATCTTGGGTTAATTTATTATATTCTTCGTTACTCATGCCAT-3'	86	N/A	PAGE
5 mismatches per binding site	5'-TGGTTACGTTCTAATCTCAAACTTCTTTAGCACAGGATCCTTTTTATCTTGGGTTAATTTATTATATTCTTCGTTACTCATGCCAT-3'	86	N/A	PAGE
10 mismatches per binding site	5'-TCGTTTCGGTCCAAGCTCAAACTACTTTGGTACATGATCCGTTTTATCTTGGGTTAATTTATTATATTCTTCGTTACTCATGCCAT-3'	86	N/A	PAGE
Probe1[a,b]	5'-Thiol-T_{20}-TTCCAGATTACAACTTCACCA-3'	21	5ThioMC6-D	HPLC
Probe2[a,b]	5′-Thiol-T_{20}-AAAGAACCTCTGCTCAACAAG-3'	21	5ThioMC6-D	HPLC

[a] Sequences were reported by Storhoff et al.[5]
[b] Each probe contained a spacer of 20 thymine bases denoted as T_{20}.

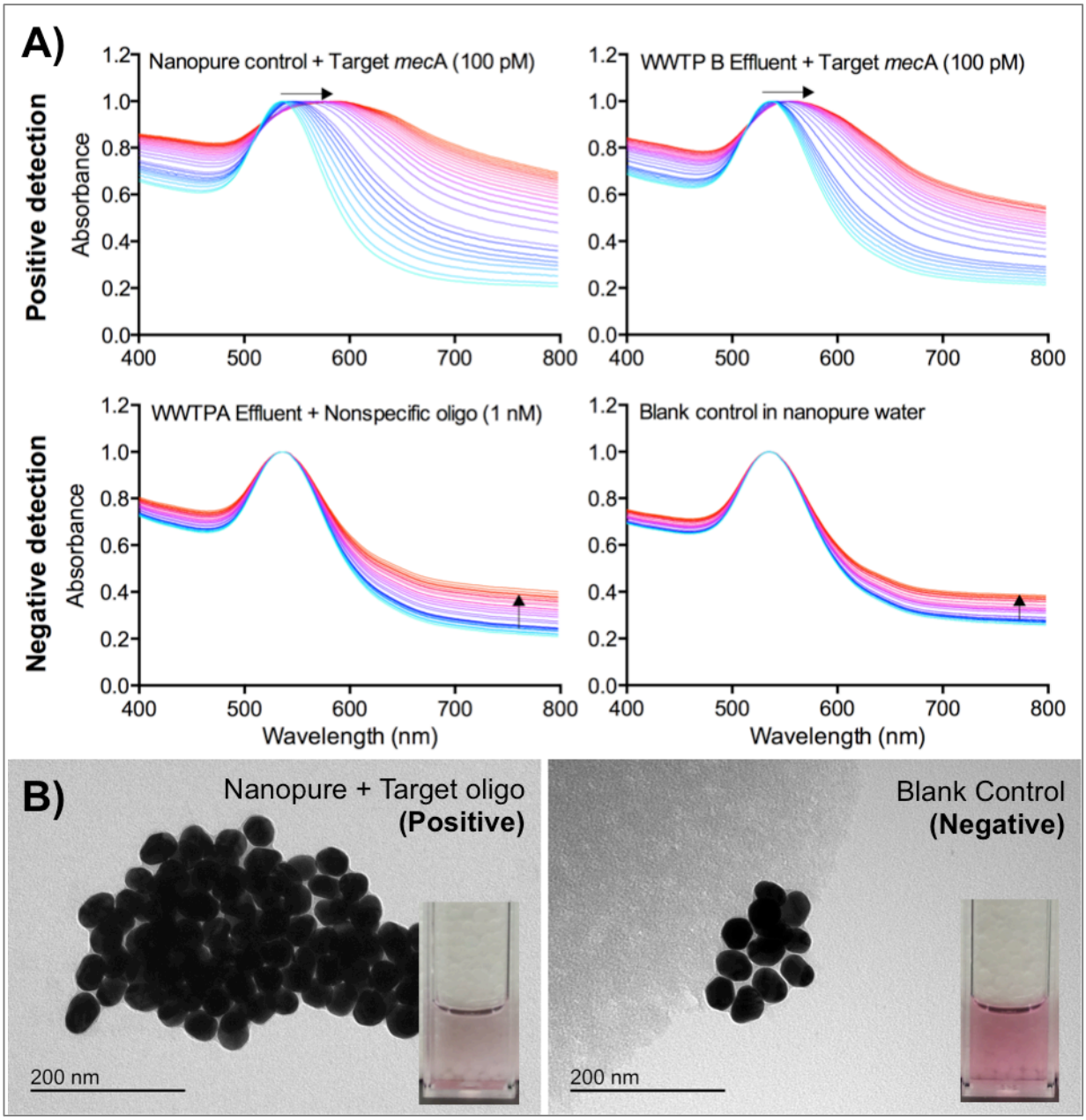

Figure 5.3. Monitoring and characterization of hybridization-induced nanoprobe aggregation: (A) Typical sample scanning kinetics results in presence and absence of WWTP effluent and/or target *mec*A gene (Arrows indicate spectral evolution with increasing time. Normalized spectra are shown); and (B) TEM and solution images in the presence or absence of target-induced nanoprobe aggregation.

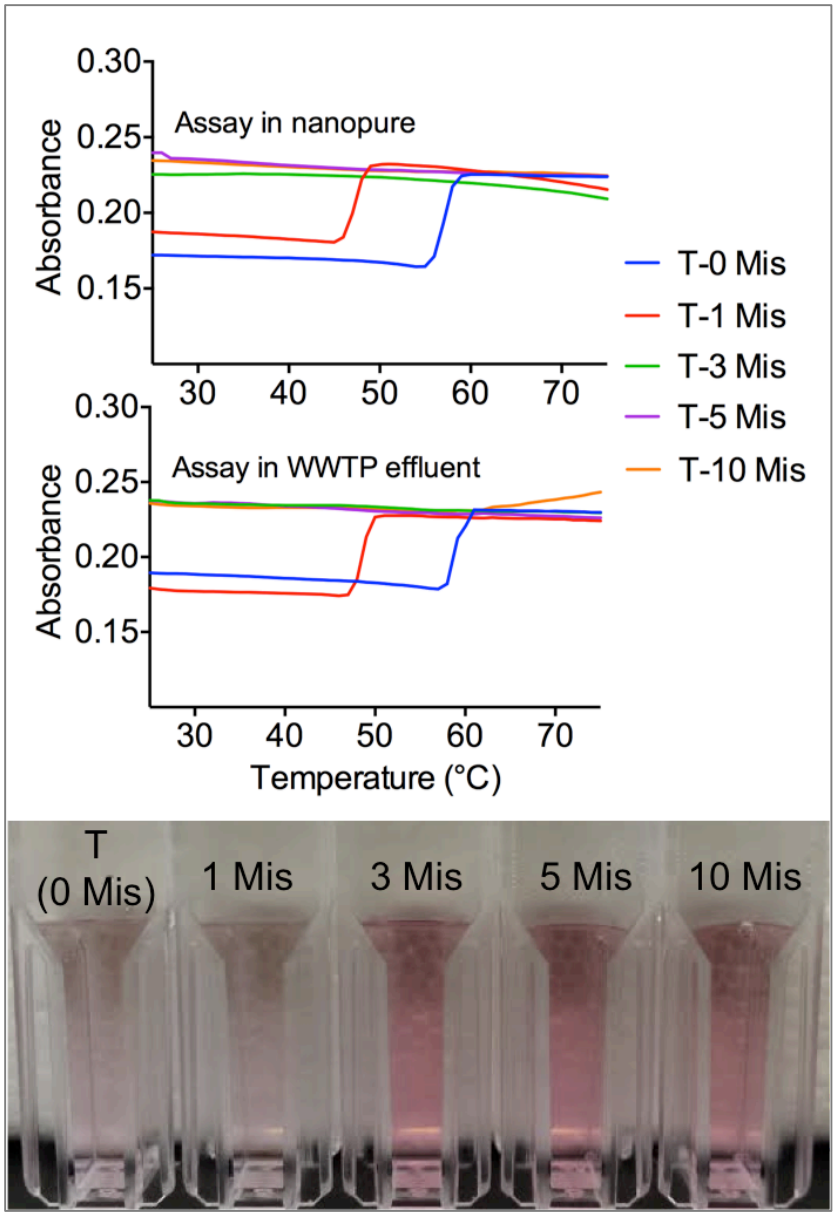

Figure 5.4. Melt curve analyses of nanoprobe-target hybrids in the presence of targets with a range of sequence mismatches. Targets with 0, 1, 3, 5 and 10 mismatches per nanoprobe binding site (T-0 Mis to T-10 Mis) were analyzed in the absence (top; control assay in nanopure) and presence (center) of WWTP effluent from WWTP A. The *Tm* in the nanopure control were found to be 56.8 °C (± 0.5 °C, n=4) and 47.7 °C (± 0.6 °C, n=3) for T-0 Mis and T-1 Mis, respectively. In WWTP effluent, the *Tm* were 59 °C and 48.35 °C for T-0 Mis and T-1 Mis, respectively. No hybridization was observed in the presence of targets with 3 or more mismatches. A picture of the assay product in WWTP effluent is shown on the bottom.

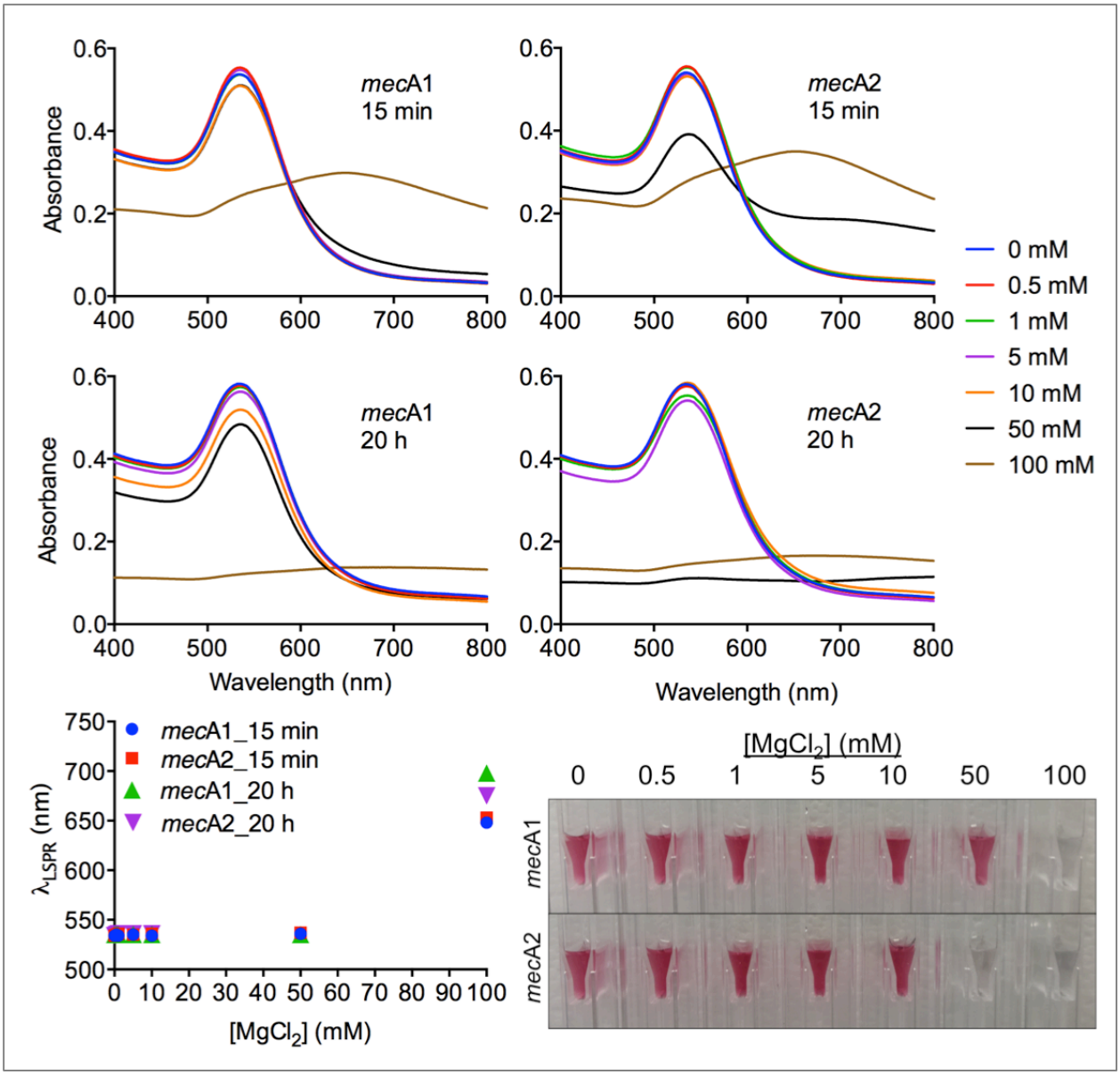

Figure 5.5. Nanoprobe stability in $MgCl_2$. Nanoprobes were pelleted at 3000 ×g for 5 min, and then resuspended in the specified $MgCl_2$ concentration after removing the supernatant. UV-Vis absorption spectra were collected after 15 min (top) and after 20 h (center). The λ_{LSPR} values were plotted against $MgCl_2$ concentration (bottom left). An image of the nanoparticle solution was collected after 20 h (bottom right).

The stability of oligonucleotide-functionalized AuNPs in monovalent and divalent cation solutions has been previously described.[17, 18, 25] In general, oligo-AuNPs are known to be stable in up to 1 M NaCl. However, stability is generally dependent upon oligonucleotide size, composition, and base-pairing potential.[25] Here we further assessed our nanoprobe

stability by pelleting and resuspending over a range of $MgCl_2$ concentrations (Figure 5.5). Our results suggest that the nanoprobes are highly stable in [$MgCl_2$] < 50 mM. Nanoprobe stability was further assessed by UV-Vis and DLS analyses over 20 h in environmentally-relevant EPA moderately hard water. No λ_{LSPR} redshift was observed after 20 h (Figure 5.6), suggesting that the particles remained stable in the presence of monovalent and divalent cations. A gradual decrease in nanoprobe size (3.7 and 5.5 nm after 20 h for probes *mec*A1 and *mec*A2, respectively) was observed via DLS (Figure 5.6). This decrease in hydrodynamic diameter is likely the effect of inter- and/or intra-oligonucleotide charge shielding induced by the added divalent cations, which resulted in more tightly packed oligonucleotide secondary structures. The nanoprobe Zeta potential was also measured in PBS-T at -20.2 and -24.0 mV for probes *mec*A1 and *mec*A2, respectively.

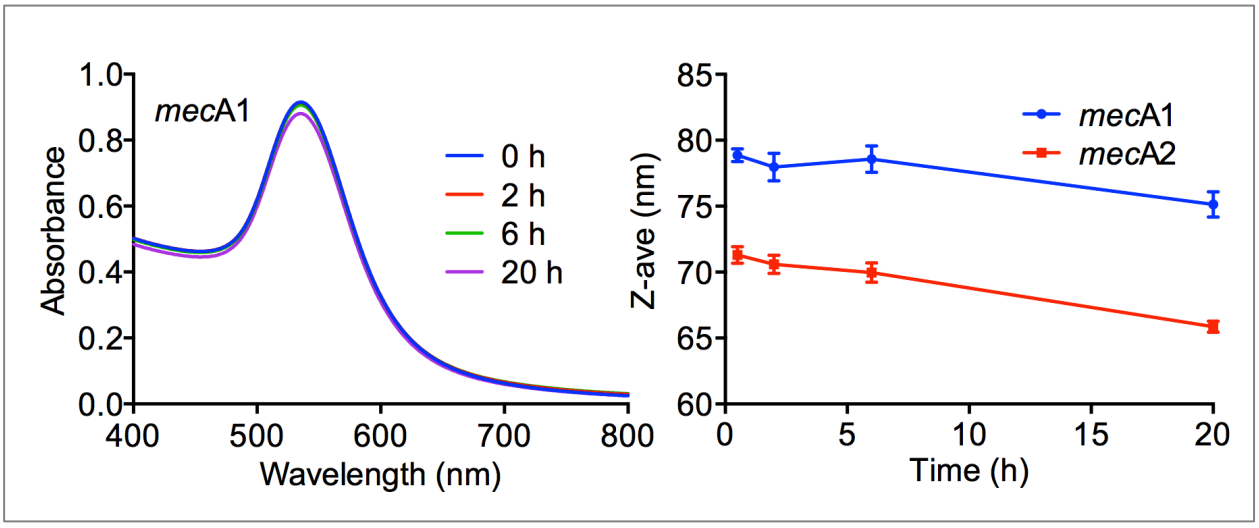

Figure 5.6. UV-Vis Absorbance (left) and DLS size measurements (right) of nanoprobes in EPA moderately hard water over 20 h. The Absorbance spectra for nanoprobe *mec*A2 are not shown, but are almost identical to the spectra shown for nanoprobe *mec*A1 on the left.

mecA detection in WWTP effluent. The *mec*A detection assay was tested in the presence of WWTP effluents from four WWTPs, including one from a large metropolitan city in India, in order to quantify the functionality in the presence of potential interferences. The nanoprobes were consistently stable and performed comparably in WWTP effluent relative to nanopure water. This suggests that potential interferences by varying ionic strength, complex organic matter, chelators, and other unknown constituents may not

post the kind of barrier that they do for enzyme-based detection assays, such as polymerase chain reaction (PCR).[26]

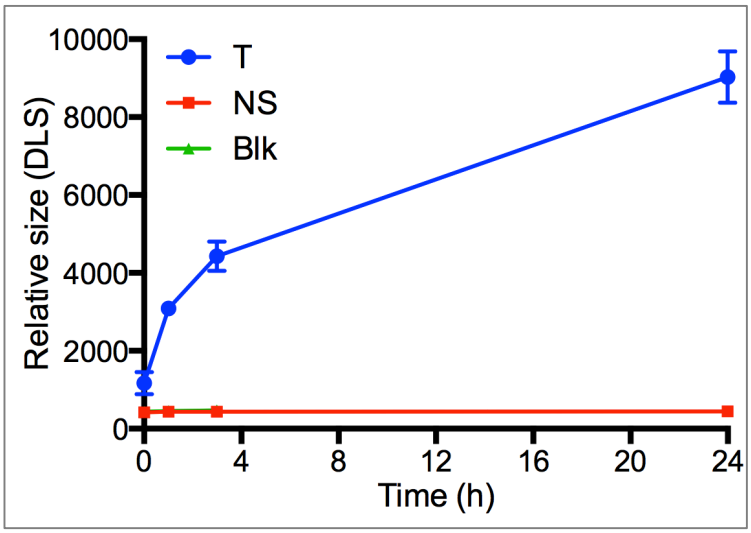

Figure 5.7. DLS monitoring of particle size changes due to hybridization-induced aggregate formation. Target (T) and nonspecific (NS) oligo concentrations were 50 nM. Important Note: Aggregate size values measured via DLS represent estimates for relative comparison between aggregated and nonaggregated samples rather than actual accurate particle size measurements. This limitation is because the accuracy of the measurements is affected by particle size polydispersity, which is high in aggregated samples; thus, as particles aggregate, the data becomes increasingly inaccurate.

The target detection assays were repeatable both in the presence and absence of WWTP effluent. Figure 5.3A provides a comparison of typical scanning kinetics results under different test conditions. A clear redshift of the LSPR band is observed in the presence of *mec*A, whereas no LSPR shift was observed in the absence of target or in the presence of a nonspecific control oligonucleotide. A clear difference can be observed visually as a result of target-induced nanoprobe aggregation (Figure 5.3B). Aggregation was further confirmed by TEM images of aggregates formed in the presence and absence of *mec*A gene segments (Figure 5.3B) and by DLS monitoring (Figure 5.7). Although small aggregates associated with the edge of visible droplets were observed in TEM images of samples prepared in the absence of the target, these small aggregates are thought to be the result of sample drying during grid preparation rather than the product of interactions between the particles within the sample. Conversely, the larger aggregates observed in

the target samples were consistently larger matrices that occurred in lower frequency and were not associated with the edges of the dry droplets.

Hybridization and nanoprobe aggregation kinetics were monitored for 16-24 h after the initial denaturing step. Nanoprobe aggregation occurred quickly during the first 3-5 h, and then more gradually up to about 10 h (Figures 5.8 and 5.9). Thereafter, a plateau was reached where the λ_{LSPR} either remained constant (for most samples) or increased slightly (for some samples). Boxplots compare the λ_{LSPR} values between t= 10 h and t=16 h (Figure 5.10). Narrower boxes reflect a relatively steady λ_{LSPR}, whereas wider boxes indicate a higher rate of λ_{LSPR} increase. An LOD of 70 pM ($\approx 4\times10^7$ genes/μL) was determined as described in the Supporting Information. Although this LOD is high in its present form, this study provides proof-of-concept to support future optimization. For example, a significant LOD decrease may be attained after integrating target concentration and SERS-mediated signal amplification into the assay.

An upper limit to the detection range was also observed. The upper and lower detection limits likely are constrained by different factors. At low *mec*A concentrations, there is insufficient target to induce an observable hybridization-induced LSPR redshift. Conversely, at high *mec*A concentrations, nanoprobe binding sites become saturated, thereby minimizing or preventing aggregate formation. Our data suggest that the optimum nanoprobe-to-target ratio should be between 1:7 to 1:9000. However, these ratios may change depending on the target concentration and on the method of detection. For instance, SERS should theoretically detect one molecule in the presence of two probes, granted that they are located within the same sample.

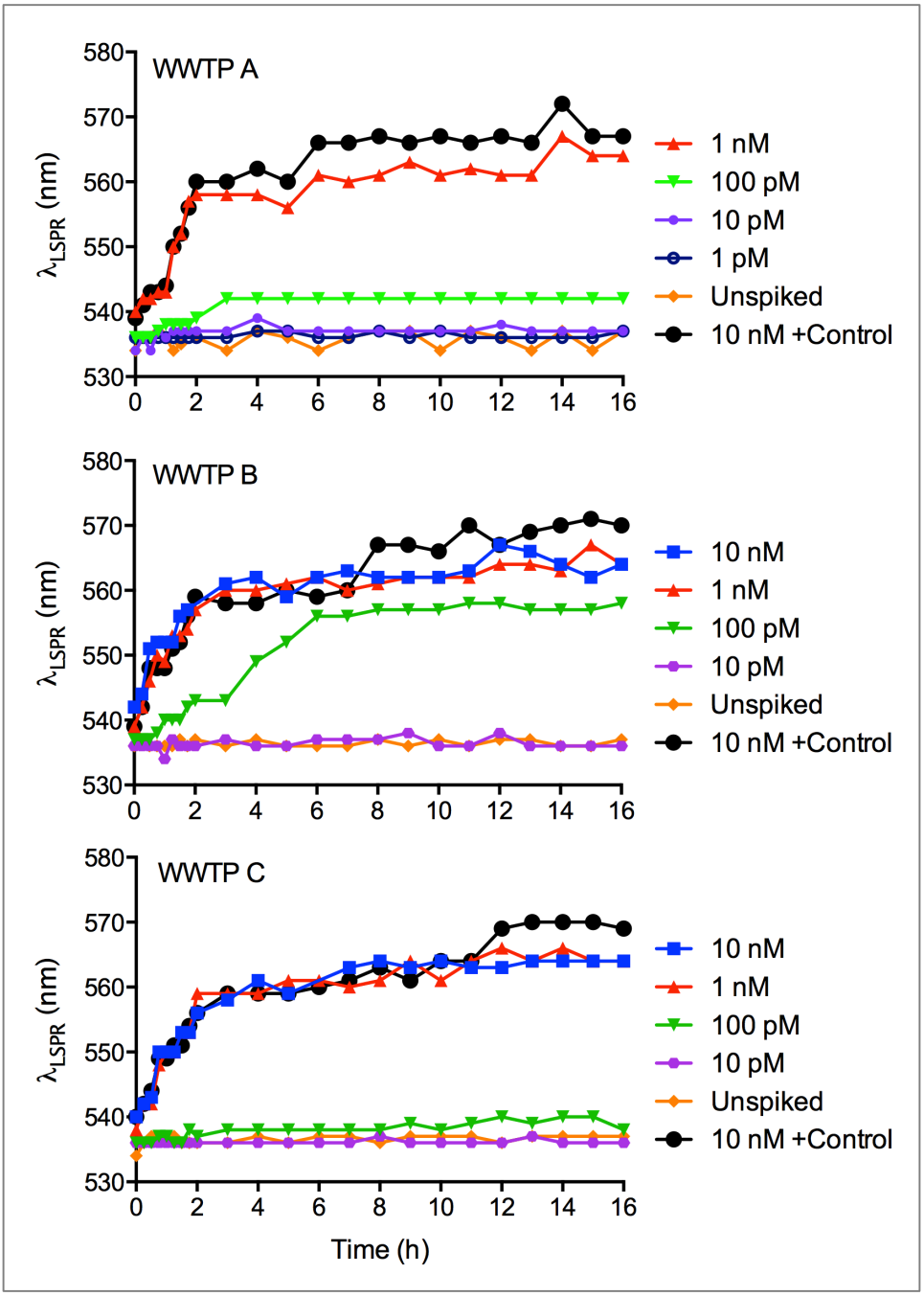

Figure 5.8. λ_{LSPR} shift during real-time scan of hybridization kinetics in WWTP samples for a range of target *mec*A gene concentrations.

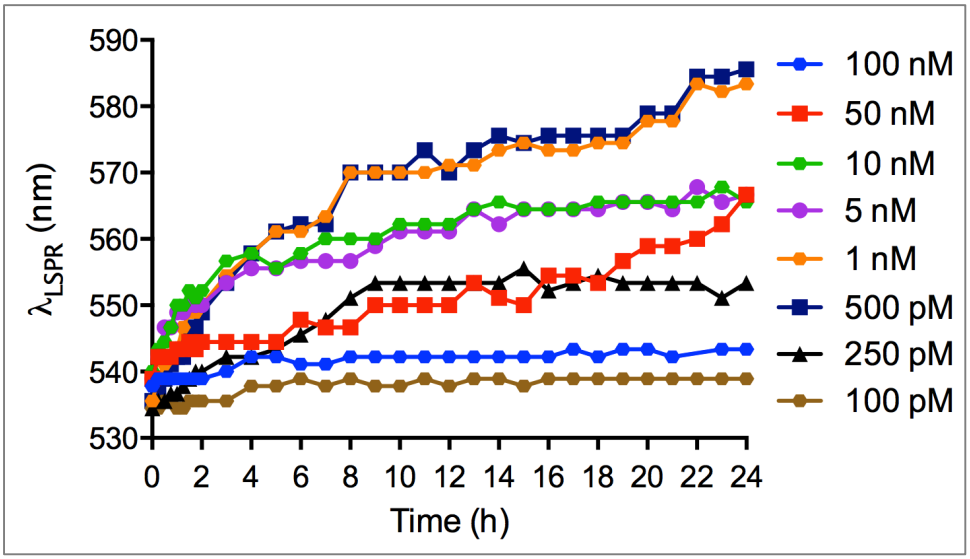

Figure 5.9. LSPR shift during real-time scan of hybridization kinetics in nanopure control samples for a range of target *mec*A gene concentrations.

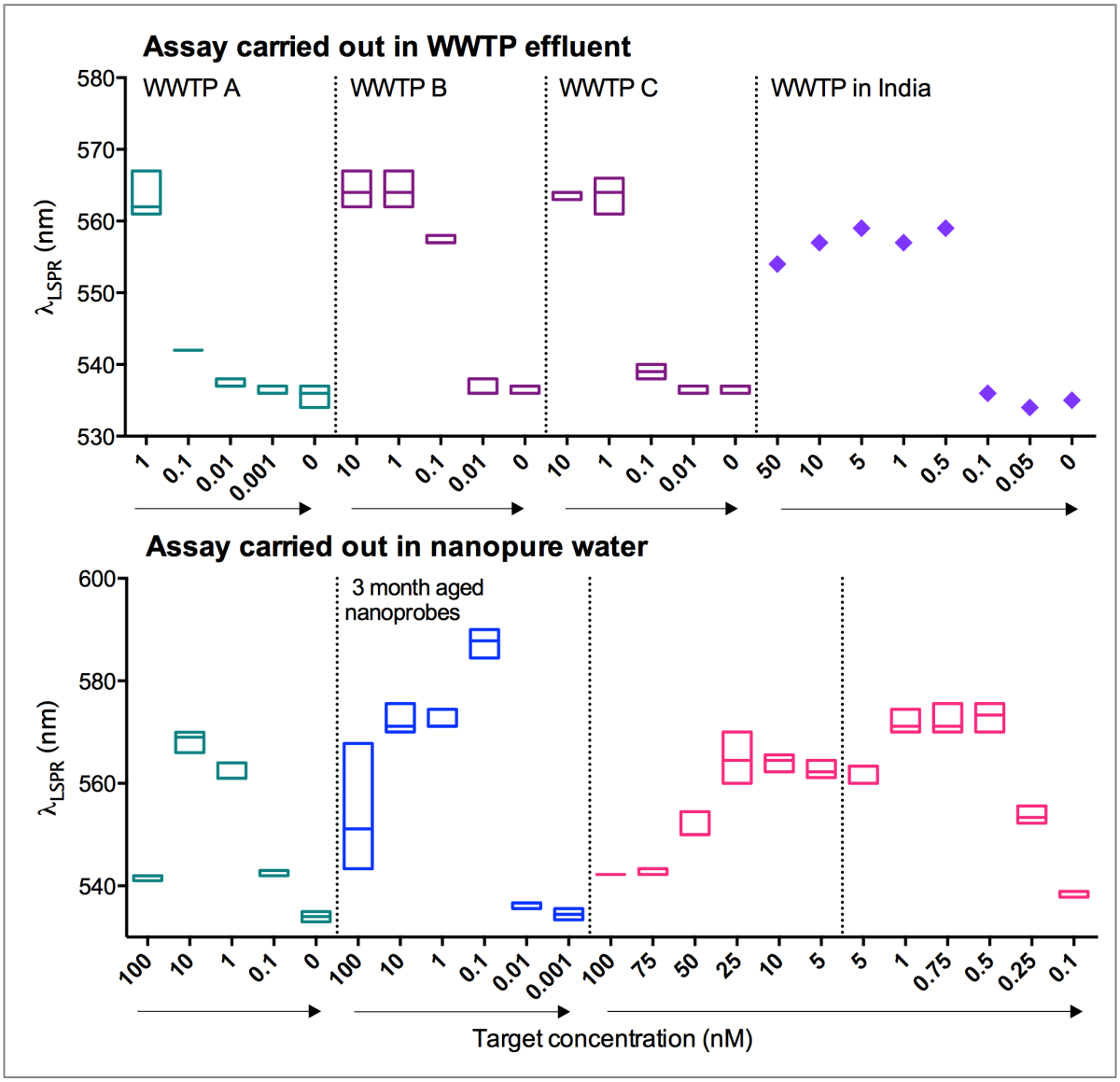

Figure 5.10. Target *mec*A detection in presence (top) and absence (bottom) of WWTP effluents. Boxplots represent maximum absorbance wavelengths observed between t=10 h and t=16 h. A single point at t=18 h is shown for samples tested in presence of effluent from a WWTP in India. Higher absorbance indicates redshift due to hybridization-induced nanoprobe aggregation, and thus indicates positive detection. Different colors represent different nanoprobe batches. Arrows indicate decreasing target *mec*A gene concentrations. The results of an experiment performed using 3-month old nanoprobes (stored at 4 °C) are shown for comparison as an indicator of the stability of reagents with time. All experiments in presence of WWTP effluents were done in presence of a positive control in nanopure water (data not shown). A nonspecific control was also tested in nanopure water, and in WWTP A and Indian WWTP effluents, and showed no interaction (results not shown).

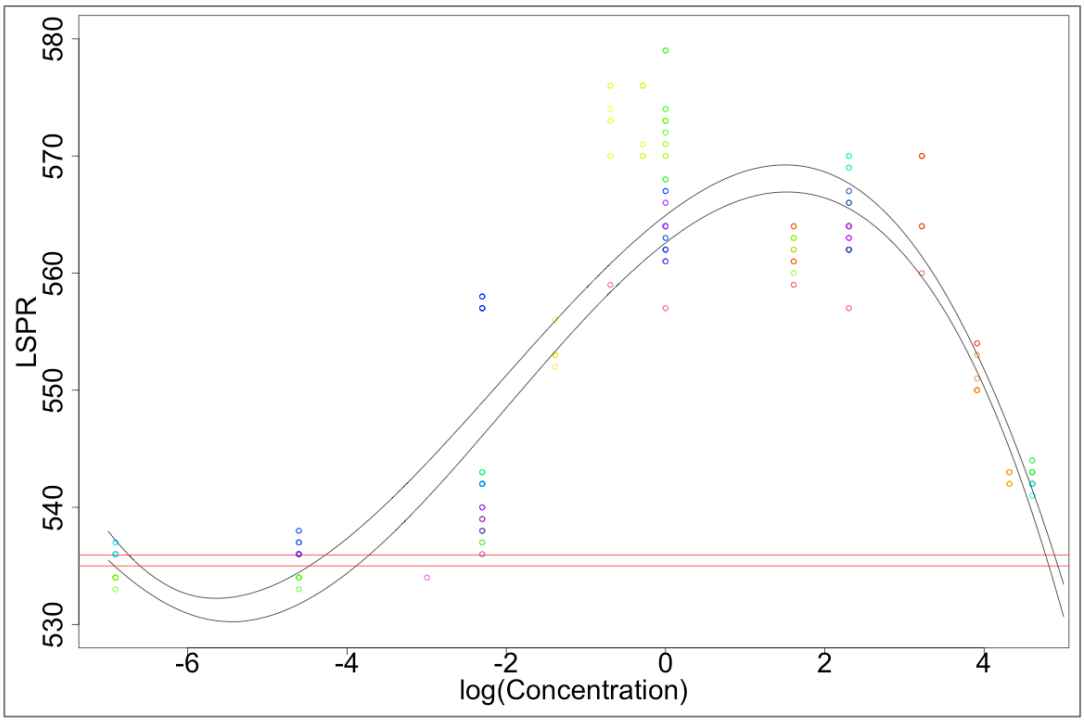

Figure 5.11. Data fitting and Limit of Detection (LOD) determination. The black curves represent the Bootstrap-generated 95% confidence intervals for a cubic polynomial fit to the log-transformed non-zero concentration λ_{LSPR} data. The upper and lower horizontal red lines represent two-times the standard error of the averaged λ_{LSPR} data at zero target concentration. Application of a linear mixed effects model confirmed that the type of medium (i.e., presence or absence of WWTP effluent) had no significant effect on the λ_{LSPR} values at nonzero target concentration. Bootstrapping results suggested a lower detection range between 13 and 23 pM target concentration where the non-zero concentration λ_{LSPR} values were significantly larger than the zero concentration λ_{LSPR} values. However, a conservative LOD of 3× the highest value in that range, or 70 pM (≈4×10^7 genes/μL), is reported.

Detection of mecA associated with genomic and non-target environmental DNA. In addition to a single-stranded *mec*A gene segment, we also tested the performance of the nanoprobes for detecting *mec*A present in genomic DNA extracted from MRSA. A sample containing DNA extracted from MRSA-negative digested sludge served as a negative control. These results (Figure 5.12) illustrate that the assay is suitable for detection of the *mec*A gene within complex genomic DNA.

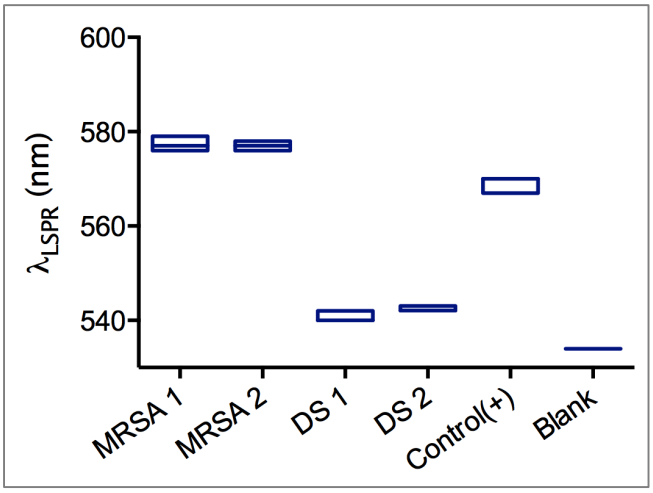

Figure 5.12. *mec*A gene detection from a genomic MRSA DNA extract (MRSA 1, MRSA 2) and from a MRSA-negative digested sludge DNA extract (DS1, DS2), compared to positive control (Control(+)- 5 nM target in single stranded form) and blank (nanoprobes only, with no added DNA). MRSA and DS assays were carried out in duplicates. Boxplots represent maximum absorbance wavelengths observed between t=10 h and t=16 h. Higher absorbance indicates redshift due to hybridization-induced nanoprobe aggregation, and thus indicates positive detection.

Effluent gene concentrations and future work. Now that nanoprobe chemical and thermal stability has been established, future work will focus on developing and optimizing assays with lower LODs. Environmental ARG concentrations are generally low. Herein, both the *S. aureus*-specific *nuc* gene and the methicillin resistance-specific *mec*A ARG were detected in at least one effluent sample from the WWTPs applied in this study (Figure 5.13); however, their concentrations were below the standard concentration range and thus unquantifiable. Others have detected *mec*A in WWTP effluents via quantitative PCR.[27, 28] It is well-known that ARGs can be detected at higher concentrations in samples from highly impacted environments, such as hospital wastewater and agricultural runoff,[13, 27, 29] and that some WWTP processes can influence the proliferation of ARGs.[15, 16] Still, low levels of ARGs may also have environmental relevance, which we envision could be addressed in part through incorporating a DNA extraction and concentration step. Further, coupling of this nanosensor technology with target concentration nanocomposites may enable simultaneous SERS detection of multiple ARGs in addition to significantly lowering the LOD. Thus, the nanosensors examined herein show great

potential due to their stability and selectivity in complex media and are a promising means for rapid ARG detection and monitoring.

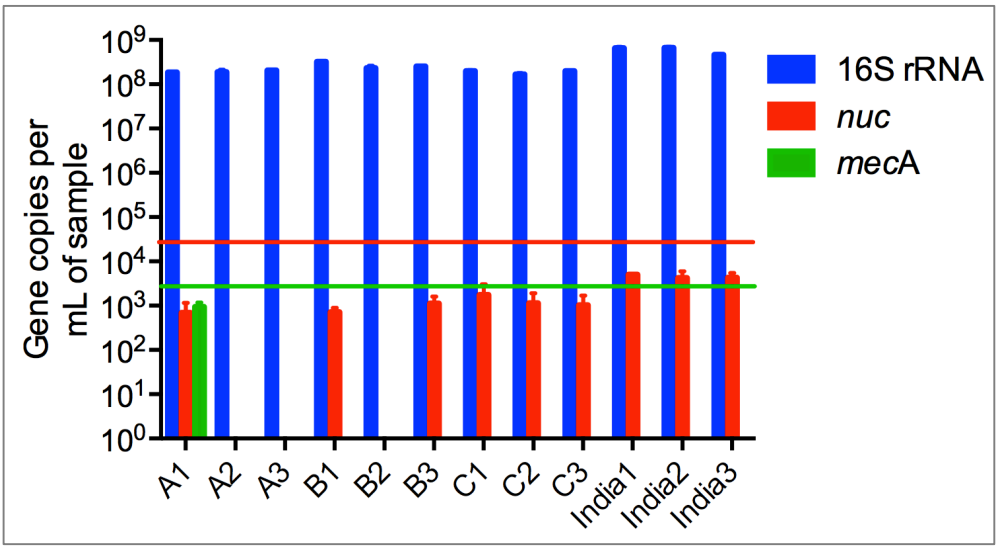

Figure 5.13. qPCR quantification of 16S rRNA, nuc and mecA genes from WWTP effluents. Triplicate DNA extractions were carried out from filter membranes after filtering 200 mL of final effluent sample (Secondary effluent for India WWTP). There was no blank qPCR-amplification for either *nuc* or *mec*A genes; however, gene concentrations were below standard quantification range. Red and green bars represent lowest standard that amplified for *nuc* and *mec*A genes, respectively.

ACKNOWLEDGEMENTS

This work was supported by US National Science Foundation grants CBET-1133746 and OISE-1545756. Additional support for MVR was provided by the Virginia Tech Graduate School.

REFERENCES

1. Laxminarayan, R.; Duse, A.; Wattal, C.; Zaidi, A. K. M.; Wertheim, H. F. L.; Sumpradit, N.; Vlieghe, E.; Hara, G. L.; Gould, I. M.; Goossens, H.; Greko, C.; So, A. D.; Bigdeli, M.; Tomson, G.; Woodhouse, W.; Ombaka, E.; Peralta, A. Q.; Qamar, F. N.; Mir, F.; Kariuki, S.; Bhutta, Z. A.; Coates, A.; Bergstrom, R.; Wright, G. D.; Brown, E. D.; Cars, O., Antibiotic resistance-the need for global solutions. *Lancet Infect. Dis.* **2013,** *13*, 1057-1098.

2. Woolhouse, M.; Farrar, J., An intergovernmental panel on antimicrobial resistance. *Nature* **2014,** *509*, 555-557.

3. Carrel, M.; Perencevich, E. N.; David, M. Z., USA300 methicillin-resistant *Staphylococcus aureus*, United States, 2000-2013. *Emerging Infect. Dis.* **2015,** *21*, 1973-1980.
4. Mine, Y.; Higuchi, W.; Taira, K.; Nakasone, I.; Tateyama, M.; Yamamoto, T.; Uezato, H.; Takahashi, K., Nosocomial outbreak of multidrug-resistant USA300 methicillin-resistant *Staphylococcus aureus* causing severe furuncles and carbuncles in Japan. *J. Dermatol.* **2011,** *38*, 1167-1171.
5. Lindsay, J. A., Hospital-associated MRSA and antibiotic resistance-What have we learned from genomics? *Int. J. Med. Microbiol.* **2013,** *303*, 318-323.
6. Shore, A. C.; Coleman, D. C., Staphylococcal cassette chromosome mec: Recent advances and new insights. *Int. J. Med. Microbiol.* **2013,** *303*, 350-359.
7. Peacock, S. J.; Paterson, G. K., Mechanisms of methicillin resistance in *Staphylococcus aureus*. *Annu. Rev. Biochem.* **2015,** *84*, 577-601.
8. Nikaido, H., Multidrug resistance in bacteria. *Annu. Rev. Biochem.* **2009,** *78*, 119-146.
9. Deleo, F. R.; Chambers, H. F., Reemergence of antibiotic-resistant *Staphylococcus aureus* in the genomics era. *J. Clin. Invest.* **2009,** *119*, 2464-2474.
10. Skippington, E.; Ragan, M. A., Lateral genetic transfer and the construction of genetic exchange communities. *FEMS Microbiol. Rev.* **2011,** *35*, 707-735.
11. Marti, E.; Variatza, E.; Balcazar, J. L., The role of aquatic ecosystems as reservoirs of antibiotic resistance. *Trends Microbiol.* **2014,** *22*, 36-41.
12. Forsberg, K. J.; Reyes, A.; Bin, W.; Selleck, E. M.; Sommer, M. O. A.; Dantas, G., The shared antibiotic resistome of soil bacteria and human pathogens. *Science* **2012,** *337*, 1107-1111.
13. Pruden, A.; Larsson, D. G. J.; Amezquita, A.; Collignon, P.; Brandt, K. K.; Graham, D. W.; Lazorchak, J. M.; Suzuki, S.; Silley, P.; Snape, J. R.; Topp, E.; Zhang, T.; Zhu, Y. G., Management options for reducing the release of antibiotics and antibiotic resistance genes to the environment. *Environ. Health Perspect.* **2013,** *121*, 878-885.
14. Pruden, A., Balancing water sustainability and public health goals in the face of growing concerns about antibiotic resistance. *Environ. Sci. Technol.* **2014,** *48*, 5-14.
15. Mao, D. Q.; Yu, S.; Rysz, M.; Luo, Y.; Yang, F. X.; Li, F. X.; Hou, J.; Mu, Q. H.; Alvarez, P. J. J., Prevalence and proliferation of antibiotic resistance genes in two municipal wastewater treatment plants. *Water Res.* **2015,** *85*, 458-466.
16. Luo, Y.; Yang, F. X.; Mathieu, J.; Mao, D. Q.; Wang, Q.; Alvarez, P. J. J., Proliferation of multidrug-resistant New Delhi Metallo-β-lactamase genes in municipal wastewater treatment plants in northern China. *Environ. Sci. Technol. Lett.* **2014,** *1*, 26-30.
17. Zhang, X.; Servos, M. R.; Liu, J. W., Instantaneous and quantitative functionalization of gold nanoparticles with thiolated DNA using a pH-assisted and surfactant-free route. *J. Am. Chem. Soc.* **2012,** *134*, 7266-7269.

18. Hurst, S. J.; Lytton-Jean, A. K. R.; Mirkin, C. A., Maximizing DNA loading on a range of gold nanoparticle sizes. *Anal. Chem.* **2006,** *78*, 8313-8318.
19. Wetmur, J. G., Acceleration of DNA renaturation rates. *Biopolymers* **1975,** *14*, 2517-2524.
20. Storhoff, J. J.; Lucas, A. D.; Garimella, V.; Bao, Y. P.; Muller, U. R., Homogeneous detection of unamplified genomic DNA sequences based on colorimetric scatter of gold nanoparticle probes. *Nat. Biotechnol.* **2004,** *22*, 883-887.
21. Frens, G., Controlled nucleation for the regulation of the particle size in monodisperse gold suspensions. *Nature Phys. Sci.* **1973,** *241*, 20-22.
22. Turkevich, J.; Stevenson, P. C.; Hillier, J., A study of the nucleation and growth processes in the synthesis of colloidal gold. *Discuss. Faraday Soc.* **1951,** *No. 11*, 55-75.
23. Leng, W. N.; Vikesland, P. J., MGITC facilitated formation of AuNP multimers. *Langmuir* **2014,** *30*, 8342-8349.
24. Thompson, D. G.; Enright, A.; Faulds, K.; Smith, W. E.; Graham, D., Ultrasensitive DNA detection using oligonucleotide-silver nanoparticle conjugates. *Anal. Chem.* **2008,** *80*, 2805-2810.
25. Tan, S. J.; Kahn, J. S.; Derrien, T. L.; Campolongo, M. J.; Zhao, M.; Smilgies, D. M.; Luo, D., Crystallization of DNA-capped gold nanoparticles in high-concentration, divalent salt environments. *Angew. Chem. Int. Ed.* **2014,** *53*, 1316-1319.
26. Schrader, C.; Schielke, A.; Ellerbroek, L.; Johne, R., PCR inhibitors - occurrence, properties and removal. *J. Appl. Microbiol.* **2012,** *113*, 1014-1026.
27. Wan, M. T.; Chou, C. C., Spreading of β-lactam resistance gene (*mec*A) and methicillin-resistant *Staphylococcus aureus* through municipal and swine slaughterhouse wastewaters. *Water Res.* **2014,** *64*, 288-295.
28. Borjesson, S.; Melin, S.; Matussek, A.; Lindgren, P. E., A seasonal study of the mecA gene and Staphylococcus aureus including methicillin-resistant S. aureus in a municipal wastewater treatment plant. *Water Res.* **2009,** *43*, 925-932.
29. Storteboom, H.; Arabi, M.; Davis, J. G.; Crimi, B.; Pruden, A., Tracking antibiotic resistance genes in the South Platte river basin using molecular signatures of urban, agricultural, and pristine sources. *Environ. Sci. Technol.* **2010,** *44*, 7397-7404.

CHAPTER 6. Conclusions

CONCLUSIONS AND FUTURE WORK

Contamination of water resources is one of the greatest challenges facing global human and environmental health today. Traditional wastewater treatment is designed to treat a limited number of contaminants, while emerging contaminants of chemical and biological origin are largely ignored.[1] Antibiotic resistance genes (ARGs), however, behave unlike typical contaminants because they can become amplified, shared and mobilized within the environment.[2] High-biomass and selective environments, such as activated sludge basins in wastewater treatment plants (WWTPs), potentially represent ideal breeding grounds for emergence, proliferation and dissemination of antibiotic resistance.[3, 4] This highlights the need for rapid, efficient, low-cost detection strategies that can be applied for biocontaminant monitoring and characterization, in order to ultimately guide mitigation at such points of interest. The ideal aim would be to power a paradigm shift whereby strategies are implemented for minimizing emerging contaminant amplification, accumulation and dissemination via key hotspots in a manner that is harmonized with other goals, such as water sustainability.[5] The work described in this dissertation was aimed at highlighting promising areas of research that can move us towards more efficient and effective biocontaminant detection and monitoring strategies, which could ultimately aid in informing a paradigm shift in how wastewater is treated. The results reported advance the knowledge of nano(bio)sensing techniques but also highlight some associated limitations.

Chapter 2 described the characterization of ARG distributions in two WWTPs and their effluent-receiving water bodies in a highly-populated city in eastern India. The results reported thus far suggest distinct differences between antibiotic resistance loads in the tested wastewaters and those reported in the literature. This may be a reflection of the country's developing economy but lagging public sanitation infrastructure, in addition to being the number one antibiotic consumer in the world.[6] Future metagenomics analyses are expected to provide higher-resolution antibiotic resistance gene distribution fingerprints that may help understand relative impacts of wastewater sources. Overall, it is hoped that Chapter 2 provides insight about local impacts contributing to global

dissemination of antibiotic resistance, especially after comparisons with similar data from other countries; and that it highlights the magnitude and global scale of the problem of antibiotic resistance as well as the need for innovative solutions, such as the sensing technologies discussed in later chapters.

Chapter 3 described the development of aptamer-functionalized gold nanosensors for SERS-mediated detection of *Staphylococcus aureus*, a model pathogen of concern. Although the technology described has not yet reached full potential, there are clear advantages to advancing this novel detection system, the most important (and possibly life-saving) of which is the ability to target and detect live pathogens of concern within minutes to few hours, with little sample handling or preparation. Other advantages related to sustainable applications of novel technologies are highlighted. For example, aptamers that confer specificity are easier and cheaper to synthesize than antibodies. Sensitivity can then be achieved via surface enhanced Raman spectroscopy (SERS), which employs the surface enhancement potential of gold nanoparticle substrates. Gold nanoparticles have shown little toxicity and, due to their size, their use would involve minimal material applications and waste products. Furthermore, nanosensor reuse strategies based on aptamer denaturing (for target release) and separation (possibly via centrifugation or filtration) could be implemented in order to further extend nanosensor life.

The research described in Chapter 4 began as an alternative way of testing aptamer affinity towards *S. aureus* using impedimetric biosensors. Although these experiments yielded little insight about aptamer-target interactions, some unexpected observations were made regarding tested blocking agents with respect to bacterial attachment onto impedimetric biosensors. These observations were considered of value for general biosensor development and optimization as they highlighted important aspects and limitations associated with minimization of nonspecific interactions in biosensing systems. Interestingly, we observed that closely related *Staphylococcus* species (*S. aureus* and *S. intermedius*) behaved differently in terms of their attachment affinities onto functionalized (blocked) gold electrodes. These results, in addition to blocking agent-specific observations and recommendations for optimizations, are published and expected to provide insight for improvement of electrochemical detection systems by maximizing specificity and minimizing interferences.

Finally, Chapter 5 described the development of oligonucleotide-functionalized gold nanosensors for the detection of antibiotic resistance genes. The nanosensors reported here were demonstrated to be highly stable and selective under environmentally relevant conditions. The nanosensors were tested in spiked effluents of four wastewater treatment plants, including a wastewater treatment plant in a densely populated Indian city. Although detection limits were high due to the detection mechanism, future improvements can be made by incorporating a concentration substrate that also enables SERS-based detection. This would dramatically decrease detection limits and potentially support the multiplex detection of ARGs of interest with little sample preparation and minimal inhibition from organic sources. Other advantages related to sustainability, similar to those reported for Chapter 3, also apply for this detection system; including the potential for nanosensor reuse after a denaturing and separation process.

Overall, the results discussed in this dissertation provide insight on potential areas of promise and limitation associated with the novel (nano)biosensing technologies reported. These technologies are a promising alternative as faster ways to detect, screen and monitor pathogens and ARGs in the environment. The results described in Chapter 2 highlight the magnitude of the antibiotic resistance problem, and support the need for improved technologies. Future work is expected to focus on optimization of the described technologies, as well as further characterization of global ARG emergence and dissemination patterns.

REFERENCES

1. Pruden, A.; Larsson, D. G. J.; Amezquita, A.; Collignon, P.; Brandt, K. K.; Graham, D. W.; Lazorchak, J. M.; Suzuki, S.; Silley, P.; Snape, J. R.; Topp, E.; Zhang, T.; Zhu, Y. G., Management options for reducing the release of antibiotics and antibiotic resistance genes to the environment. *Environ. Health Perspect.* **2013,** *121*, 878-885.

2. Martinez, J. L.; Baquero, F.; Andersson, D. I., Predicting antibiotic resistance. *Nature Reviews Microbiology* **2007,** *5*, 958-965.

3. Mao, D. Q.; Yu, S.; Rysz, M.; Luo, Y.; Yang, F. X.; Li, F. X.; Hou, J.; Mu, Q. H.; Alvarez, P. J. J., Prevalence and proliferation of antibiotic resistance genes in two municipal wastewater treatment plants. *Water Res.* **2015,** *85*, 458-466.

4. Zhang, T.; Zhang, X. X.; Ye, L., Plasmid metagenome reveals high levels of antibiotic resistance genes and mobile genetic elements in activated sludge. *PLoS One* **2011,** *6*.
5. Pruden, A., Balancing water sustainability and public health goals in the face of growing concerns about antibiotic resistance. *Environ. Sci. Technol.* **2014,** *48*, 5-14.
6. Laxminarayan, R.; Chaudhury, R. R., Antibiotic Resistance in India: Drivers and Opportunities for Action. *PLoS Med.* **2016,** *13*.